– An international journal for New Concepts in Global Tectonics –

NCGT JOURNAL

Volume 7, Number 1, March 2019. ISSN 2202-0039. www.ievpc.org
Editor-in-Chief: Louis HISSINK (louis.hissink@bigpond.com)

CONTENTS

From the Editor In this issue ……002

Articles

Multi-parametric Earthquake Forecasting the New Madrid From Electromagnetic Coupling between Solar Corona and Earth System Precursors, Leybourne et al……003

Earthquakes of 1811-1812, City of New Madrid, Missouri, USA……..026

Essays On Global Tectonics, Peter James,……..…033

Electromagnetic Monitoring of the New Madrid Fault US Area with the RDF System Radio Direction Finding of the Radio Emissions Project, Straser et al,……..043

The Potential of Biotic and Abiotic Hydrocarbons in Karakoram, Pakistan, Haleem Magsi…....063

About the NCGT Journal ……073
Appendix: Electric Earth, third installment, Michael Csuzdi

Donate To The IEVPC

The International Earthquake and Volcano Prediction Center (IEVPC) has an important humanitarian mission of saving lives through employment of the latest state-of-the-art technology and processes to predict large earthquakes and volcanic eruptions.

http://www.ievpc.org/donate.html

Please feel free to contact the CEO of the IEVPC, Mr. Bruce Leybourne, at mail@ievpc.org.

For contact, correspondence, or inclusion of material in the NCGT Journal please use the following methods:

NEWCONCEPTSINGLOBAL TECTONICS. 1. E-mail: louis.hissink@bigpond.com.com; 2. Mail, air express, etc., 33 Fields Road, Tanja, NSW 2550, Australia (files in MS Word or ODT format, and figures in gif, bmp or tif format) as separate files; 3. Telephone, +61 419 283 775. *DISCLAIMER*: The opinions, observations and ideas published in this journal are the responsibility of the contributors and do not necessarily reflect those of the Editor and the Editorial Board. *NCGT Journal* is a refereed quarterly international online journal and appears in March, June, September and December. For Mac computer users, this journal in pdf format must be opened with Acrobat or Acrobat Reader. ***ISSN number***; ISSN 2202-0039.

FROM THE EDITOR

In this issue

This issue contains a comprehensive paper describing the latest ideas concerning the electromagnetic (EM) coupling of the Sun and Earth and the forecasting of earthquakes. Straser et al have additionally written a detailed study of the monitoring of the New Madrid Fault system using remote Radio Direction Finding of precursor signals. James continues his series of essays with number four discussing earthquake prediction, while Magsi has proposed another potential source of abiotic hydrocarbons in Pakistan. Finally we have copied the tourist in formation published by the city of New Madrid in Missouri, USA, on the great earthquake of 1811-1812 that adds additional observations associated with the earthquake, in particular the 17 month appearance of the great comet that reached its brightest appearance during the earthquakes. Finally the third installment of Michael Csuzdi's work Electric Earth is reproduced.

It is obvious colossal and catastrophic earthquakes have occurred during the historical past resulting in an enormous loss of life and destruction of infrastructure. If another 1811-1812 event occurred today the destruction would be even more catastrophic, so it is crucial that our understanding of earthquake generation is improved and we attempt to show a new direction of study focussing on EM effects by which this goal may be achieved.

The association of exogenous forcings provided by nearby passing meteorites and comets causing igneous eruptions at the earth's surface was previously proposed by Konstantin Khazanovitich-Wulff in a series of papers published in NCGT News. In that model electromagnetic effects were induced in the Earth's crust by the passing meteoritic bolide causing perturbations in the ionosphere that resulted induced surface kimberlite pipe formation, among many other tectonic effects. So it is interesting to learn that the great New Madrid earthquake was associated with a passing comet, and raises the possibility that the comet might have been the primary forcing of the larger New Madrid earthquakes.

However the idea that an exogenous forcing was capable of initiating tectonic effects at the Earth's surface flies totally into the face of the present day paradigm of geological uniformitarianism in which only endogenous gravitational forcings are permitted, with the ad hoc exception of the blindingly obvious circular craters on the Earth's surface interpreted as meteorite impacts. However there does seem to be a growing body of evidence that earthquakes are linked to crustal EM effects, the nature of which remains obscure. Deep seated earthquakes, as described by James in this issue, led to, among many other observations, the model of plate tectonics where the purely mechanical solution of sliding tectonic plates were proposed for the earthquakes. This explanation was logical given that the only physical force was gravity and its derivatives. However if plasma science is right, that 99.997% of the visible universe is comprised of matter in the plasma state, then it logically follows that a similar ratio between plasma/condensed matter will also occur in the Earth. This leads to the realization that if plasma forces are tectonically dominant and described by the equations of Maxwell and Heaviside, then gravitational forces will of necessity be irrelevant.

This insight leads to the possibility of a vast new area of geological study and research where the role of plasma, (and all volcanic eruptions are eruptions of plasma, albeit it in a viscous state), is the dominant surface geological forcing. Even flowing water is liquid plasma if plasma is defined as ionized matter.

It seems we have arrived at the cusp of another Kuhnian paradigm change, where the Victorian era clockwork universe and geology is withering in the presence of a growing geo-plasma force, and that's the direction we at NCGT Journal will be taking, perhaps with even a new publication focusing directly on the plasma component. I might also add that the publication format of the NCGT journal is under review and will be updated to a new format more appealing to the younger generation(s) behind us.

Multi-parametric Earthquake Forecasting the New Madrid From Electromagnetic Coupling between Solar Corona and Earth System Precursors

Disclosure: A condensed 6-page version of this paper is currently under review with The 13th International Multi-Conference on Society, Cybernetics and Informatics: IMSCI Orlando 6 – 9 July, 2019.

by

Bruce Leybourne, Ms., IEVPC – CEO, Sebastian, Florida, USA
Valentino Straser, Department of Science and Environment, UPKL Brussels
Hong-Chun Wu, Institute of Labor Occupational Safety and Health, Formosa Scientific Center, Taiwan
Giovanni Gregori, PhD., Professor, Istituto di Acustica e Sensoristica O. M. Corbino (INM-CNR), Roma, Italy
Arun Bapat, PhD. Former Head Earthquake Engineering - Central Water and Power Research Station (CWPRS), Pune, India
Natarajan Venkatanathan, PhD., Electrical and Electronics Engineering, SASTRA University, Thanjavur, Tamil Nadu, India
Louis Hissink, IEVPC – Research Director, NCGT Journal – Chief Editor, NSW, Australia

Acknowledgement: In recognition of Dr. Dong Choi's tenacious research as past Director of International Earthquake and Volcano Prediction Center (IEVPC) and from his persistent efforts as Chief Editor of New Concepts in Global Tectonics (NCGT) Journal toward the goals of this paper we honor his memory by including him as an honorary Co-Author posthumously.

ABSTRACT

Forecasting large earthquakes M ≥ 6.0 with satellite monitoring and Radio Direction Finding (RDF) techniques of Electro-Magnetic (EM) precursors associated with earthquakes are possible. Researches with International Earthquake and Volcano Prediction Center (IEVPC - www.ievpc.org) have uncovered phenomena driving earthquakes that should be considered in a framework of strong global EM coupling between solar corona and the entire Earth system, through EM induction driving ionosphere-air-earth currents. Catastrophic earthquakes have repeatedly stricken the New Madrid Seismic Zone during the last 4 major solar hibernation cycles since 1400 AD. Research suggests it is reasonable to expect another cycle of strong magnitude 6.0 to 8.0 earthquakes in the New Madrid region during the upcoming, solar hibernation or solar minimum period starting around 2020. Possibly it's already begun as evidenced by very little Sunspot activity. Large earthquakes generally occur early in the lower part of the cycle. The 1811–12 earthquakes, occurred in the midst of Dalton Solar Minimum (1793-1830), causing many types of ground failures including lateral spreading and ground subsidence by soil liquefaction across the Mississippi River flood plain and tributaries at least 15,000 square kilometers. The Mississippi River changed course in several places. Studies by the United States Geological Survey (USGS), and damage assessments by Federal Emergency Management Agency (FEMA), estimate damages to infrastructure approaching $600 billion of damage. Understanding the common denominators between seismic precursors associated with a solar EM driver should be of concern. Analyzing data on ionization phenomena in areas under tectonic stress such as: Outgoing Long-wave Radiation (OLR); Total Electron Content (TEC); atmospheric effects, such as Jet Stream and other meteorological phenomena related to earthquake clouds and lights is necessary. IEVPC case studies show many M ≥ 6.0 earthquakes seismic locations were identified with Jet Stream precursors that interrupt velocity flow-lines crossing above the earthquake epicenter 1–70 days prior to the event lasting 6–12 hours at ~100 km distance from Jet Stream's precursor. Maximum local temperatures within the potential earthquake zones become higher than normal by 5-7°C, gradually increasing over few days. A rise in the range of 7-12°C or more may indicate imminent earthquakes 3 - 4 days beforehand. High regional OLR and TEC values indicate possible earthquakes. Radio broadcasting may go to higher frequencies, while landlines and inflight communications can be disturbed within the epicenter area 3-4 days beforehand, television broadcast within 15 hours of an event. While mobile phones within 30-40 km of an event may become non-functional within 100 minutes of an event. Global seismological archives indicate 3-4 weeks before large M ≥ 8.0 earthquakes, dry wells, rivulets, and brooks may be flooded with oozing ground water. These innovative research and observational techniques for detecting EM and geomagnetic seismic precursors have rarely been implemented, as earthquakes are simplistically considered the result of grinding plate motions, and their true EM nature (solar EM induction triggering lightning from below) has been ignored. Crustal emission of radio waves (detected with RDF) at very low frequency in the band above 20kHz manifests about 20 hours before an earthquake within the epicenter area. By combining RDF information of appropriately spaced antennae array stations (of some tens of km) one can locate the source of EM emission by triangulation discriminating source direction, position, and distance from the station, providing data on the temporal variation of frequency, magnitude, and source intensity. Many of the methods above have been individually verified as valid for earthquake forecasting.
See: http://www.ievpc.org/earthquake-papers.html.

Keywords: *New Madrid, Earthquakes, Energy Transmigration, Solar Minimum, Stellar Transformer Induction, Space Weather, Solar System, Endogenous Energy, Electric Universe, Earthquake Forecasting, Gravity, Magnetic Dipole Moment, Lightning, Mantle Circuits, Volcanoes, Coronal Mass Ejections, Solar Flares, Axial-Radial Solar Induction, Climate Change.*

1. INTRODUCTION

Catastrophic earthquakes have repeatedly stricken the New Madrid Seismic Zone (Fig. 1) mid-continental USA during the last 4 major solar hibernation cycles since 1400 AD (Fig. 2), [1- Casey et al., 2016]. Therefore, we can reasonably expect another cycle of strong magnitude 7.5 to 8.0 earthquakes in the New Madrid region during the upcoming, solar hibernation or solar minimum period, which starts around 2020. Possibly it's already begun as evidenced by very little Sunspot activity. Since its

establishment in 2012, IEVPC researchers[1] have uncovered phenomena driving earthquakes that should be considered in a framework of strong global EM coupling between solar corona and the entire Earth system, through EM induction driving ionosphere-air-earth currents.

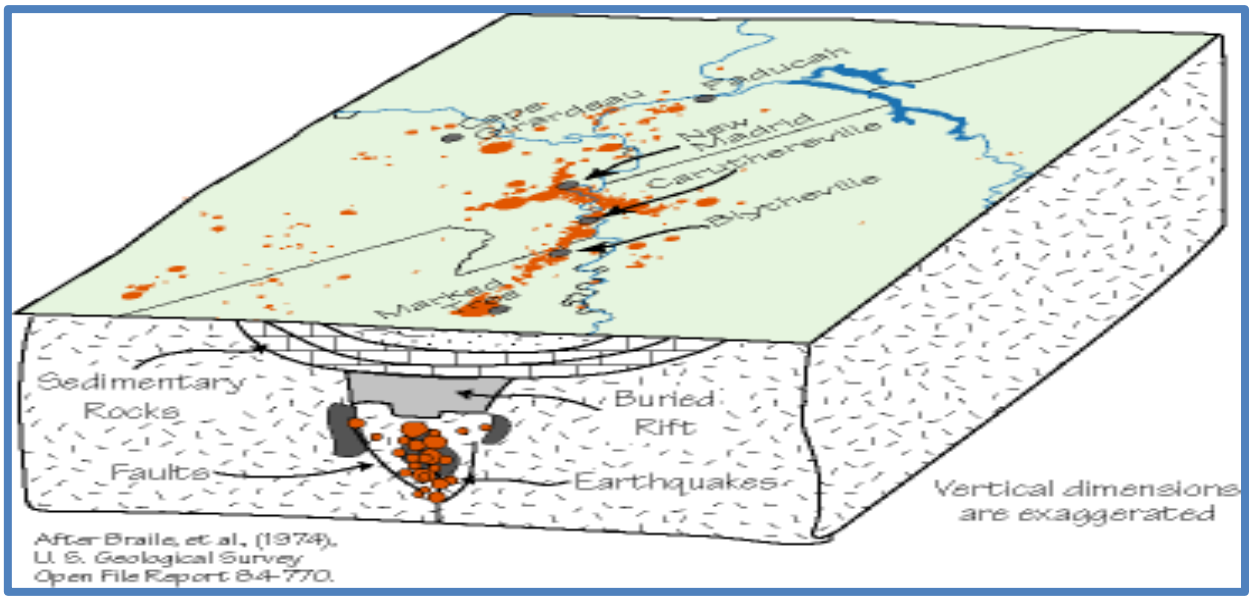

Fig.1. New Madrid Seismic Zone showing schematic section of buried Reelfoot Rift mid-continental USA. http://maps.unomaha.edu/Maher/GEOL3300/Bonuslectures/Reactivation.html. Source:USGS.

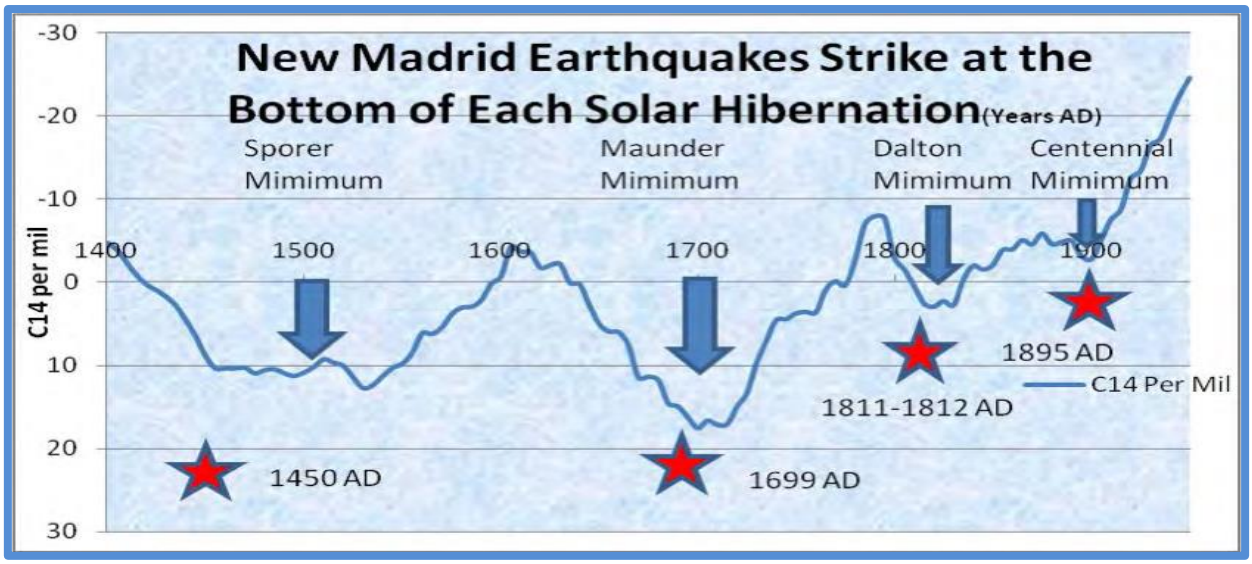

Fig. 2. Solar Activity Deduced from C^{14} Proxy Variation. History of New Madrid earthquakes compared to solar minimums or "solar hibernations" from 1400-1950 AD. The years of major New Madrid earthquakes are shown in red stars with dates. Source: [1- Casey et al., 2016], Data: [2- Reimar et al., INTCAL04].

IEVPC studies reported over the years in the *New Concepts in Global Tectonics Journal* have shown the link between deep and shallow earthquakes, which was originally established by Blot [3- Blot, 1976] as the Energy Transmigration (ET) concept. Transmigration rates of thermal energy towards the surface from deep-seated earthquakes are on the order of 0.15km/day. The physics of seismic and volcanic transmigration has been discussed by Gregori [4- Gregori, 2015c], who distinguishes three kinds of approach: the Blot-Choi viewpoint, which is here considered, the Tsunoda [5- Tsunoda, 2009a]; [6- Tsunoda, 2010]; [7- Tsunoda, 2010a] planetary-scale investigation, and the Vikulin approach [8- Vikulin et al., 2012], which is based on statistics of global seismic catalogues.

[1] Valentino Straser states, "*The complexity of the problem of forecasting major geophysical events is an urgency not only for science, but above all for humanity, today more than ever before, given the degree of civilization. To face this challenge, IEVPC interdisciplinary work is necessary that takes into account the different skills and methods of investigation of the associated researchers. This work was born from this experience, which aims to be above all a research project*".

The ET concept allows forecast of strong shallow quakes, magnitude 6.5 or greater several years in advance, based on the appearance of strong deep-seated earthquakes. Many of the IEVPC's successful predictions have validated the ET concept. Within the upper mantle, energy transmigration generally takes place in two modes [9- Choi, 2017b]. 1.) One surfaces through inclined fracture zones of the Wadati-Benioff zone [10- Benioff, 1949], a planar zone of seismicity corresponding with a down-going slab driven by mantle convection [11- Holmes, 1978] considered as subduction zones within Plate Tectonic Theory. 2.) Another enters sealed porous zones of mantle low seismic velocity lenses or surge channels within Surge Tectonic Theory [12- Meyerhoff, 1996] and transmigrates laterally until finally rising through fracture systems. Earthquakes at 300 - 700 km are related to deep fracture systems particularly in the lower mantle 660 - 700 km or deeper. These slanted fractures and lateral low velocity lenses provide conduits for outer core-derived Electro-Magnetic (EM) energy propagating as "lightning from below", emitting long wavelength radio signals at very low frequency in the band above 20kHz, manifesting about 20 hours before an earthquake within the epicenter area [13- Straser, 2019]. Thus thermal joule energy released from large shallow EM seismic precursor activity may trigger large ground fault earthquakes fairly rapidly. According to the past literature, the general concern has always been focused on gravitation, on thermodynamics, plus stress and deformation, and isostasy (acknowledged, however, to be correct only on the regional, non-planetary, scale), etc. while EM phenomena have always been considered a secondary driver. Detecting EM and geomagnetic seismic precursors has rarely been implemented for earthquake forecasting, as earthquakes are simplistically considered the result of grinding plate motions within the Plate Tectonic paradigm, and their true EM nature (solar ***EM induction***[2] triggering "lightning from below") has been ignored by most tectonic theories until Giovanni Gregori in Earth Endogenous Energy showed that the differential tidal action on different components of the Earth's interior is an effective dynamo (the tide-driven or TD dynamo) that generates an enormous amount of endogenous energy, capable to justify the entire geodynamic and paleoclimate phenomena of the Earth. [14- Gregori, 2002]. Gregori showed that the Earth's interior is a battery. Earth's interior and outer space compose a leaky capacitor. The solar wind flow modulates the efficiency of the TD dynamo, as the longer is the period of the external inducing EM field, the deeper are the electric currents inside the Earth's mantle, and the more efficient is the TD dynamo. During solar minimum the positive/negative alternation of the sectors of the interplanetary magnetic field is such that the TD dynamo is more efficient. Thus, a greater production occurs of endogenous energy. Hence, during solar minima a greater release of endogenous energy occurs, with greater seismicity, and greater soil exhalation in the atmosphere, and more violent impact on climate (see below). The observed EM effect has previously been considered the result of a piezoelectric effect that, indeed, is a secondary and almost negligible additional effect superposed on the leading TD basic phenomenon (the piezoelectric effect is considered a release of electric energy from motion or sudden fracturing of rock). The detection of radio precursors from EM propagation before earthquakes points to problems of interpretation with this much more general and wide-looking perspective. A new theoretical framework arises.

The ***Stellar Transformer Concept*** [15- Leybourne, 2018]; [16, Leybourne et. al., 2017] contends that simple step down energy induction occurs between Sun and Earth, much like the transformer process that steps down your household energy from higher voltage transmission lines sourced from the power company. The Sun would represent a large coil from the power company, while the Earth represents the smaller coil to your home. The larger coil element generally excites current into the smaller coil element by induction of step down energy. Layers within the Earth hold and release charge acting as condensers, or capacitance layers. *Thus the larger Stellar Transformer hypothesis concludes that induction characteristics are determined by the Earth's* ***Magnetic Moment***[3] primarily considered in relationship to the Sun & Moon and to a lesser extent other planets. The energy balance is a key focus of [14- Gregori, 2002], and plenty of energy is available to explain all geodynamic and climatic phenomena. There is need only to exploit the details of this planetary-scale EM interaction. Vector induction components of torque generating power for Earth's magnetic moment are outlined below.

Earth's Axial (y) dipole induction effects of the poloidal **(E)** electric field primarily on polar connected north-south circuits of the mid-ocean ridges, western Pacific rim, and inner core, associated with magnetic moment of the total field strength and polarity variability of mostly the Sun related to Earths planetary orientation and Moon as related to position of Earth's liquid outer core;

Earth's Radial (x) induction effects of the toroidal **(E)** electric field, associated primarily with variations of the magnetic moment of solar winds magnetic field strength and polarity variability primarily affecting Earth's outer core and E-W oriented fracture systems. The south pole has most energy transfer from a ring effect along the ridge encircling Antarctica;

---

[2] ***Electro-Magnetic*** **or** ***Magnetic Induction*** is the production of an electromotive force, or voltage, across an electrical conductor in a changing *Magnetic* field. The induction characteristics are determined by current alignments between layers in the Earth and polarity relationships between of the Earth, Sun and other planets. The alignment and polarity determine the attraction or repulsive forces in *Plasma Core* physics and determine charging and discharging forces on our planet.

[3] The ***Magnetic Moment*** is defined as a quantity that represents the *Magnetic* strength and orientation of a magnet or other object that produces a *Magnetic* field. The *Magnetic Dipole Moment* of an object is defined in terms of the torque the object experiences in a given *Magnetic* field. The strength and direction of this torque depends not only on the magnitude of the *Magnetic Moment* but also on its orientation relative to the direction of the *Magnetic* field and is therefore ***considered a vector***. The direction of the *Magnetic Moment* points from the South to North Pole within the magnet in this case the Earth. The magnetic field of a *Magnetic Dipole* is proportional to its *Magnetic Dipole Moment*. The dipole component of an object's magnetic field is symmetric about the direction of its *Magnetic Dipole Moment*, and decreases as the inverse cube of the distance from the object. The strength of a *Magnetic Dipole* is called the *Magnetic Dipole Moment*. ***Considered a measure of a dipole's ability to turn itself into alignment within a given external magnetic field.*** In a uniform magnetic field, the magnitude of the dipole moment is proportional to the maximum amount of torque on the dipole, which occurs when the dipole is at right angles to the magnetic field. The *Magnetic Dipole Moment*, often simply called the *Magnetic Moment*, may be ***defined then as the maximum amount of torque*** caused by magnetic force on a dipole that arises per unit value of surrounding magnetic field in vacuum (Wikipedia & Britannica).

Earth's Vertical (z) induction effects, associated primarily with magnetic moment linked to Sun-moon tidal variations affecting volcanic and magmatic electric joule energy production of sea-urchin spines or anode plasma tufts. Considered connectors between the oppositly (+/-) charged double layers of the radial-toroidal **(E)** and axial-poloidal **(E)** electric fields.

Each vector has a primary effect when considered as separate vectors, but in reality these are not separable circuits and should be considered together as coupled with the Sun's total variability and output, and ideally with position and magnetic fields of the moon and other planets. To simplifiy understanding of the relationships, solar coronal holes that are aligned with the Sun's north-south polar axis can be considered axial induction elements, while those aligned with the equator can be considered radial induction elements. Many coronal hole configurations represent some combination of the axial and radial elements. This is important to understand because the elements on Earth are directly energized by alignment relationships between these Sun and Earth elements controlled by magnetic moment orbital physics. These dark coronal holes on the Sun represent the induction current elements of our ***Solar Stellar Transformer*** (Fig. 3), charging/discharging the Sun from elements within the arm of our spiral galaxy and thereby the Solar System including Earth, via electro-magnetic wavelength and frequency response, within an Electric Universe framework [17- Thornhill and Talbott, 2007].

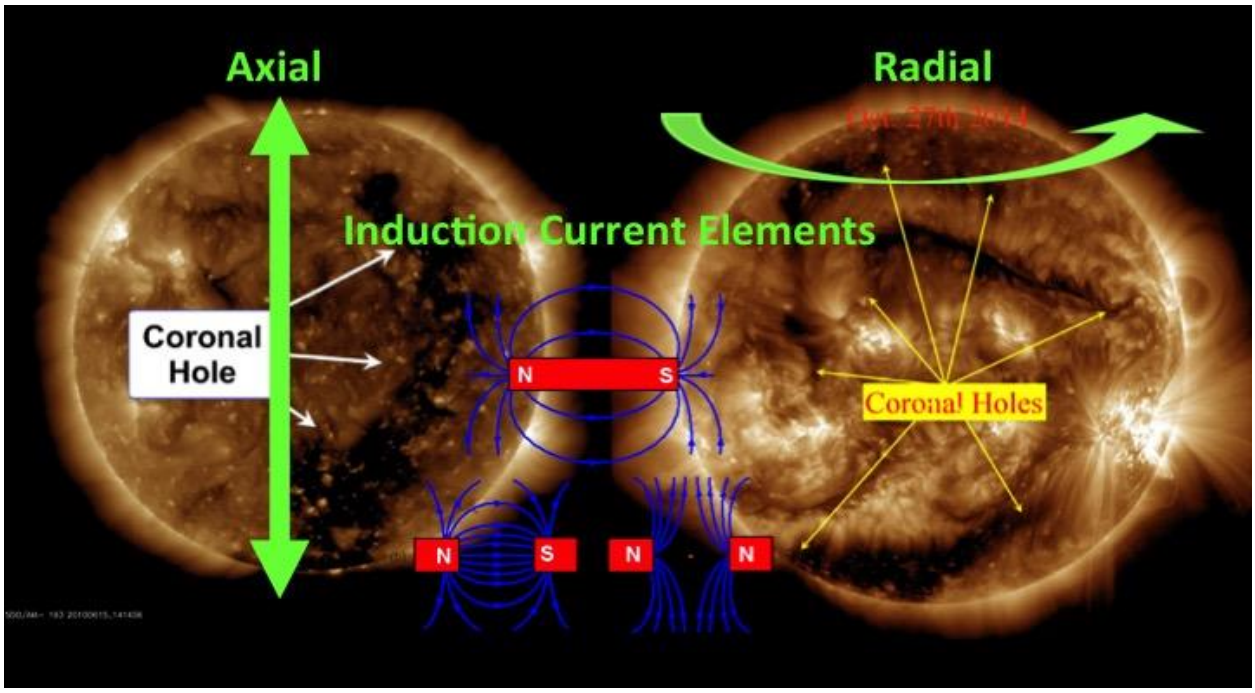

Fig. 3. Solar Stellar Transformer Induction Current Elements Coronal holes express induction elements in axial vs. radial orientations determining axial vs. radial affects on Earth systems. Polarity determines attractive/repulsive force determining charging/discharging relationships [15, 16].

2. DETERMING EFFECTS ON EARTH

In space above the Earth's poles there are aurora plasma rings, inducing ground currents within the mid-ocean ridges, especially the mid-ocean ridge encircling the South Pole (Radial Induction) (Fig. 4). A direct coupling with the Earth's most powerful induction current elements occurs within its mantle and inner/outer core. Mantle circuit trends can be mapped with satellite mantle gravity imaging of the thermal signatures given off by induction current elements of the mid-ocean ridge circuits (Fig. 5). Complex magnetic modeling techniques reveal multi-phase circuit configurations of the Polar Regions, reviewed in previous writings "Evolution of as a Stellar Transformer" [16- Leybourne et. al., 2017]. For example, circuit activation and switching of these global scale electric circuits mapped by satellite gravity and magnetics signatures can be understood in terms of shifting earthquake and lightning hotspot activity. The Southeast Indian Ridge mantle circuit provides South Pole grounding links to lighting activity in the African Congo.

A global momentum shift in Lightning from the African Congo to Lake Maracaibo, Venezuela occurs in conjunction with the 11-14 year Sunspot cycles and signals a change of Earth's charging phase, which switches to the East Pacific Rise. This is the Earth's largest ridge and a most active mantle circuit linked to earthquakes, volcanic activity, and huge climate change [15, 16]. An interdisciplinary forecasting approach using an innovative electro-dynamic model of our solar system can be built with geophysical intelligence. This builds a comprehensive framework for understanding Earth's interactions with space weather.

Fig. 4. Global Electric Circuit Conventional Model includes Ground Inductions Currents (GIC) magnetically coupled to Aural Ring Currents torqued by Field Aligned Induction currents from magnetosphere coupling to solar forcing. (Forbes, J. - University of Colorado – Boulder). Step down aurora energy to the Mid-Ocean Ridges encircling Antarctica would generate powerful radial ground induction currents (Smoot, N.C. - Sr. Fellow IASCC).

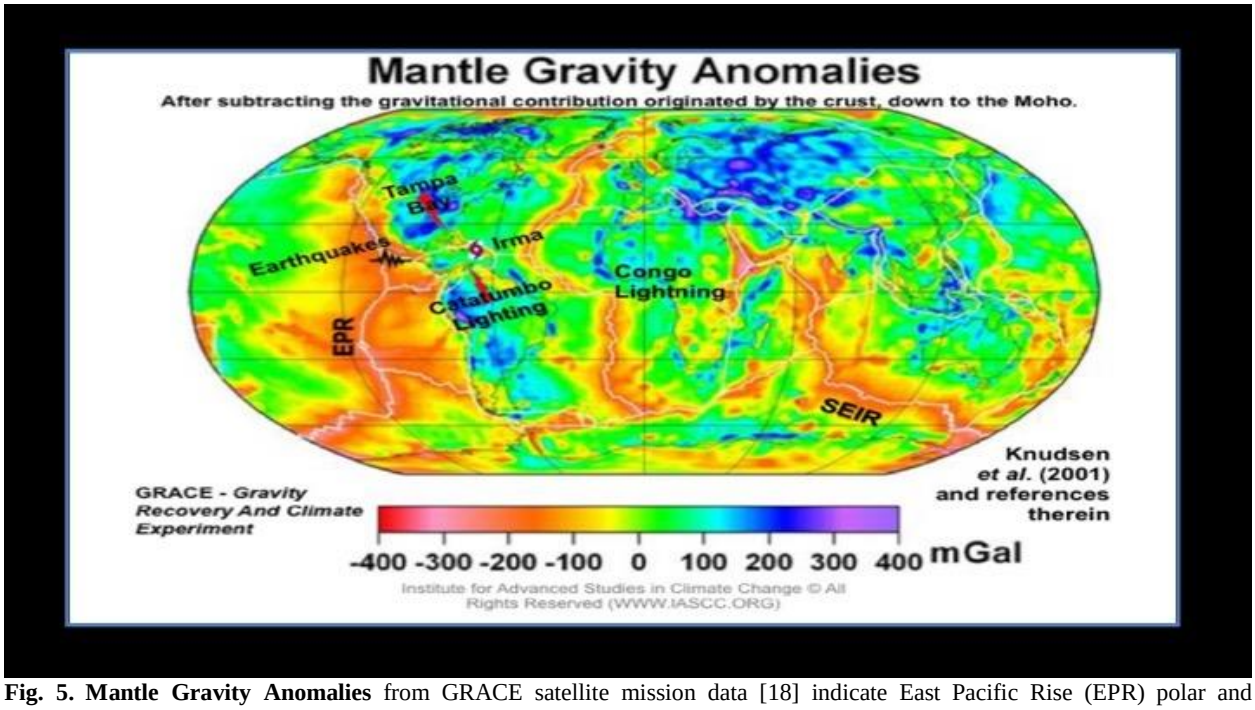

Fig. 5. Mantle Gravity Anomalies from GRACE satellite mission data [18] indicate East Pacific Rise (EPR) polar and continental circuit connections to Catatumbo, Tampa Bay lightning anomalies, and Southeast Indian Rise (SEIR) connections to the African Rift/Congo global lighting anomalies.

3. NEW MADRID SCOPE AND SIGNIFICANCE

The 1811–12 earthquakes (Fig. 6), associated with the Dalton Minimum (Fig. 2), had deveasting concequences in a relatively unpopulated area at the time compared to now. Studies by USGS and damage assessments by FEMA within the past decade estimate damages to infrastructure within the New Madrid Seismic Zone approaching over $600 billion worth of damage [19-Elnashai, et al., 2009]. Understanding the common denominator between analyzed seismic precursors with an associated solar EM driver should be of major concern.

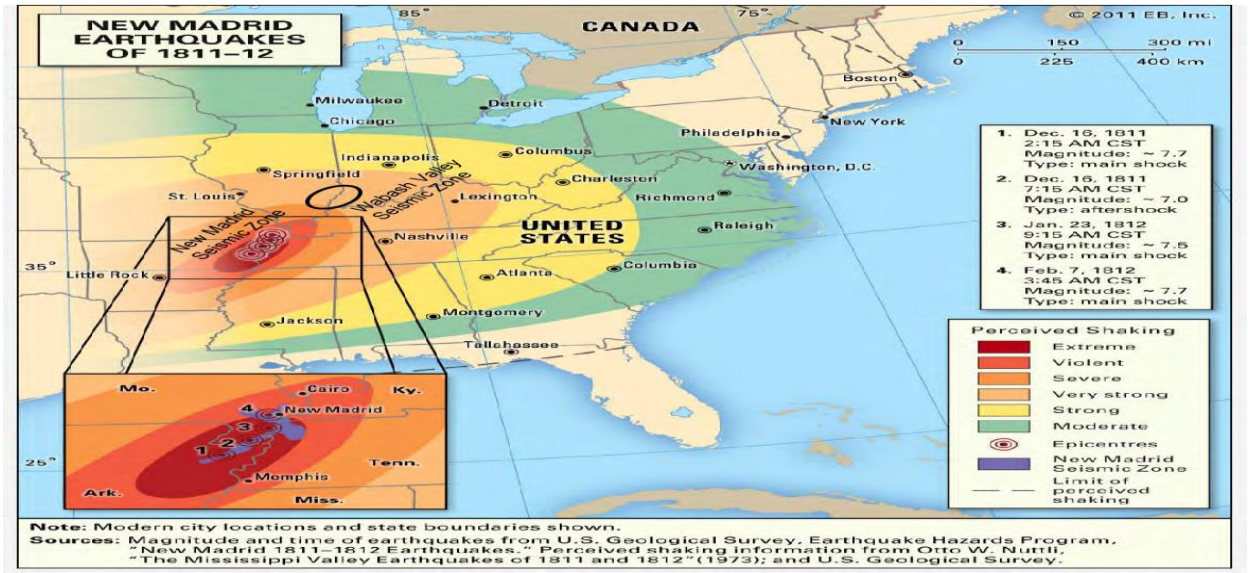

Fig. 6. Map of the New Madrid earthquakes of 1811-12. Base map cited from Encyclopedia Britannica, Inc. (http://www.britannica.com/EBchecked/topic/1421133/New-Madrid-earthquakes-of-1811-12). Wabash Valley Seismic Zone.

USGS Impact Statement: "Likely impacts from future large earthquakes hazards involve more than just strong ground shaking from passing seismic waves. The 1811–12 earthquakes caused many types of ground failures including landslides along the Mississippi River bluffs from Mississippi to Kentucky. Ground failures also included lateral spreading and ground subsidence by soil liquefaction across the Mississippi River flood plain and along tributaries to the Mississippi River over at least 15,000 square kilometers. Today, a repeat event could be expected to produce similar effects in northeastern Arkansas, southeastern Missouri, western Tennessee and Kentucky, and southern Illinois. Roadways in the Mississippi Valley of Arkansas and Missouri (such as Interstate 55) could become impassable because of bridge failures and fissuring of road surfaces. Venting of large quantities of water, sand, and mud as a result of liquefaction could flood fields and roads and disrupt agriculture for weeks to months. Flooding of farmland, where agricultural chemicals are stored onsite, could contaminate rivers and streams. Failure of levees, especially during high water, would contribute to flooding, and failures of riverbanks could make the Mississippi River and its tributaries difficult to navigate for many weeks. The City of Memphis and the surrounding metropolitan area of more than one million people would be severely impacted. Memphis has an aging infrastructure, and many of its large buildings, including unreinforced schools and fire and police stations, would be particularly vulnerable when subjected to severe ground shaking. Relatively few buildings were built using building codes that have provisions for seismic-resistant design. Soil liquefaction and related ground failures are likely to occur in downtown Memphis along the Mississippi River and along the Wolf River that passes through Memphis. The older highways and railroad bridges that cross the Mississippi River, as well as older overpasses, would likely be damaged or collapse in the event of a major New Madrid earthquake. Some of the bridges and pipelines crossing the Wolf River might be damaged or destroyed. Although Memphis is likely to be the focus of major damage in the region, St. Louis, Mo., Little Rock, Ark., and many small and medium-sized cities would also sustain damage" [20 - Frankel, et. al., 2009].

3. SOLAR RELATIONSHIPS

Historic records and analysis (Fig. 7 & Fig. 8) show convincingly an increase in quake and volcanic activities during the solar low cycles throughout the globe [21- Choi and Maslov, 2010]. These solar cycles linked to this anti-correlation theoretically [15, 16] as a Stellar Transformer are caused by solar system induction charging cycles. When the magnetic fields of the Sun, Earth and other celestial bodies within our solar system begin to be characterized by a lower frequency during the solar minimums, fluctuations of the external magnetic field determine a much more efficient TD dynamo. Thus a larger release of endogenous energy causes a greater thermal expansion of different parts of the Earth's crust. This results into a greater crustal stress, seismicity, and more violent climate excursions (drought/flood, hurricanes, extreme events, etc.). That is, mentally this can be simply conceptualized as a long-lasting lightning from below. This is feasibly explained by Gregori [14, 22- Gregori, 2009], and by the interpretation of the recent and still ongoing MiniMax of Cycle 24 [23- Clette et al., 2014]. According to the following rationale, Gregori states… "Unlike what is generally and arbitrarily believed, the Earth is not a hot-ball cooling in space on the billion-year time scale. In contrast, the Earth operates like a battery that recharges and discharges at different times. On the geological time-scale, the typical pace is the period of a "heartbeat" i.e. ~28.4 Ma, although effects are also immediately observed (shown e.g. by the modulation of volcanic cycles that are clearly correlated with long-period solar activity). Battery recharging occurs through the tide-driven (*TD*) dynamo. The discharge occurs through sea-urchin spines that propagate from the core-mantle boundary (*CMB*) through the Earth's surface. The currents induced by the long-period EM induction into the mantle, and caused by the solar wind, supply the "static" magnet of the *TD* dynamo. The larger are these mantle currents, the more efficient is the *TD* dynamo, hence the production of endogenous heat. On the short period, i.e. almost immediate, time-scale, this is manifested like anomalous exhalation of geogas into the ocean/atmosphere system, with consequent climate anomalies. But, also a faster uplift occurs of superswells, a greater geodynamic activity, a larger global seismicity, and increased energy supply to

volcanism, whether volcanoes are directly supplied by spines or by friction heat consequent to geodynamic activity. Indeed, since a few years while the MiniMax period is in progress, all these effects are presently being unquestionably observed and reported everyday by mass media all over the world."

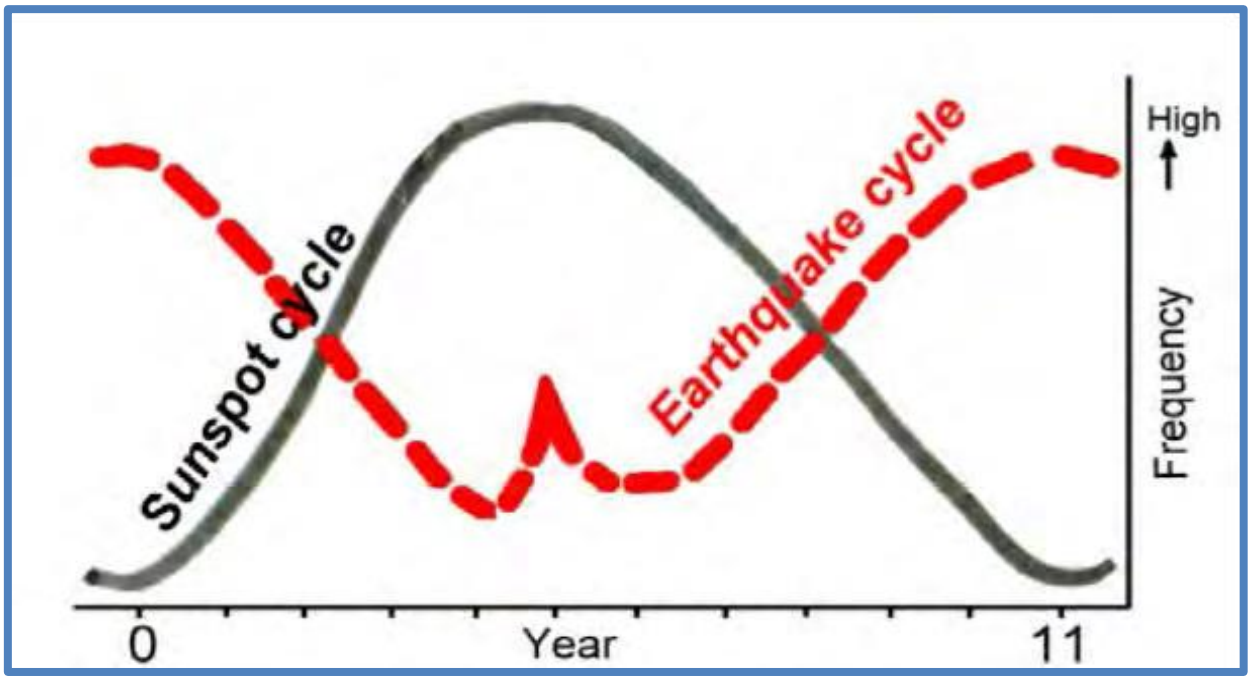

Fig. 7. Anti-correlation between the solar and earthquake cycles [21- Choi and Maslov, 2010].

IEVPC understands and monitors precursor signals (http://www.ievpc.org/id74.html) associated with these disruptive events, and have developed innovative methods of earthquake forecasting. Based on the next arrival of a major, prolonged, solar low period, or solar hibernation cycle we expect another series of large earthquakes to strike the New Madrid region during this solar minimum cycle, 2007 to 2040 AD [1]. The correlation of major earthquakes and solar activity in terms of climate change and geophysical associations discussed by Walker [24, 25, 26] found earthquake links to El Niño as early as 1988. Then followed up by Leybourne [27, 28] in 1996 and 2001, with *El Niño Tectonic Modulation in the Pacific Basin*. An initial paper [29- Casey, 2008] on the regular pattern of climate oscillations linked to solar activity using the Relational Cycle Theory (RC Theory) has demonstrated itself to be among the most successful in climate prediction, underscoring the basic reliability of the theory and its associated seven elements of climate change. Subsequently [30- Casey, 2010] in a preliminary paper, proposed the connection between the RC Theory and major earthquakes and volcanic activity. Others [31- Choi et. al., 2014], have also found the strong relationship between solar lows and increased seismic and volcanic activities.

The arrival of another solar minimum is in harmony with the increased seismic activity in the Caribbean and offshore Central America along Pacific coast, and Mexico, as represented by a large M = 7.5 earthquake offshore Honduras on 10 January 2018. Further support comes from the extremely high water temperature of the Gulf of Mexico observed in March 2018, which followed the January M = 7.5 quake. This is corroborated by a recent M = 7.5 earthquake in the Caribbean in January 2018 [32- Choi et al., 2018]. The extremely high seawater temperature appeared in the Gulf of Mexico in March 2018 following the January M = 7.5 quake. This implies highly increased thermal activity in the region. Undoubtedly, the Caribbean - Gulf of Mexico region has already entered heighted energy release phase likely related to the decreasing solar activity or solar hibernation. It has been established that the energy release from the Earth's outer core dramatically increases during the major solar low cycles. Seismo-volcanic quiescence cited from [33- Choi, 2010] and [34- Tsunoda et al., 2013], and the "Earth core active phase" from [21- Choi and Maslov, 2010].

It has also been found that seismic energy transmigrates northward synchronized with the recent accelerated north magnetic polar movement during the declining solar cycle in the Central America-Caribbean area (Fig. 9). This is confirmed by suddenly increased earthquake activity since 1990 when the solar cycle 22 peaked and a longer solar cycle (which includes the 11-year solar cycles 23, 24 and possibly 25 and 26) started. Increased energy inputs from the southern hemisphere expand northward as explained from the mid-ocean ridge coupling to ridges encircling Antarctic (increased radial induction) with increased space weather events as explained by Stellar Transformer concepts [15, 16]. A combination of these facts may well explain the historic devastating New Madrid earthquakes that occurred during every solar minimum, four in a row, since 1400 AD.

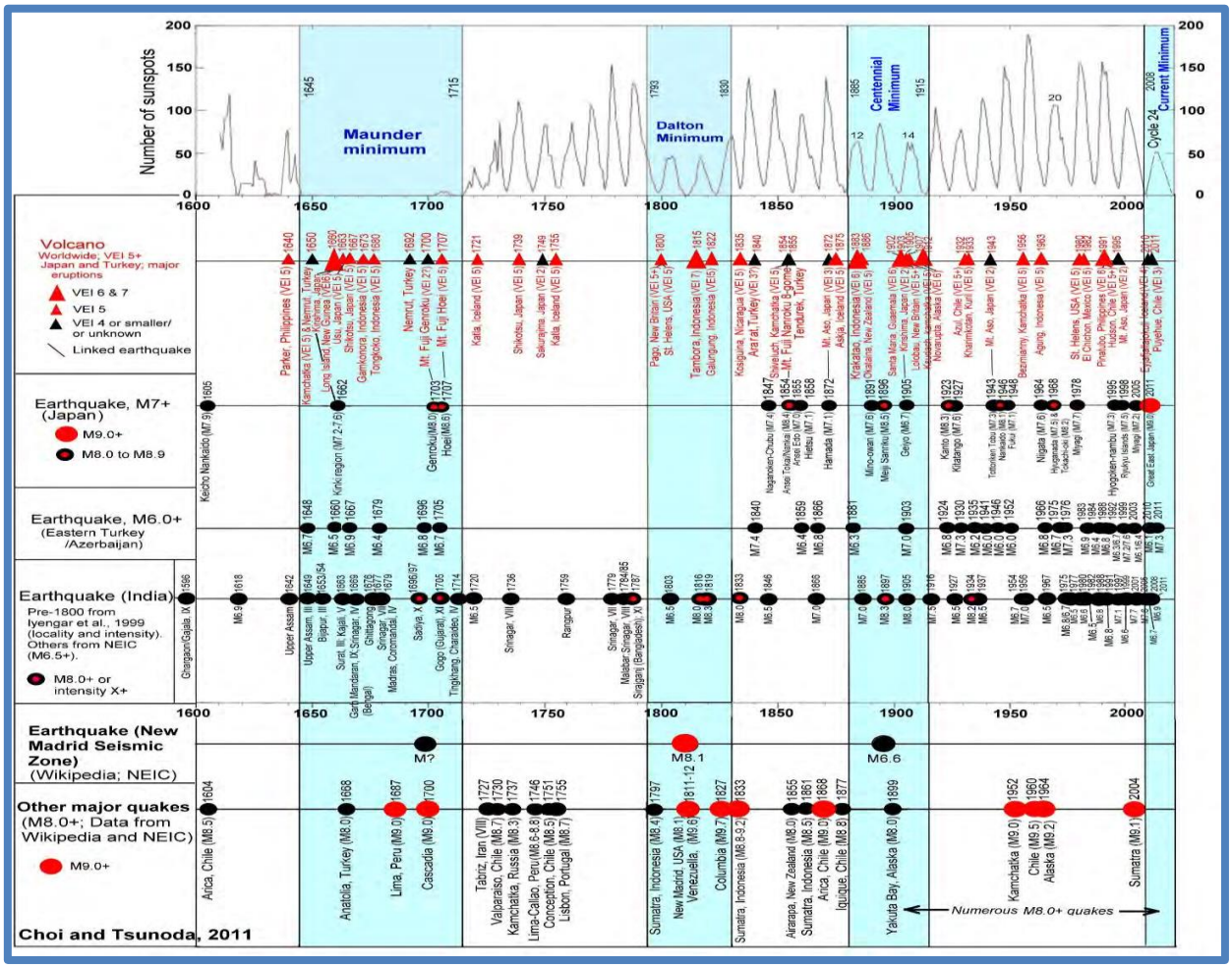

Fig. 8. Solar cycle and world volcanic/seismic activities. All of the NMSZ quakes occurred around the middle of the solar low periods. Cited from [35- Choi and Tsunoda, 2011] and [36- Choi, 2013b].

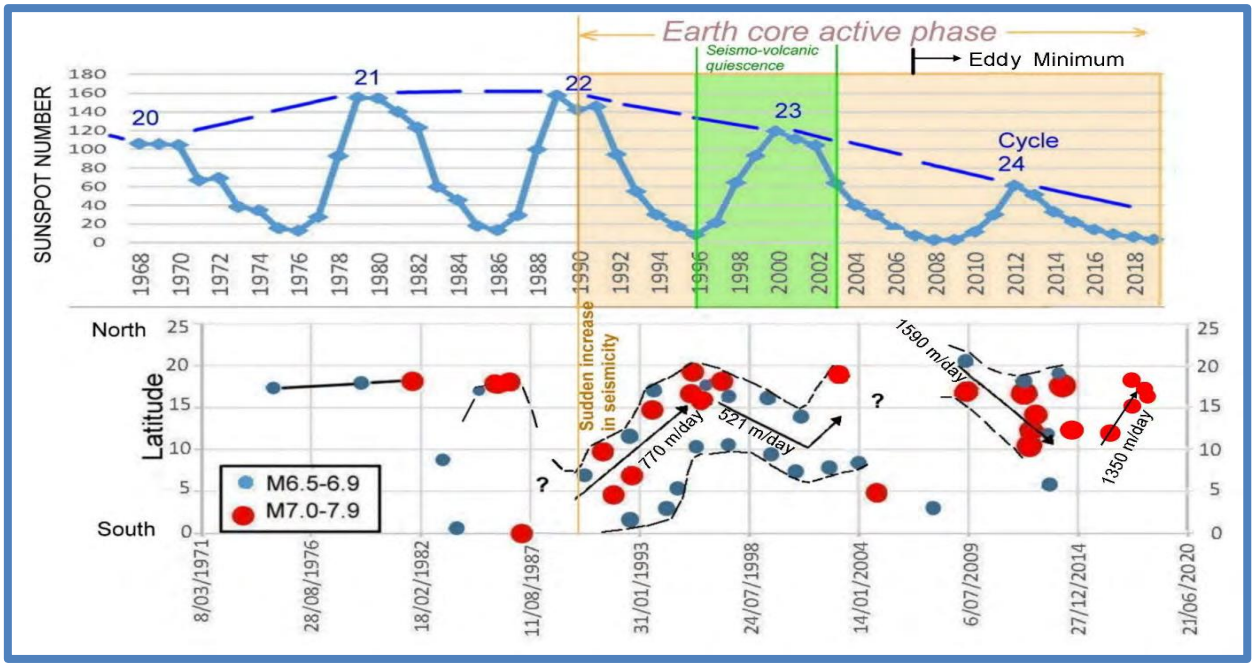

Fig. 9. Solar cycles and earthquake propagation trend in Central American Pacific coast [37- Choi, 2014]. Note a general trend when earthquakes move northward as the solar cycle is in decline, but southward when the solar cycle rises. Data missing from 2005 to 2009.

RADIO DIRECTION FINDING (RDF) OF SOLAR INDUCED EM SEISMIC PRECURSORS [13]

The Radio Direction Finding (RDF) Network, developed by the Radio Emissions Project is based on technology that evolved starting from the late 1800s thanks to the studies of Heinrich Hertz, who discovered the directionality of an open loop of wire used as an antenna. The first monitoring station was built in Lariano (Rome, Italy), and was created by the Luminous Transient Phenomena that occur in Earth's Atmosphere (LTPA) Observer Project and the Radio Emissions Project. This allows 24/7 monitoring of a wide bandwidth of the Earth's background electromagnetic emissions to trace radio anomalies in seismically active areas for a "crustal diagnosis" in real time, on a global scale [13- Straser et al., 2019]. By combining RDF information of appropriately spaced antennae array stations (of some tens of km) one can locate the source of EM emission by triangulation. The network of receiving stations identify the goniometric axis of a radio signal and discriminate source direction, position and distance from the station. The system provides data on the temporal variation of frequency, magnitude, and source intensity. During the experimentation of the Radio Emissions Project it was possible to detect strong and precise radio emissions that precede destructive earthquakes worldwide [38- Straser et al., 2015]; [39- Straser et al., 2016]; [40- Cataldi et al., 2017].

The station began to provide the first data on the origin of electromagnetic signals in March 2017 [13], while the monitoring of the New Madrid Fault began almost a year later. Pre-seismic crustal emissions of radio waves are detected with RDF at very low frequency in the band above 20kHz manifesting about 20 hours before an earthquake within the New Madrid Fault epicenter area. On 2 February 2018 the electromagnetic monitoring of the United States began in the New Madrid [13] revealed 57 earthquakes M ≥ 2.5, including earthquakes of magnitude 3.3 and 4.4 in December 2018. In this case the "dark purple" azimuth was kept under strict control focused on the New Madrid Fault 8,500 km away from the monitoring station in Italy (Fig. 10).

Fig. 10. World mapping of the RDF system of the Radio Emissions Project [13]- Distance of 8500 km indicated by violet azimuth in NW direction to monitor New Madrid Fault area from RDF monitoring station in Lariano (Rome, Italy). Source: Google Maps.

The experiment was able to record numerous incoming signals, identifying their azimuthal origin by discarding all others accordingly, then checking their electromagnetic frequency, time of appearance, and bandwidth. The earthquakes analyzed in the course of the experiment were preceded by electromagnetic frequencies between the SELF and VLF bands, 1000 Hz and 32000 Hz, which appeared a few hours to a few days before earthquakes. Radio receivers designed for the amplification of low-frequency electromagnetic signals by Daniele and Gabriele Cataldi detected these frequencies. The frequency of the radio-anomalies is inversely proportional to the average electromagnetic frequency of the seismic magnitude signals. The periods in which there are many electromagnetic emissions always precede earthquakes of a strong or greater intensity than the average of the period (Fig. 11). Groups of signals or single very intense signals preceded the occurrence of earthquakes.

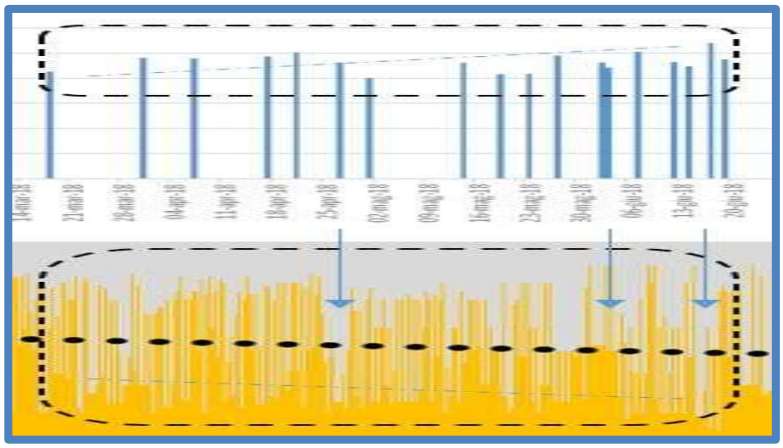

Fig. 11. Impulse signals with significant frequency variation and little temporal variation precede magnitude of seismic events with low variations.

It is also evident that solar activity has an important influence on the electromagnetic emissions detected with the RDF system. The study in this case has found that these emission concentrations in a given period of time somewhat follow the Sunspot Number inversely proportional, ie solar activity (Fig. 12).

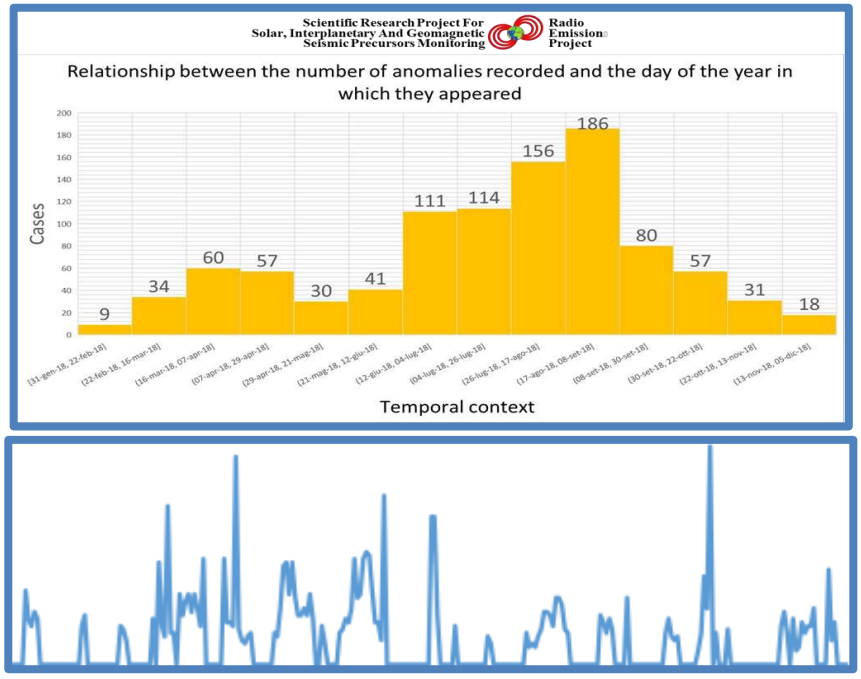

Fig. 12. Inversely Proportional number of radio-anomalies time series [13] (upper inset) somewhat follows the number of Sunspots (lower inset). Source: http://www.sidc.be.

OTHER SIGNIFICANT PRECURSORS

Understanding the common denominator between analyzed seismic precursors with an associated solar EM driver should be of concern. The comparison is carried out by collecting data on ionization phenomena in areas under tectonic stress such as: Outgoing Long-wave Radiation (OLR); Total Electron Content (TEC); atmospheric effects, such as Jet Stream and other meteorological phenomena related to earthquake clouds and lights as in the case of the Luminous Transient Phenomena that occur in Earth's Atmosphere (LTPA) Observer Project discussed above. For example: the Jan. 16, 1995 Kobe earthquake was preceded by earthquake lights [41- Tsukuda 1992]; similar observations were reported from Mexico and other seismic regions of the world [42- King, 1983]; [43- Lomnitz, 1994].

Global seismological archives indicate 3-4 weeks before large M ≥ 8.0 earthquakes, dry wells, rivulets, and brooks may be flooded with oozing ground water. Changes in the geomagnetic field, gravity field, electric potential, rise in well-water, appearance of springs etc. are quite well known [44- Plastino et al 2002].

There are also reports of rises in sub-surface, surface and atmospheric temperatures. Usually the rise in temperature starts about 150 to 200 days before the earthquake occurs. The rise takes the form of a ramp-shaped plot. About three to five days before the earthquake it suddenly shoots up and peaks on the day of the earthquake. The observed rise on the day of the earthquake could be anything in the range of 6.0 to 10° C. On the day of the Kashmir Earthquake of October 8, 2005, the atmospheric temperature was 10° C higher than the average temperature. Increased infrared radiation recorded by satellites has been a good earthquake precursor [45- Qiang, et al 1990].

OUTGOING LONGWAVE RADIATION (OLR) PRECURSOR ANOMALIES [46]

Average maximum local temperatures within the potential earthquake zones are higher than normal by 5-7°C, gradually increasing over few days. Usually a rise in the range of 7-12°C or more indicates an imminent earthquake. The temperature rise is observed ~3-4 days before earthquakes. If the values of OLR and TEC are very high this is another possible earthquake indicator inside a suitable large area. Outgoing Long wave Radiation (OLR) measurement, a satellite-based measurement can be used as an effective tool to identify the earthquake preparation zones. Atmospheric and surface phenomena like anomalous Outgoing Longwave Radiation (OLR) normally appear 5 to 30 days before the occurrence of moderate and big earthquakes. Preliminary analysis of a recent Peru earthquake occurring on September 25, 2013 with the magnitude of 7.0 is shown [46- Venkatanathan, N., and Natyaganov, V., 2013].

Outgoing Longwave Radiations (OLR) are electromagnetic low energy infrared radiations departing from the Earth surface into Space. Anomalous OLR is observed in imminent earthquake zones. In recent years, numerous studies published on the appearance of significant transient thermal anomalies before devastating earthquakes were reported [46- Venkatanathan et al, 2013]; [47- Tronin et al, 2002]; [48 & 49- Saraf and Choudhury, 2005a & b]; [50- Ouzounov et al, 2006]; [51- Ouzounov et al, 2007]; [52- Oyama et al, 2011]; [53- Jing et al, 2013]. Some researchers link OLR anomalies and specific clouds – seismic-tectonic indicators [54- Doda et al., 2011] are associated with a local increase in deep degassing through lithospheric faults before strong earthquakes, such as hydrogen sulfide, methane, and underground water in the form of superheated steam creating conditions for a critical point of Mendeleev. This is indirectly related to numerous "smokers" found recently in many places on the ocean floor.

The appearance of anomalous transient radiation can be correlated with the tectonic stress and thermodynamic processes in the atmosphere. OLR measures radiation from ground, lower atmosphere, and clouds together. An algorithm calculates the OLR, at 8 to 12 μm [55- Gruber and Krueger, 1984]. An anomalous OLR flux can be defined as change in energy index (dE_index), which signifies the statically defined maximum change in the rate of OLR for a given location and time specific spatial locations and predefined times [56- Ouzounov et al, 2011]. The appearance of the short lived OLR anomaly is observed before the occurrence of the Peru earthquake. The manifestation of an OLR anomaly can normally be related to the magnitude of the earthquake. It varies from few days to one month prior to the earthquake occurrence. The time line of the appearance of these transient anomalies varies from earthquake to earthquake, probably due to the different nature of the tectonic settings of these places.

Short-lived anomalies appeared thrice before the occurrence of the earthquake on September 25, 2013. An example of first anomaly appeared on September 07, 2013, and it lasted till September 10, 2013. The intensity of the daily current field OLR value slowly increased from September 07, 2013 and it reached peak value on September 10, 2013 (Fig. 13a, b, c & d).

From September 07, 2013 to September 09, 2013 the anomalous daily current field OLR value was recorded by the NOAA satellite during its “night” pass and the daily current field OLR value was 4 times greater than daily base field OLR value during the “day” pass of NOAA satellite on September 10, 2013. The OLR anomaly started disappearing from September 10, 2013 “night”, and it was completely disappeared on September 11, 2013, which was recorded by NOAA satellite during “day” pass (Fig. 13e).

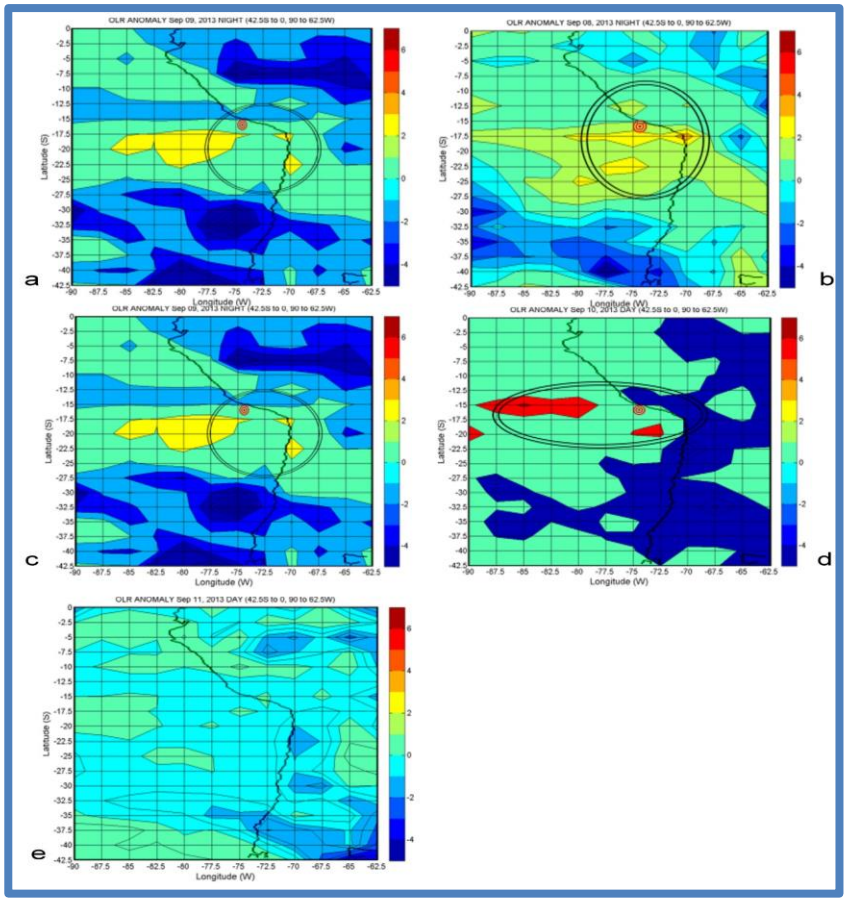

Fig. 13 (a, b, c, d & e): OLR Anomaly evolution for the first time observed before the earthquake occurred at 50km S of Acari, Peru (15.882°S, 74.543°W) on September 25, 2013. Anomalies are circled and epicenter was marked by red concentric circle [46].

After the disappearance of OLR anomaly on September 11, 2013 no abnormality was recorded till September 17, 2013 satellite "night" pass and appeared again on September 18, 2013, which was recorded on a satellite's "day" pass image. At one location (10S, 80W) the satellite OLR value was 4 times more than base field OLR values. Another anomaly was concentrated at the location (17.5S, 72.5W) with current field OLR value was 3 times more than base field OLR value.

After the disappearance of second anomaly in the nearby region, a quiet period in terms of current field OLR value prevailed until September 20, 2013, and satellite recorded normal current field OLR value during its "night pass". Finally, before the earthquake occurred on September 25, 2013, for the third time the anomaly appeared on September 21, 2013. This time the current field OLR value was 3 times more than the base field OLR value at the nearby location (12.5S, 75W), which was observed by satellite "night" pass. The intensity and area of the anomaly increased on September 22, 2013 compared to previous day night and less intense anomaly was recorded on September 23, 2013 at the location (17.5S, 72.5W), it completely disappeared the day before and after the occurrence of earthquake on September 25, 2013, 16:42 (UTC).

The OLR data derived from the NOAA satellites show that the OLR anomaly can be used as a trustworthy precursory signal. It is possible to elevate the earthquake prediction to the exceptional level of precision if we use multi-parameter precursory studies. This can be certainly accomplished by well-coordinated global networking with help of space and ground based methodologies for forecasting earthquakes.

SEISMO-ELECTRO-MAGNETIC EFFECT [57]

When the temperature of any magnetic body increases, the magnet starts losing its magnetic properties. The magnetism decreases as the temperature rises. The temperature at which the magnet entirely loses its magnetism is known as the Curie temperature or Curie point. In the case of the thrust type of earthquake mechanism, two sides or parts move over one another. The frictional movement during the initial stages is very small. A few days (about 150 to 200 days) before the occurrence of a destructive earthquake the temperature starts rising. This effect is extensively manifested at sub-surface temperature level. About 3 to 5 days before the occurrence of an earthquake the rise is sharp and rapid and it peaks on the day of earthquake. As a result of the rise in sub-surface temperature in the hypo-central region, the geomagnetic field declines. The reduction in the magnetic field adversely affects the transmission and propagation of electric and electromagnetic signals coined the Seismo-Electro-Magnetic Effect [57- Bapat, 2003]. It affects radios, telephones and televisions. If a radio station is transmitting a signal at a particular frequency, say 1000 kHz, then the same will be received about ten to twenty hours before the occurrence of the earthquake at 1100, 1200, 1300 .... 1700, 1800, 1900, 2000 kHz or more. In the case of televisions, there are repeated audio, visual and spectral disturbances. The number of disturbances goes on increasing till the occurrence of the earthquake. It has been seen that these effects are manifested about two to three days in advance and are observed intensely about ten to twenty hours before the earthquake. Thus radio broadcasting may go to higher frequencies, while landlines and inflight communications can be disturbed within the epicenter area 3-4 days beforehand, television broadcast within 15 hours of an event. While mobile phones within 30-40 km of an event may become non-functional within 100 minutes of an event.

The entire zoological species consisting of reptiles, animals, ants, insects, birds etc. become restless and move in a feared condition in many directions without any proper orientation. All of them make shrilling loud noise and in attacking mood. Even domestic pets become hostile to the owner. This happens about 14 to 15 hours before earthquake. There is large number of reports about abnormal animal behavior [58- Rikitake, 1984]. It has also been observed that some sensitive human beings are useful as earthquake precursors. This is observed in hospitals. It was found that the number of deliveries and outpatients increases to five to seven times the daily averages [59- Bapat, 2005).

These innovative research and observational techniques for detecting EM and geomagnetic seismic precursors have rarely been implemented as earthquakes are simplistically considered the result of grinding plate motions, and their true EM nature (solar EM induction triggering lightning from below) has been ignored.

JET STREAMS PRECURSOR ANOMALIES [56]

IEVPC case studies reported in the *New Concepts in Global Tectonics Journal* show many $M \geq 6.0$ earthquake locations were identified with Jet Stream precursors (Fig. 14). In fact, the interruption of velocity flow-lines that cross above an earthquake epicenter occurs 1–70 days prior to the event, with duration 6–12 hours, at ~100 km average distance between Jet Stream's precursor and epicenter [60- Wu, 2015].

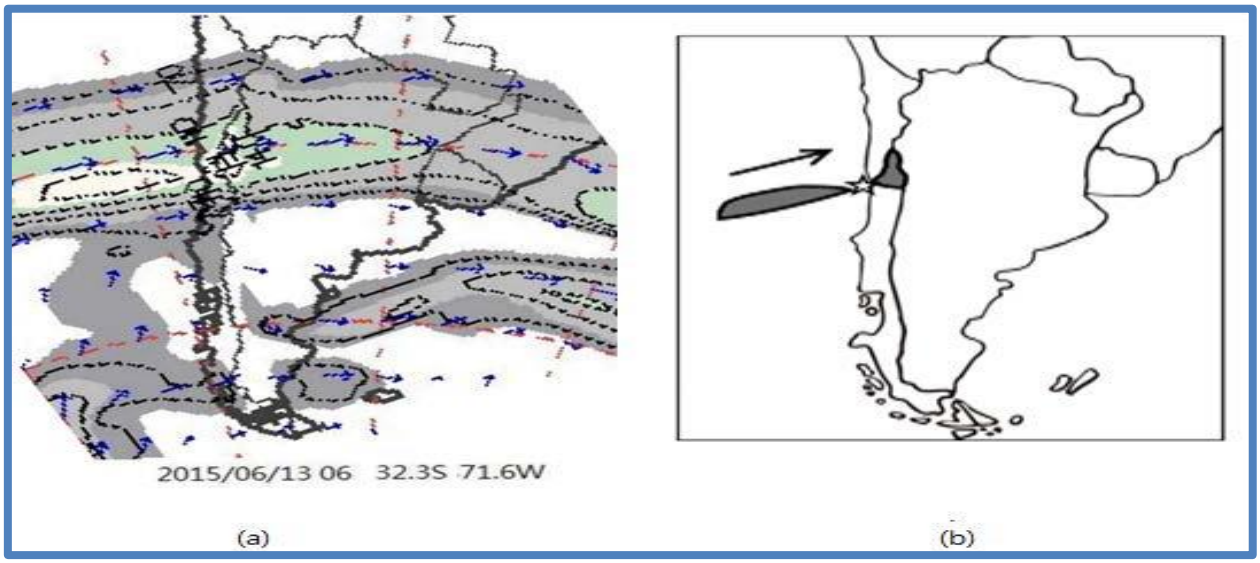

Fig. 14. The anomalous behavior of jet stream: (a) The original jet stream map (S.F. State University), (b) The jet stream at a speed of 130 knots (234km/hour) was interrupted at the epicenter on 13 June 2015 at 06:00 (UTC). The epicenter was located at the interrupted region.

In the past, many scientists around the world have reported the occurrence of atmospheric anomalies prior to earthquakes. Simultaneous analysis of jet-stream maps and 58 earthquake data with M > 6.0 have been made. It has been found that interruption or velocity flow lines cross above an epicenter of earthquake take place 1–70 days prior to event. The duration of this phenomenon was 6–12 hours. The average distance between epicenters and jet stream's precursor was about 36.5 km. In most cases, a satisfactory accuracy was obtained in regard to epicenters with deviations less than 70 km, and narrow time windows. Satellite observation found possible atmospheric disturbances in jet stream velocity before the powerful M = 8.3 Chile Earthquake on 16 Sep. 2015. The jet stream was interrupted at the epicenter on 13 June 2015 at 06:00 UTC (Fig. 14), 96 days prior to the major M = 8.3 Chile Earthquake, and the epicenter deviation was less than 80 km. The prediction posted on 2015/06/14 had the time range from 2015/06/13 to 2015/07/13, in Central Chile at the location (32.3S, 71.6W) and magnitude M > 5.5. The actual event was an M = 8.3 about two months later than predicted on 2015/09/16 - 22:54:33 UTC in Central Chile at location (31.570°S, 71.654°W) at a depth of 25.0 km [60- Wu, 2015]; [61- Wu, et. al, 2015]; [62 & 63- Wu and Tikhonov, 2015a & b].

5. SEISMICITY & TECTONIC FRAMEWORK

The earthquakes occurring in the NMSZ come from a unique tectonic settings. It is strongly related to the global-scale geological structure related to the North-South American Super-anticline (NSAS) that runs from South America, via the Caribbean and Mississippi Valley, to the Canadian Shield (Fig. 15, [64- Choi, 2013a]). It is a fundamental geological structure formed in the early stage of the Earth's formation – in the Archean. There is another antipodal super-anticline that extends from SW Pacific, via SE Asia and South China, to Siberia. These anticlinal structures have influenced the subsequent development of the Earth by repeated magmatic and tectonic activities throughout the Phanerozoic, especially since Mesozoic.

Earthquake and volcanic energies in the Central America come from the outer core under the Caribbean Sea and transmigrate to the Pacific coast through the oceanized horst structures, one of which now forms the Cayman Trough [37- Choi, 2014]. The direction of energy movement is controlled by the level of thermal energy input into the Caribbean dome from the outer core, which is inversely correlated with the solar cycle. During the declining solar cycle, earthquake and volcanic swarms move northward, but during the rising cycle, southward. This energy transmigration cycle pattern explains why the catastrophic New Madrid earthquakes have occurred exclusively during the major solar minimums. Bearing the above in mind, a very strong earthquake in the offshore Caribbean north of Honduras (M = 7.5) along the Cayman Tough on 10 January 2018 caught our attention, because of its possible seismic energy link to the New Madrid Seismic Zone through the (brown lines) NSAS (Fig. 15). This earthquake occurred at the junction of this global-scale NSAS of Archean-origin and the E-W trending Cayman Fault. The seismic energy of this quake is considered to have derived from the outer core through gigantic fracture systems developed in the mantle deep under the Caribbean. [32- Choi et al., 2018].

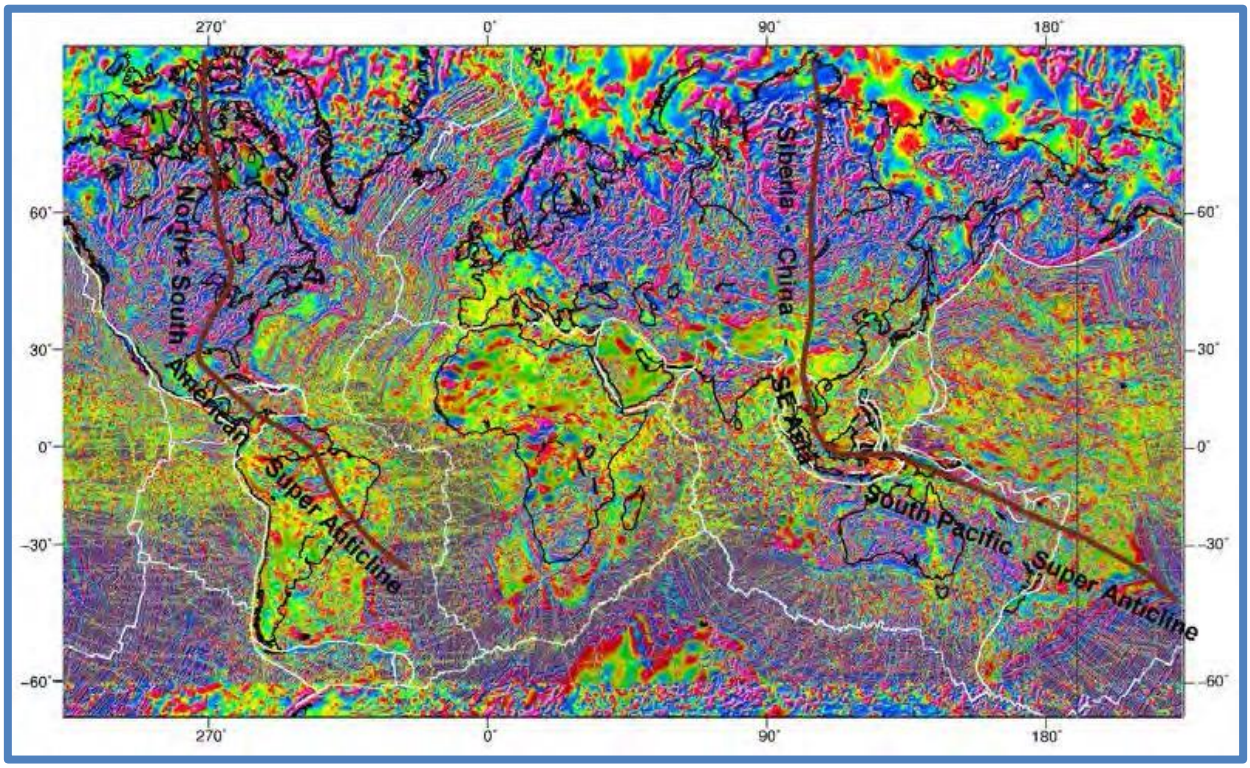

Fig. 15. Antipodal Archean-origin Super-anticlines on the globe [64- Choi, 2013a]; [65- Choi and Kubota, 2015]. These anticlines have been repeatedly reactivated during Proterozoic and Phanerozoic. Note that the Caribbean Sea and the Mississippi Valley are situated on the axis of the anticline. Base map, World magnetic anomaly map, by [66- Korhonen et al., 2007].

Magnetic anomalies (violet and red signatures) of the Precambrian or Archean (Original Crust) trace southward from the Great Lakes and then trend eastward toward the New Madrid Seismic Zone in Fig. 16. These anomalies are generally produced by variations in the distribution of iron minerals, usually magnetite, in the rocks of the Earth's crust. Igneous and metamorphic crystalline rocks can be very magnetic. By comparison, sedimentary rocks are usually nonmagnetic. Magnetic anomalies therefore provide a way of mapping exposed and buried crystalline rocks of these Precambrian rift basin signatures exhibited in eastern North America. Others include: Keweenawan Midcontinent Rift; Fort Wayne Rift; Rough Creek Graben an east–west extension of the Reelfoot Rift; and Cambrian Rome Trough and provide ancient connections to the outer core EM energies stimulated by solar induction.

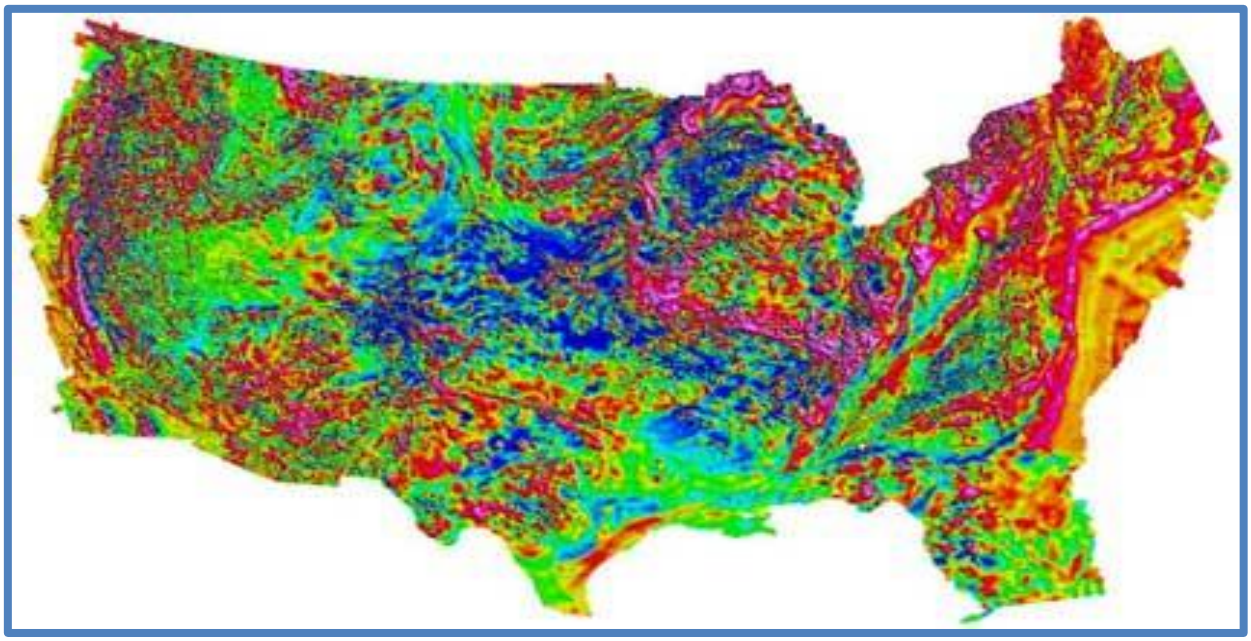

Fig. 16. North American Magnetic Anomaly Map Aeromagnetic compilation of the conterminous United States, updated in 2002. Geological Society of America Committee for the Magnetic Anomaly Map of North America, 1987, Geological Society of America, continent-scale map-003, scale 1:5,000,000, 4 sheets [67- Zietz, I., 1982].

Seismic hazard map of North America (Fig. 17), shows earthquake realtionships to this ancient crystalline Archaen basement rock.

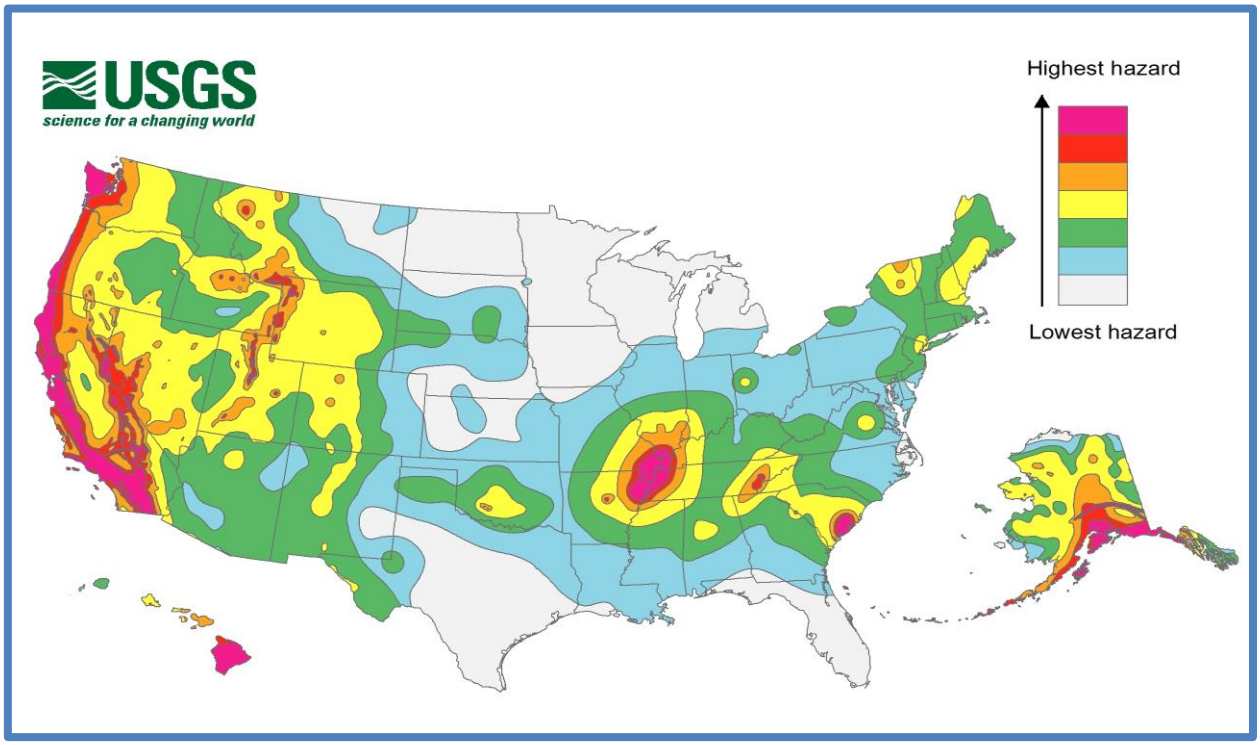

Fig. 17. U.S. Seismic Hazard Map of North America. https://earthquake.usgs.gov/hazards/hazmaps/ Source: USGS

Ongoing seismicity in the southeastern United States, as with intraplate seismicity in general, is not well understood. The area has had significant earthquakes and vaiable seismicity patterns with several moderate to large earthquakes over the past two centuries. Two noteable events include an M = 7 in Charleston, South Carolina in 1886 [68- Chapman et.al., 2016], and an M = 5.8 in the Central Virginia Seismic Zone (CVSZ) in 2011 [69- Wolin et al., 2012]. In addition to the seismicity clusters associated with these large events, other distinct regions of increased seismicity exist in the Eastern Tennessee Seismic Zone (ETSZ) located parallel to the strike of the Appalachian Mountains in eastern Tennessee and westernmost North Carolina [70- Powell and Thomas, 2016]. Ongoing seismicity over much of central and western South Carolina, parts of northern Georgia, and southwestern North Carolina is commonly referred to as the South Carolina Seismic Zone (SCSZ) [71- Li et al., 2007]. In addition, a North-South oriented Marianna fault line in Eastern Arkansas, has produced large magnitude $M \geq 7$ earthquakes in the greater area over several thousand years on more than one occasion. It's had a recent outbreak of earthquakes and is located south of Forrest City (45 miles West of Memphis) striking south to Helena-West Helena, and travels through Lee County, near Marianna. This active fault line has produced magnitude seven earthquakes. Increases in intraplate seismicity along lateral gradients in lithospheric thickness have been observed globally [72- Mooney et al. 2012]. Some contributing factors of intraplate seismicity proposed include: oceanic fracture zones of inherited weakness, thin or weak mantle lithosphere, abrupt changes in lithospheric thickness or strength, presence of terrane boundaries or sutures, presence of increased fluid pore pressure from fluctuations in meteoric water or mantle CO_2 emissions, intersecting fault zones, presence of failed rifts, and faults favorably aligned with the regional stress fields [72- Mooney et al., 2012]; [73- Sykes, 1978]; [74- Babuška et al., 2007]; [75- Talwani, 1988]; [76- Costain, 2008]; [77- Zoback, 1992]; [78- Bartholomew and van Arsdale, 2012]. Interestingly no solar EM induction or joule energy inputs seem to have been proposed for this anomalous seismicity.

An anomaly on the order of 100 × 150 km or less of Eocene volcanics in western Virginia and in the central part of eastern West Virginia, just west of the Central Virginia Seismic Zone (CVSZ) exhibit a notable "earthquake shadow" or gap in observed seismicity relative to surrounding areas [79- Bollinger and Gilbert, 1974]. A very localized low-velocity anomaly directly underlies the Eocene volcanism [80 & 81- Mazza et al., 2014 & 2017] indicating an unknown hypothesized loss of mantle lithosphere during the Eocene, surrounded by otherwise relatively uniform mantle lithosphere. A similar pattern is observed with the Central Virginia Seismic Zone (CVSZ). This cluster, associated with the M = 5.8, 2011 Mineral, Virginia earthquake, is located just east of the low-velocity anomaly that underlies the Eocene volcanoes described earlier. That low-velocity anomaly is, in turn, the location of the seismic shadow first described by [79- Bollinger and Gilbert, 1974]. Almost all previous tomographic inversions that cover the eastern United States show some evidence of reduced seismic velocities in northern Virginia and easternmost West Virginia [82- Biryol et al., 2016]; [83- Pollitz and Mooney, 2016]; [84- Shen and Ritzwoller, 2016]; [85- Buehler and Shearer, 2017]; [86- Burdick et al., 2017]; [87- Savage et al., 2017]. A further question remains about how such a low velocity can be sustained over a period of 48 m.y. A posible explanation is that Eocene joule energy inputs that reduced the seismic velocity in this area by shifting the underlying geochemisty or anistropy, may now be dormant.

Gravity anomalies (Fig. 18) are produced by density variations within the rocks of the Earth's crust and upper mantle. These density variations also trace southward from the Great Lakes a long snake-like gravity feature heading south from the tip of Lake Superior, similar but different than that seen earlier in the magnetic data. Large density signatures in Texas are also connected to the New Madrid Seismic Zone related to the buried presence of the Archean Precambrian crystalline basement or later younger volcanic rock emplacements.

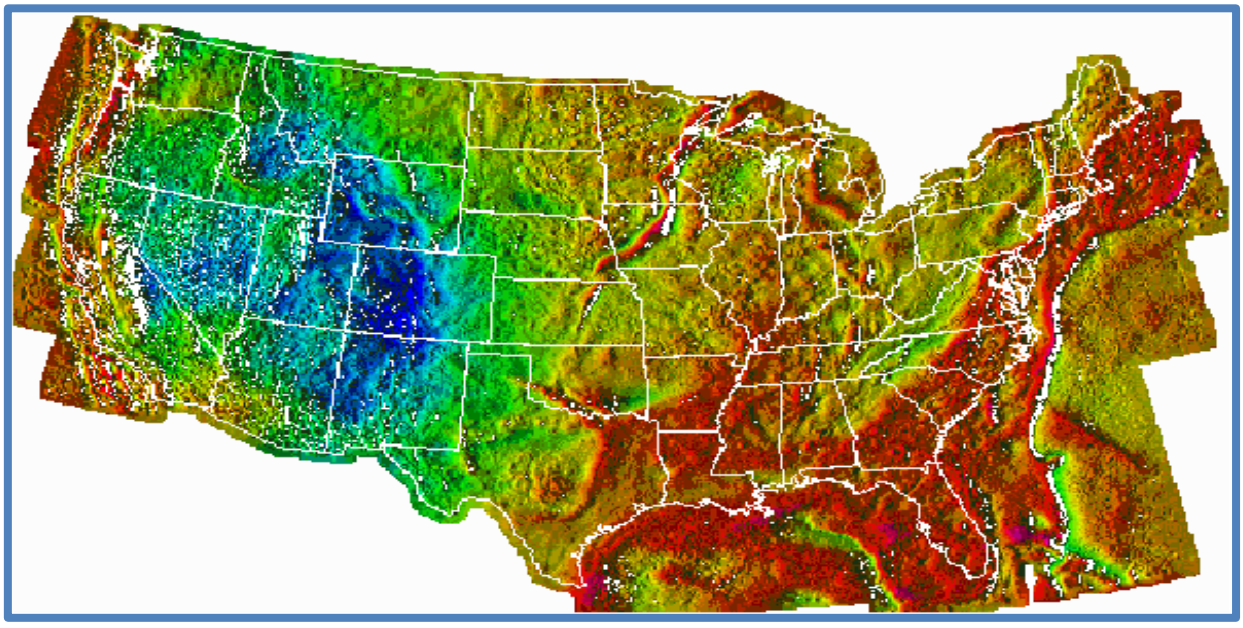

Fig. 18. Bouguer Gravity Anomaly Data Color shaded-relief map showing the complete- for the conterminous United States (onshore) and free-air gravity anomaly data offshore. Red shades indicate areas of high gravity values produced by high average densities in the Earth's crust and upper mantle; blue shades indicate areas of low gravity values produced by low average densities. Illumination is from the west. Source: USGS

A more profound and detailed discussion (Gregori and Leybourne, in preparation) focuses on the general geometrical patterns of deep Earth, including the explanation of the mysterious network of mid-ocean ridges. The result is a perfect deep tetrahedron, and its' observed geometry at the Earth's surface is modified by the sliding of the lithosphere on top the asthenosphere (better known as continental drift). One edge of the tetrahedron runs between California and the North Pole, through the NMSZ, and the Hudson Bay. The relative increase of wildfire, observed roughly along the line between Dallas and Winnipeg (NASA, Earth Observatory), is an index of the expected greater soil exhalation of methane. Also this more precise analysis confirms the concern about the seismicity of the NMSZ during an extreme low solar activity period.

RIFT SEISMIC VELOCITY ANOMALIES

Tomographic images generated from the broadband seismic stations monitoring upper mantle shear-wave velocities from this passive margin setting provides constraints on the evolution of mantle lithosphere [88- Wagner et.al., 2018]. The results suggest that lithospheric mantle continues to evolve in this relatively "stable" continental passive margin setting, being subject to episodes of delamination, foundering, and erosion processes that are still not well understood. The Rome Trough and Reelfoot Rift high-velocity layer is separated from the Moho by 10–20 km. For the Reelfoot Rift the high-velocity layer appears to be deflected downward while maintaining constant thickness beneath the sub-Moho low-velocity layer. In contrast, the high-velocity layer beneath the low velocities that coincide with the Rome Trough does not appear to be deflected downward at all. The reduced sub-Moho velocities are observed in regional surface-wave inversions in the eastern United States [83- Pollitz and Mooney, 2016]; [87- Savage et al., 2017]; [89- Chen et al., 2016]. However, the shallow low-velocity anomalies observed, contrast with the more dramatic and deeper low-velocity structures observed by [89- Chen et al., 2016] beneath the southwestern extension of the Reelfoot Rift. Similarly, the continent-wide tomographic inversion of [85- Buehler and Shearer, 2017] shows reduced uppermost-mantle velocities along the Reelfoot Rift.

Almost all of the earthquakes are related to low velocity lenses, which are underlain by deep fracture systems (expressed as linear fast zones) in the lower mantle. This low velocity layer is ubiquitously observed throughout the globe [90- Choi et al., 2017). Mantle structure of the Caribbean can be understood by analyzing seismo-tomographic images. Several tomographic images were analyzed; [91- Widiyantoro, 1997]; [92- Romanowicz, 2003]; [93- van Benthem et al., 2013]; [94- Ervin and McGinnis, 1975]. Seismo-tomographic images show a conspicuous 400 km wide low velocity lens with two small peaks developed in the axial area of the NSAS at the 400-500 km depth under the Caribbean (Fig. 19). This lens is considered a porous zone filled with electromagnetically charged fluid and gas, which plays a role as an energy transmigration volcanic surge channel. An anomalously low velocity lens is also recognized in the New Madrid Seismic Zone at the 25 to 50 km depth at the top of the

mantle on the axis of the NSAS. These velocity anomaly lenses in these areas seem connected. This volcanic surge channel appears to have repeatedly reactivated since the Proterozoic, which altered the mantle and crustal composition to form collapsed axial structures of the Caribbean dome and the Mississippi Valley. These three tomographic images unequivocally portray the low velocity mantle shallows northward toward the Gulf of Mexico (Fig. 19). This northward shallow extension of the slow mantle seems to continue further north, which is confirmed in velocity/density profile in the New Madrid Seismic Zone at the top of the mantle, 25 to 50 km [94- Ervin and McGinnis, 1975]. This interpretation explains most of the geological/geophysical features of the region and agrees with an in-situ origin of the Caribbean Dome, oceanized since Mesozoic [95 & 96- James, 2016 & 2018]; [97- James et al., 2009] or may go back to Paleozoic time [98 & 99- Pratch, 2008 & 2010].

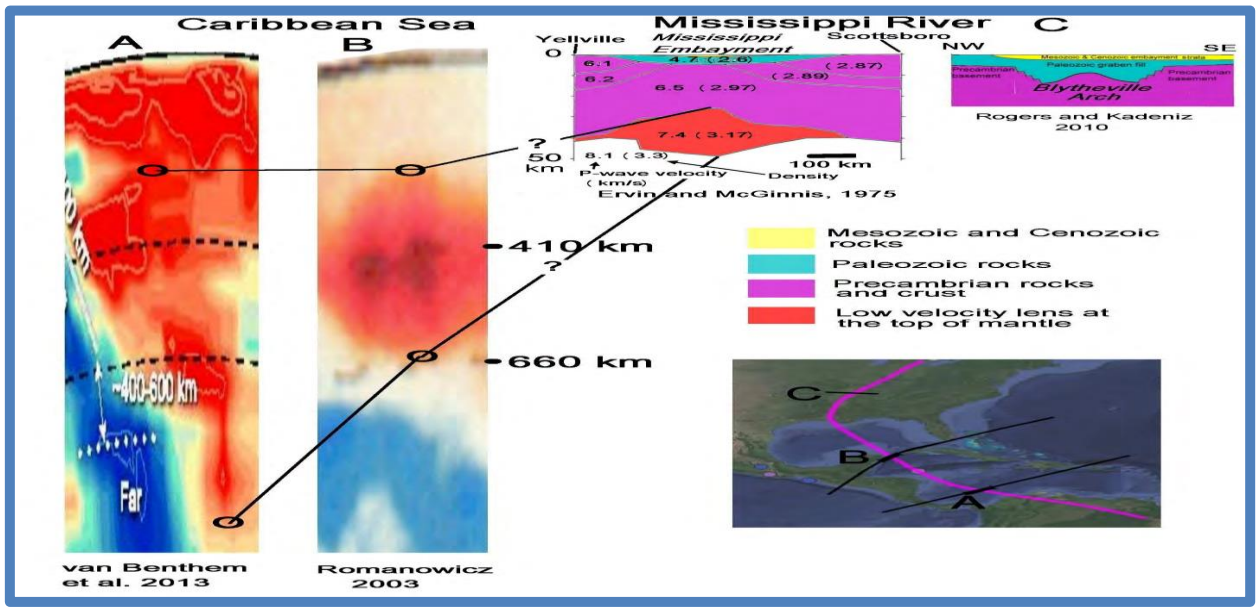

Fig. 19. Low seismic velocity zones in the Caribbean and the Mississippi Valley, composite showing their northward shallowing. The Mississippi Valley profiles indicate that the Valley was formed by an anticlinal structure, which collapsed before the Paleozoic. Note the mantle with decreased velocity and density (7.4/3.17) under the Mississippi Embayment, suggesting that it served as an energy transmigration channel during the time of tectonic activity forming the present-day Mississippi Valley.

Recall the very strong Caribbean (M = 7.5) earthquake along the axis of the North-South American Super-anticline, north of Honduras where it meets with the E-W deep-seated Cayman Fault on 10 January 2018 that caught our attention? It was the second strongest earthquake since 1970 in the Caribbean region; the largest being 7.6 on the Pacific coast in 2012. Note that six out of the eight M = 7.0+ quakes occurred in 2007 or after. The year 2007 is the starting year of the modern Solar Minimum [1- Casey et al., 2016], as previously discussed.

CONCLUSIONS

Since the establishment in 2012, IEVPC has run many test programs to study precursor signals and to establish a geological model that best explains the appearance of precursor signals and earthquakes. Our policy is an open, multi-parameter approach, involving some of the world's best seismologists and geologists. The team has successfully predicted many strong earthquakes, some of which have been published in scientific journals. Most methods have been individually verified as valid for earthquake forecasting. http://www.ievpc.org/earthquake-papers.html.

An effective operative approach to seismic "prediction" management can occur through 4 levels [100, Gregori et al., 2018]. The focus of the present paper is on *level 1* that is aimed to envisage seismicity on the large scale-size and long time-range. *Level 2* is aimed to get a better definition of the hazard both in space and time, by means of a global monitoring of crustal stress, similarly to the planetary monitoring of meteorology in order to forecast weather. *Level 3* is aimed to monitor the evolution of every pre-chosen active fault with the target to forecast a possible seismic shock (location and timing with a 1-2 day advance). *Level 4* is aimed to forecast the timing of a possible (though never certain) shock with the precision of a few minutes.

Many sound reasons support Solar EM induction model for New Madrid seismicity. It relies on realistic consideration of several matters of fact. This paper documented scientific grounds for linking deep geological structure of the Caribbean Sea to its northern area, the New Madrid Seismic Zone. The following points were documented. 1). The latest gigantic earthquake, January 2018 magnitude 7.5 offshore north Honduras, occurred at the junction of one of Earth's most fundamental structures, the North-South American Super-anticline and the E-W Cayman deep fault, recalling the relationships of *Axial vs. Radial induction.* 2). The quake occurred above a major low velocity lens at 400 to 500 km depth, which is considered an energy transmigration volcanic surge channel likely filled with ionized liquid and gas. 3). The low velocity lens shallows northward to Gulf of Mexico and appears to extend to the New Madrid Seismic Zone, where a distinctive low velocity lens is developed at the top of the mantle. 4). Seismic activity has dramatically increased since 1990, especially since 2007. These years are significant, because

the former is the starting year of a one-order longer solar cycle, and the latter the starting year of the current Solar Minimum. 5). A comparison of Central American earthquakes and solar cycle shows that during the declining years of solar cycles, seismic energy transmigrates northward with magnetic polar motions (magnetic moment synchronization also occurs at atomic scales), and during the rising period southward. 6). The above facts explain the damaging New Madrid earthquakes that exclusively occurred during the last four major solar minimums. 7). There are strong scientific grounds to forecast another series of major earthquakes in the New Madrid Seismic Zone during the current solar minimum.

The NMSZ developed on the major Precambrian-origin super-anticline axis where magmatic, thermal, and tectonic activities have been concentrated, particularly since Mesozoic when the Gulf of Mexico and the Caribbean have started to form. This activity is still continuing today. Thus the historic record clearly shows that large seismic events in the NMSZ have occurred during the Sun's inactive periods. The sequence of 1811-12 quakes is only one of them. In the light of the now confirmed start of a prolonged, solar hibernation for the coming 30 years or so, which are comparable to Dalton Minimum or worst case, a Maunder Minimum ("Little Ice Age"), a repeat of the 1811-12 earthquakes should be expected. The window of highest risk for another major New Madrid earthquake extends roughly from 2021 through 2038. Seismic and volcanic activities in the Caribbean may foretell energy release in the New Madrid region with a delay of only a few years. This warning is further emphasized by the fact that earthquake activity has increased dramatically in recent years in the Caribbean, as represented by the M = 7.5 northern offshore Honduras earthquake in January 2018. We consider this gigantic quake is a harbinger of the coming New Madrid quake. Based on IEVPC's innovative electro-dynamic geologic/tectonic model, expanded within a Stellar Transformer framework, understanding of the Earth's interactions with space weather can be improved. This provides an understanding of some common electromagnetic denominators associated with earthquakes.

REFERENCES

[1] Casey, J.L., Choi, D.R., Tsunoda, F. and Humlum, O., 2016. Upheaval! Whey catastrophic earthquakes will soon strike the United States? Trafford Publishing. 332p.

[2] Reimer, P. J., Baillie, M. G. L., Bard, E., Bayliss, A., Beck, J. W., Blackwell, P. G., Bronk Ramsey, C., Buck, C. E., Burr, G. S., Edwards, R. L., Friedrich, M., Grootes, P. M., Guilderson, T. P., Hajdas, I., Heaton, T. J., Hogg, A. G., Hughen, K. A., Kaiser, K. F., Kromer, B., McCormac, F. G., Manning, S. W., Reimer, R. W., Richards, D. A., Southon, J. R., Talamo, S., Turney, C. S. M., van der Plicht, J., & Weyhenmeyer, C. E. (2009). IntCal09 and Marine09 radiocarbon age calibration curves, 0-50,000 years cal BP. *Radiocarbon, 51*(4), 1111-1150.

[3] Blot, C., 1976. Volcanisme et sismicité dans les arcs insulaires. Prévision de ces phénomènes. Géophysique, v. 13, Orstom, Paris, 206p.

[4] Gregori, Giovanni P., 2015c. Migration of foreshocks and/or volcanic eruptions. The "Blot's migration Law", *New Concepts Global Tectonics Journal*, 3, (2), 233-239.

[5] Tsunoda, Fumio, 2009a. Habits of earthquakes – Part 1: Mechanisms of earthquakes and lateral thermal seismic energy transmigration, *New Concepts Global Tectonics Newsletter*, (53), 38-46. (Originally published as Tsunoda, 2009).

[6] Tsunoda, Fumio, 2010. Habits of earthquakes – Part 2: Earthquakes corridors in East Asia, *New Concept Global Tectonics Newslett*er, (54), 45-56.

[7] Tsunoda, Fumio, 2010a. Habits of earthquakes – Part 3: Earthquakes in the Japanese Islands, *New Concepts Global Tectonics Newslett*er, (55), 35-65.

[8] Vikulin, A. V., D. R. Akmanova, S. A. Vikulina, and A. A. Dolgaya, 2012. Migration of seismic and volcanic activity as display of wave geodynamic process, *New Concepts Global Tectonics Newslett*er, (64), 94-110. [with minor modifications after *Geodyn. Tectonophys*., 3, 1-18, 2012].

[9] Choi, D.R., 2017b. The great 17 July 2017 offshore Kamchatka earthquake, its link to deep energy source, and geological significance. NCGT Journal, v. 5, no. 3, p. 379-390.

[10] Benioff, Hugo (1949). "Seismic evidence for the fault origin of oceanic deeps". Bulletin of the Geological Society of America. Geological Society of America. **60 (12)**: 01 Dec., 1949, pp.1837–1866. doi:10.1130/0016-7606(1949)60[1837:seftfo]2.0.co;2.

[11] Holmes, A., 1978. Principles of Physical Geology (3 ed.). Wiley. pp. 640–41. ISBN 978-0-471-07251-5.

[12] Meyerhoff, A.A., Taner, I., Morris, A.E.L., Agocs, W.B., Kamen-Kaye, Bhat, M.I., Smoot, N.C., Choi, D.R. and Meyerhoff-Hull, D. (ed.), 1996. Surge tectonics: a new hypothesis of global geodynamics. Kluwer Academic Publishers, 323p.

[13] Straser, V., Cataldi, D., and Cataldi, G., 2019, Electromagnetic Monitoring of the New Madrid Fault U.S. Area with the RDF – Radio Direction Finding of the Radio Emissions Project, *NCGT Journal*, v. 7, no. 1.

[14] Gregori, G.P., 2002. Galaxy-Sun-Earth relations. *Beiträge zur Geoschichte der Geophysik und Kosmischen Physik*, Band 3, Heft 4, 471p.

[15] Leybourne, B.A., 2018. Stellar Transformer Concepts: Solar Induction Driver of Natural Disasters Forecasting with Geophysical Intelligence, *Journal of Systemics, Cybernetics and Informatics*, Orlando, FL, V. 16, N. 4, pp. 26-37, ISSN: 1690-4524.http://www.iiisci.org/journal/sci/Contents.asp?var=&next=ISS1804 http://www.iiis.org/ViewVideo2018.asp?id=21

[16] Leybourne, B.A., James 'Mick' Davis, Giovanni P. Gregori, John M. Quinn, and N. Christian Smoot, Evolution of Earth as a Stellar Transformer, *New Concepts in Global Tectonics Journal*, V. 5, No. 1, pp. 144-155, March 2017. See: www.iascc.org/the-science

[17] Thornhill, W. and Talbott, D., 2007. ***The Electric Universe***, Mikamar Publishing (May 24, 2007), 132p.

[18] Knudsen, Per, Ole Andersen, Shfaqat Abbas Khan, and Jacob Høyer, Ocean tide effects on *GRACE* gravimetry, 8 p. in *Sideris (2001)*. Sideris, Michel G., (ed.), 2001. Gravity, geoid, and geodynamics 2000, *IAG Symposia*, 123, 398 pp., Springer-Verlag, New York.

[19] Elnashai, A.S., et al., 2009. Impact of New Madrid Seismic Zone earthquakes on the Central USA, volume 1. MAE Center Report No. 09-03, October.

[20] Frankel, A.D., Applegate, D., Tuttle, M.P. and Williams, R.A., 2009. Earthquake hazard in the New Madrid Seismic Zone remains a concern: U.S. Geological Survey Fact Sheet 3071, 2p.

[21] Choi, D.R. and Maslov, L., 2010. Earthquakes and solar activity cycles. NCGT Newsletter, no. 54, p. 36-44.

[22] Gregori, Giovanni P., 2009. The Earth's interior – Myth and science, *New Concepts Global Tect. Newslett*., (53), 57-75.

[23] Clette, F., Svalgaard, L., Vaquero, J.M., Cliver, E.W.: 2014, Revisiting the Sunspot Number. A 400-Year Perspective on the Solar Cycle. Space Sci. Rev., 186, 35. https://doi.org/10.1007/s11214-014-0074-2.

[24] Walker, D.A., 1988. Seismicity of the East Pacific: correlations with the Southern Oscillation Index? *EOS Trans. AGU*. V. 69, p. 857.

[25] Walker, D.A., More evidence indicates link between El Ninos and seismicity. *EOS Trans. AGU.* 76 (33) 1995.

[26] Walker, D.A., 1999. Seismic Predictors of El Nino Revisited. *EOS Trans. AGU*, v. 80, no. 25.

[27] Leybourne, B.A., A tectonic forcing function for climate modeling, *EOS, Transactions, American Geophysical Union, Western Pacific Geophysics Meeting*, 1996, May 28th supplement, #A42A-10.

[28] Leybourne, B.A., and M.B. Adams, El Nino tectonic modulation in the Pacific Basin. *Marine Technology Society Oceans '01 Conference Proceedings,* Honolulu, Hawaii, Nov. 2001.

[29] Casey, J.L., 2008. The existence of 'relational cycles' of solar activity on a multi-decadal to centennial scale, as significant models of climate change on Earth. *Space and Science Research Center, Research Report 1-2008* – The RC Theory. p. 1-8. www.spaceandscience.net

[30] Casey, J.L., 2010. Correlation of solar activity minimums and large magnitude geophysical events. *Space and Science Research Center, Research Report 1-2010* (Preliminary), p. 1-5.

[31] Choi, D.R., Casey, J., Maslov, L. and Tsunoda, F., 2014. Global increase in seismic and magmatic activities since 1990 and their relation to solar cycles. The Global Climate Status Report (GCSR), Edition 2, 2014. Space and Science Research Corporation, p. 7-19.

[32] Choi D.R., Casey, J.L., Leybourne, B.A. and Gregori, G.P., 2018. The January 2018 M7.5 offshore North Honduras earthquake: its possible energy link to the New Madrid Seismic Zone, Mississippi Valley, *New Concepts in Global Tectonics Journal*, Mar. v.6, no. 1, pp. 21-36.

[33] Choi, D.R., 2010. The January 2010 Haiti seismic disaster viewed from the perspective of the energy transmigration concept and block tectonics. NCGT Newsletter, v. 54, p. 36-44.

[34] Tsunoda, F., Dong R. Choi, Kawabe, T., 2013. Thermal energy transmigration and fluctuation. NCGT Journal, v. 1, no. 2, p. 65-80.

[30-35] Choi, D.R. and Tsunoda, F., 2011. Volcanic and seismic activities during the solar hibernation periods. NCGT

Newsletter, no.61, p. 78-87.

[36] Choi, D.R., 2013b. Earthquake/volcanic activities and solar cycles. The Global Climate Status Report. Edition 3–2013, September, p. 10-19. Space and Science Research Corporation. Orlando.

[37] Choi, D.R., 2014. Seismo-volcanic energy propagation trends in the Central America and their relationship to solar cycles. *NCGT Journal*, v. 2, no. 1, p. 19-28.

[38] Straser, V., Cataldi, G. and Cataldi, D., 2015. Radio-anomalies: a tool for earthquake and tsunami forecasts. European Geosciences Union (EGU) General Assembly 2015, Natural Hazard Section (NH5.1), Sea & Ocean Hazard - Tsunami, Geophysical Research Abstract, vol. 17, Vienna, Austria. Harvard-Smithsonian Center for Astrophysics, High Energy Astrophysics Division, SAO/NASA Astrophysics Data System.

[39] Straser, V., Cataldi, G. and Cataldi, D., 2016. SELF and VLF electromagnetic signal variations that preceded the Central Italy earthquake on August 24, 2016. NCGT Journal, vol. 4, no. 3, p. 473-477. Harvard-Smithsonian Center for Astrophysics, High Energy Astrophysics Division, SAO/NASA Astrophysics Data System.

[40] Cataldi, D., Cataldi, G. and Straser, V., 2017. SELF and VLF electromagnetic emissions which preceded the M6.2 Central Italy earthquake that occurred on August 24, 2016. European Geosciences Union (EGU), General Assembly 2017. Seismology (SM1.2)/Natural Hazards (NH4.7)/Tectonics & Structural Geology (TS5.5). The 2016 Central Italy Seismic sequence: overview of data analyses and source models. Geophysical Research Abstracts Vol. 19, EGU2017-3675.

[41] Tsukuda, T., 1992. Sizes and some features of luminous sources associated with the 1995 Hyogo-Ken Nanbu earthquake. *J. Phy. Earth*, v. 45, p. 73-82.

[42] King, C.Y., 1983. Electromagnetic emission before earthquake. *Nature*, v. 301, p. 377.

[43] Lomnitz. C., 1994. Fundamentals of earthquake prediction, 326p. New York, N.Y. Plastino, W., Bella, F., Catalano, P.G. and Giovambattista, R.D., 2002. Radon groundwater anomalies related to the Umbria-Marche Sept. 19, 1997 earthquake. *Geophysics International*, v. 41, p. 369-375.

[44] Plastino, W., Bella, F., Catalano, P.G. and Giovambattista, R.D., 2002. Radon groundwater anomalies related to the Umbria-Marche Sept. 19, 1997 earthquake. Geophysics International, v. 41, p. 369-375.

[45] Qiang, Z.J., Xu, X.D. and Dian, C.D., 1990. Abnormal infrared thermal of satellite forewarning of earthquake. Chinese Sci. Bull., v. 35, p. 1324-1327.

[46] Venkatanathan, N., and Natyaganov, V., 2013. Anomalous Outgoing Longwave Radiation Observations Preliminary Results of September 25, 2013 (M7.0) Peru Earthquake. *New Concepts New Concepts in Global Tectonics Journal*, v. 1, no. 4, p. 5 – 10.

[47] Tronin, A., Hayakawa, M. and Molchanov, O.A., 2002. Thermal IR satellite data application for earthquake research in Japan and China, Journal of Geodynamics, v. 33, p. 519–534.

[48] Saraf, A. K. and Choudhury S., 2005a. NOAA-AVHRR detects thermal anomaly associated with the 26 January, 2001. Bhuj earthquake, Gujarat, India, International Journal of Remote Sensing, v. 26, p. 1065–1073, doi:10.1080/ 01431160310001642368.

[49] Saraf, A.K. and Choudhury S., 2005b. Satellite detects surface thermal anomalies associated with the Algerian earthquakes of May 2003, International Journal of Remote Sensing, v. 26, p. 2705–2713.
doi:10.1080/01431160310001642359.

[50] Ouzounov, D., Bryant, N., Logan, T., Pulinets S. and Taylor P., 2006. Satellite thermal IR phenomena associated with some of the major earthquakes in 1999–2004. *Physics and Chemistry of the Earth*, v. 31, p. 154–163.

[51] Ouzounov, D., Liu, D., Kang, C., Cervone, G., Kafatos, M. and Taylor, P., 2007. Outgoing long wave radiation variability from IR satellite data prior to major earthquakes. *Tectonophysics,* v. 431, p. 211-220.

[52] Oyama, K.–I., Shimoyama, M. and Liu, J.Y., 2011. Possible interaction between thermal electrons and vibrationally excited N2. *Annals Geophysicae*, v. 29, p. 583 – 590.

[53] Jing, F., Shen, X. H., Kang, C. L. and Xiong, P., 2013, Variations of multi-parameter observations in atmosphere related to earthquake. *Natural Hazards Earth System Science*, v. 13, p. 27–33, doi:10.5194/nhess-13-27-2013

[54] Doda, L.N., Dushin, V.R., Natyaganov V.L., Smirnov N.N. and Stepanov, I.V., 2011. Earthquakes forecasts following Space and ground-based monitoring. *Acta Astronautica*, v. 69, nos. 1-2, p. 18-23.

[55] Gruber A. and Krueger A., 1984. The status of the NOAA outgoing long wave radiation dataset. *Bulletin of American Meteorological Society*, v. 65, p. 958–962.

[56] Ouzounov, D., Pulinets, S., Romanov, A., Romanov, A., Tsybulya, K., Davidenko, D., Kafatos, M. and Taylor, P., 2011. Atmosphere-ionosphere response to the M9 Tohoku earthquake revealed by multi-instrument space-borne and ground observations: Preliminary results. *Earthquake Science*, v. 24, no. 6, p. 557-564, DOI: 10.1007/s11589-011-0817-z, ISSN: 1674-4519.

[57] Bapat, A., 2003. Role of Telecom in Seismic Surveillance. Proc. Nat. Sym. On Developments in Geophys. Banaras Hindu Univ., Varanasi, p. 129 – 132.

[58] Rikitake, T., 1984. Earthquake forecasting and warning. D. Riedel Pub. Co., Dordrecht, Boston and London.

[59] Bapat, A., 2005. Learning from Seismic Precursors. The Dawn (Pakistan), 22 Oct. 2005.

[60] Wu, H.C., Anomalies in Jet Streams that Appeared Prior to the 16 September 2015 M8.3 Chile Earthquake, New Concepts in Global Tectonics Journal, V. 3, No. 3, pp. 407-408, September 2015.

[61] Wu, H.C., Tikhonov, I.N. and Cesped, A.R., 2015. Multi-parametric analysis of earthquake precursors. *Russian Journal of Earth Sciences*, v. 15, no. 3. doi:10.2205/2015ES000553, 2015.

[62] Wu, H.C. and Tikhonov, I.N., 2014a. Jet streams anomalies as possible short-term precursors of earthquakes with $MM > 6.0$. *Research in Geophysics*, Special Issue on Earthquake Precursors, v. 4, no. 1, p. 12–18. doi:10.4081/rg.2014.4939.

[63] Wu, H.C. and Tikhonov, I.N., 2014b. The earthquake prediction experiment on the basis of the jet stream's precursor. *2014 AGU Fall Meeting*, NH31A-3844.

[64] Choi, D.R., 2013a. An Archean geanticline stretching from the South Pacific to Siberia. *NCGT Journal*, v. 1, no. 3, p. 45-55.

[65] Choi, D.R. and Kubota, Y., 2015. North-South American Super-Anticline. *NCGT Journal*, v. 3, no. 3, p. 367-377.

[66] Korhonen, J.V., Fairhead, J.D., Hamoudi, M, Hemant, K., Lesur, V., Mandea, M., Maus, S., Purucker, M., Ravat, D., Sazonova, T. and Thebault, E., 2007. Magnetic anomaly map of the World (and associated DVD), Scale, 1:50,000,000, 1st edition, Commission for the Geological Map of the World, Paris, France.

[67] Zietz, I., 1982, Composite magnetic anomaly map of the United States; Part A, Conterminous United States: U.S. Geological Survey Investigations Map GP-954-A, 59 pp., 2 sheets, scale 1:2,500,000.

[68] Chapman, M.C., Beale, J.N., Hardy, A.C., and Wu, Q., 2016, Modern seismicity and the fault reponsible for the 1886 Charleston, South Carolina, Earthquake: Bulletin of the Seismological Society of America, v. 106, no. 2, https://doi.org/10.1785/0120150221.

[69] Wolin, E., Stein, S., Pazzaglia, F., Meltzer, A., Kafka, A., and Berti, C., 2012, Mineral Virginia, earthquake illustrates seismicity of a passive-aggressive margin: Geophysical Research Letters, v. 39, no. 2, 7 p., https://doi.org/10.1029/2011GL050310.

[70] Powell, C.A., and Thomas, W.A., 2016, Grenville basement structures associated with the Eastern Tennessee seismic zone, southeastern USA: Geology, v. 44, p. 39–42, https://doi.org/10.1130 /G37269.1.

[71] Li, Q., Liu, M., Zhang, Q., and Sandvol, E., 2007, Stress evolution and seismicity in the central-eastern United States: Insights from geodynamic modeling: Geological Society of America Special Paper 425, p. 149–166, doi:10.1130/2007.2425(11).

[72] Mooney, W.D., Ritsema, J., and Hwang, Y.K., 2012, Crustal seismicity and the earthquake catalog maximum moment magnitude (Mcmax) in stable continental regions (SCRs): Correlation with the seismic velocity of the lithosphere: Earth and Planetary Science Letters, v. 357–358, p. 78–83, https://doi.org/10.1016/j.epsl.2012.08.032.

[73] Sykes, L.R., 1978, Intraplate seismicity, reactivation of preexisting zones of weakness, alkaline magmatism, and other tectonism postdating continental fragmentation: Reviews of Geophysics, v. 16, no. 4, p. 621–688, https://doi.org/10.1029/RG016i004p00621.

[74] Babuška, V., Plomerova, J., and Fischer, T., 2007, Intraplate seismicity in the western Bohemian Massif (central Europe): A possible correlation with a paleoplate junction: Journal of Geody- namics, v. 44, p. 149–159, https://doi.org/10.1016/j.jog.2007.02.004.

[75] Talwani, P., 1988, The intersection model for intraplate earthquakes: Seismological Research Letters, v. 59, p. 305–310.

[76] Costain, J.K., 2008, Intraplate seismicity, hydroseismicity, and predictions in hindsight: Seismological Research Letters, v. 79, no. 4, p. 578–589, https://doi.org/10.1785/gssrl.79.4.578.

[77] Zoback, M.L., 1992, Stress field constraints on intraplate seismicity in eastern North America: Jour- nal of Geophysical Research, v. 97, no. B8, p. 11,761–11,782, https://doi.org/10.1029/92JB00221.

[78] Bartholomew, M.J., and van Arsdale, R.B., 2012, Structural controls on intraplate earthquakes in the eastern United States, *in* Cox, R.T., Tuttle, M.P., Boyd, O.S., and Locat, J., eds., Recent Advances in North American Paleoseismology and Neotectonics East of the Rockies: Geo- logical Society of America Special Paper 493, p. 165–189.

[79] Bollinger, G.A., and Gilbert, M.C., 1974, A reconnaissance microearthquake survey of the Hot Springs, Virginia area: Bulletin of the Seismological Society of America, v. 64, p. 1715–1720. Bonini, W.E., and Woollard, G.P., 1960, Subsurface geology of North Carolina–South Carolina coastal plain from seismic data: American Association of Petroleum Geologists Bulletin, v. 44, no. 3, p. 298–315.

[80] Mazza, S.E., Gazel, E., Johnson, E.A., Kunk, M.J., McAleer, R., Spotila, J.A., Bizimis, M., and Cole- man, D.S., 2014, Volcanoes of the passive margin: The youngest magmatic event in eastern North America: Geology, v. 42, p. 483–486, https://doi.org/10.1130/G35407.1.

[81] Mazza, S.E., Gazel, E., Johnson, E.A., Bizimis, M., McAleer, R., and Biryol, B., 2017, Post-rift magmatic evolution of the eastern North American “passive-aggressive” margin: Geochemistry, Geophysics, Geosystems, v. 18, no. 1, p. 3–22. https://doi.org/10.1002/2016GC006646.

[82] Biryol, C.B., Wagner, L.S., Fischer, K.M., and Hawman, R.B., 2016, Relationship between observed upper mantle structures and recent tectonic activity across the southeastern United States: Journal of Geophysical Research, v. 121, p. 3393–3414.

[83] Pollitz, F.F., and Mooney, W.D., 2016, Seismic velocity structure of the crust and shallow mantle of the Central and Eastern United States by seismic surface wave imaging: Geophysical Research Letters, v. 43, p. 118–126, https://doi.org/10.1002/2015GL066637.

[84] Shen, W., and Ritzwoller, M.H., 2016, Crustal and uppermost mantle structure beneath the United States: Journal of Geophysical Research, v. 121, p. 4306–4342, https://doi.org/10.1002/2016JB012887.

[85] Buehler, J.S., and Shearer, P.M., 2017, Uppermost mantle seismic velocity structure beneath US Array, Journal of Geophysical Research, v. 122, p. 436–448, https://doi.org/10.1002/2016JB013265.

[86] Burdick, S., Vernon, F.L., Martynov, V., Eakins, J., Cox, T., Tytell, J., Mulder, T., White, M.C., Astiz, L., Pavlis, G.L., and van der Hilst, R.D., 2017, Model Update May 2016: Upper-Mantle Hetero- geneity beneath North America from Travel-Time Tomography with Global and US Array Data: Seismological Research Letters, v. 88, p. 319–325, https://doi.org/10.1785/0220160186.

[87] Savage, B., Covellone, B.M., and Shen, Y., 2017, Wave speed structure of the eastern North American margin: Earth and Planetary Science Letters, v. 459, p. 394–405, https://doi.org/10.1016 /j.epsl.2016.11.028.

[88] Wagner, L.S., Fischer, K.M., Hawman, R., Hopper, E., and Howell, D., Lithospheric evolution in the southeastern United States, *Geosphere*; 14 (4): 1385–1410. 17 May 2018. doi: https://doi.org/10.1130/GES01593.1

[89] Chen, C., Gilbert, H., Andronicos, C., Hamburger, M.W., Larson, T., Marshak, S., Pavlis, G.L., and Yang, X., 2016, Shear velocity structure beneath the central United States: Implications for the origin of the Illinois Basin and intraplate seismicity: Geochemistry Geophysics Geosystems, v. 17, p. 1020–1041. https://doi.org/10.1002/2015GC006206.

[90] Choi, D.R., Tsunoda, F. and Kawabe, T., 2017. Thermal structure of the Earth’s mantle: Part 1. Pacific Ocean Sector. NCGT Journal, v. 5, no. 4, p. 512-521.

[91] Widiyantoro, S., 1997. Studies of seismic tomography on regional and global scale. Ph.D. Thesis, Australian National University, Canberra, Australia.

[92] Romanowicz, B., 2003. Global mantle tomography: progress status in the past 10 years. Annu. Rev. Earth Planet. Sci., v. 31, p. 303-328. doi:10,1146/annurev.earth.31.091602.113555.

[93] van Benthem, S., Govers, R., Spakman, W. and Rinus Wortel, R., 2013. Tectonic evolution and mantle structure of the Caribbean. Jour. Geophys. Research, Solid Earth, v. 118, p. 3019-3036. doi: 10.1002/jgrb.50235, 2013.

[94] Ervin, C. P., and L. D. McGinnis, 1975. Reelfoot Rift: Reactivated precursor to the Mississippi embayment, Bull. Geol. Soc. Am., 86, 1287–1295.

[95] James, K., 2016. Middle America: Intra-continental extension along ancient structures. NCGT Journal, v. 4, no. 3, p. 518-521.

[96] James, K., 2018. Not written in stone. AAPG Explorer, February 2018, p. 18-19 & 22-23.

[97] James, K., Lorente, M. and Pindell, J. (eds.), 2009. The origin and evolution of the Caribbean plate. Geol. Soc. London Spec. Pub. 328, ISBN978-1-86239-288-5.

[98] Pratsch, J.C., 2008. Letter to the Editor. NCGT Newsletter, no. 47, p. 4.

[99] Pratsch, J.C., 2010. Gulf of Mexico Basin – a collapsed Late Carboniferous mantle dome? NCGT Newsletter, no. 55, p. 74-76.

[100] Gregori, Giovanni P., Bruce Leybourne, and Louis A. G. Hissink, 2018. Natural “catastrophes”: “forecast” and management deontological obligation and common sense, *New Concepts Global Tectonics Journal*, 6, (3), 327-346.

EARTHQUAKES OF 1811-1812

Source: New Madrid Tourist Information Missouri, USA. Abridged from Seismicity of the United States, 1568-1989 (Revised), by Carl W. Stover and Jerry L. Coffman, U.S. Geological Survey Professional Paper 1527, United States Government Printing Office, Washington: 1993.

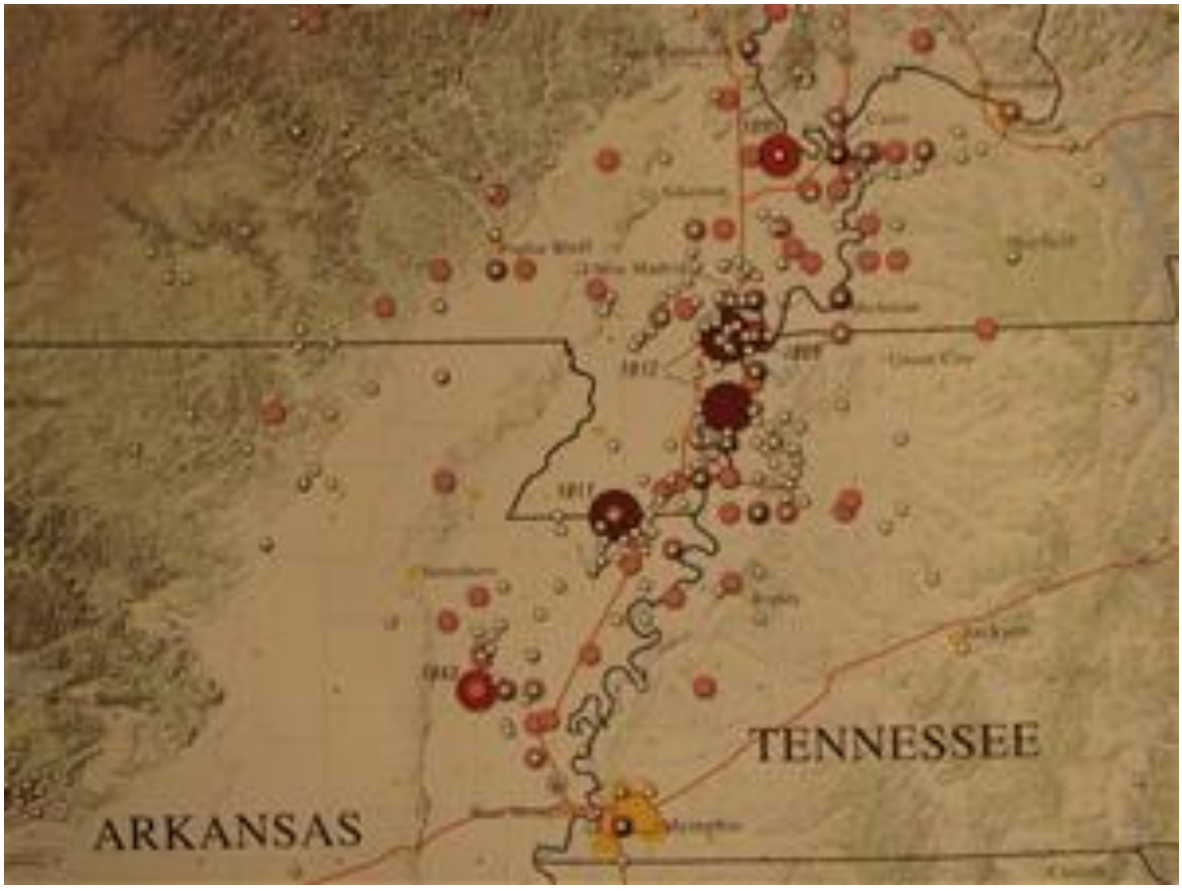

Figure 1 : *1811, December 16, 08:15 UTC. Northeast Arkansas Magnitude ~7.2 - 8.1*

On the basis of the large area of damage (600,000 square kilometers), the widespread area of perceptibility (5,000,000 square kilometers), and the complex physiographic changes that occurred, the Mississippi River valley earthquakes of 1811-1812 rank as some of the largest in the United States since its settlement by Europeans. The area of strong shaking associated with these shocks is two to three times larger than that of the 1964 Alaska earthquake and 10 times larger than that of the 1906 San Francisco earthquake.

The magnitude of these series of earthquakes, usually named the New Madrid, Missouri, earthquakes, vary considerably between the mb and MS values estimated by Nuttli. The mb was estimated from isoseismal maps, and the MS was estimated from a spectral scaling relation by Nuttli for mid-plate earthquakes. The value of MS magnitude has a functional relationship to the mb. The authors have chosen to include the Mfa magnitude because it was estimated from isoseismal maps, as were most of the historical earthquakes.

The first and second earthquakes occurred in Arkansas (December 16, 1811 - two shocks - Mfa 7.2, MSn 8.5 and Mfa 7.0, MSn 8.0) and the third and fourth in Missouri (January 23, 1812, Mfa 7.1, MSn 8.4; and February 7, 1812, Mfa 7.4, MSn 8.8). Otto Nuttli, however, has postulated another strong earthquake in Arkansas on December 16 at 18 UTC (MSn 8.0). This would make a total of five earthquakes of magnitude MSn 8.0 or higher occurring in the period December 16, 1811 through February 7, 1812.

THE FIRST EARTHQUAKE

The first earthquake caused only slight damage to man-made structures, mainly because of the sparse population in the epicentral area. The extent of the area that experienced damaging earth motion (MM intensity greater than or equal to VII) is estimated to be 600,000 square kilometers. However, shaking strong enough to alarm the general population (MM intensity greater than or equal to V) occurred over an area of 2.5 million square kilometers.

At the onset of the earthquake the ground rose and fell - bending the trees until their branches intertwined and opening deep cracks in the ground. Landslides swept down the steeper bluffs and hillslides; large areas of land were uplifted; and still larger areas sank and were covered with water that emerged through fissures or craterlets. Huge waves on the Mississippi River overwhelmed many boats and washed others high on the shore. High banks caved and collapsed into the river; sand bars and points of islands gave way; whole islands disappeared. Surface rupturing did not occur, however. The region most seriously affected was characterized by raised or sunken lands, fissures, sinks, sand blows, and large landslides that covered an area of 78,000 - 129,000 square kilometers, extending from Cairo, Illinois, to Memphis, Tennessee, and from Crowleys Ridge to Chickasaw Bluffs, Tennessee.

Although the motion during the first shock was violent at New Madrid, Missouri, it was not as heavy and destructive as that caused by two aftershocks about six hours later. Only one life was lost in falling buildings at New Madrid, but chimneys were toppled and log cabins were thrown down as far distant as Cincinnati, Ohio; St. Louis, Missouri; and in many places in Kentucky, Missouri, and Tennessee.

The Lake County uplift, about 50 kilometers long and 23 kilometers wide, upwarps the Mississippi River valley as much as 10 meters in parts of southwest Kentucky, southeast Missouri, and northwest Tennessee. The uplift apparently resulted from vertical movement along several, ancient, subsurface structures; most of this uplift has occurred during earthquakes. The Lake County uplift can be subdivided into several topographic bulges, including Tiptonville dome, Ridgely Ridge, and the south end of Sikeston Ridge. A strong correlation exists between modern seismicity and the uplift, indicating that stresses that produced the uplift still exist today.

TIPTONVILLE DOME

Tiptonville dome, which is 14 kilometers in width and about 11 kilometers in length, shows the largest upwarping and the highest topographic relief on the uplift. It is bounded on the east by Reelfoot scarp, which has a zone of normal faults (displacement about three meters) at its base. Although most of Tiptonville dome formed between 200 and 2,000 years ago,

additional uplifting deformed the northwest and southeast parts of the dome during the earthquakes of 1811-1812.

A notable area of subsidence is Reelfoot Lake in Tennessee, just east of Tiptonville dome. Subsidence there ranged from 1.5 to six meters, although larger amounts were reported. It may be that the lake was enlarged by compaction, upwarping, and subsidence occurring simultaneously during the New Madrid earthquakes.

Other areas subsided by as much as 5 meters, although 1.5 to 2.5 meters was more common. Lake St. Francis, in eastern Arkansas, which was formed by subsidence, is 64 kilometers long by 1 kilometer wide. Coal and sand were ejected from fissures in the swamp land adjacent to the St. Francis River, and the water level is reported to have risen there by eight to nine meters.

Large waves were generated on the Mississippi River by fissures opening and closing below the surface. Local uplifts of the ground and water waves moving upstream gave the illusion that the river was flowing upstream. Ponds of water also were agitated noticeably.

Otto Nuttli reported that more than 200 moderate to large earthquakes occurred on the New Madrid fault between December 16, 1811, and March 15, 1812 (5 of MS about 7.7; 10 of MS about 6.7; 35 of MS about 5.9; 65 of MS about 5.3; and 89 of MS about 4.3). Nuttli also noted that about 1,800 earthquakes of mb about 3.0 to 4.5 occurred in that same period.

1811, DECEMBER 16, 14:15 UTC, NORTHEAST ARKANSAS

On the basis of the effects reported at the same locations, the MM intensity of this earthquake has been inferred to be similar to that of the earlier shock at 08:15 UTC (see description above). Thus, the inference is that, if the documented intensities are the same or are similar at identical locations, then the maximum intensities at the epicenter must be about the same; therefore, the intensity at the epicenter of this earthquake must be at the MM intensity X-XI level. The maximum documented intensity for both earthquakes on December 16, 1811, is MM intensity VIII at Richmond, Kentucky.

1812, JANUARY 23, 15:00 UTC, NEW MADRID, MISSOURI MAGNITUDE ~7.0 - 7.8

This is the third principal shock of the 1811-1812 sequence. The first earthquake of this series on December 16, 1811, was located in northeast Arkansas. It is difficult to assign intensities to the principal shocks that occurred after 1811 because many of the published accounts describe the cumulative effects of all the earthquakes. Using the December 16 earthquake as a standard, however, a comparison between it and the shock on January 23 indicates that the intensities were about equal at similar locations. The meizoseismal area was characterized by general ground warping, ejections, fissuring, severe landslides, and caving of stream banks.

1812, FEBRUARY 7, 09:45 UTC, NEW MADRID, MISSOURI MAGNITUDE ~7.4 - 8.0

This is the fourth earthquake of the 1811-1812 series. Several destructive shocks occurred on February 7, the last of which equaled or surpassed the magnitude of any previous event. The town of New Madrid was destroyed. At St. Louis, many houses were damaged severely and their chimneys were thrown down. The meizoseismal area was characterized by general ground warping, ejections, fissuring, severe landslides, and caving of stream banks.

STRANGE HAPPENINGS DURING THE EARTHQUAKES

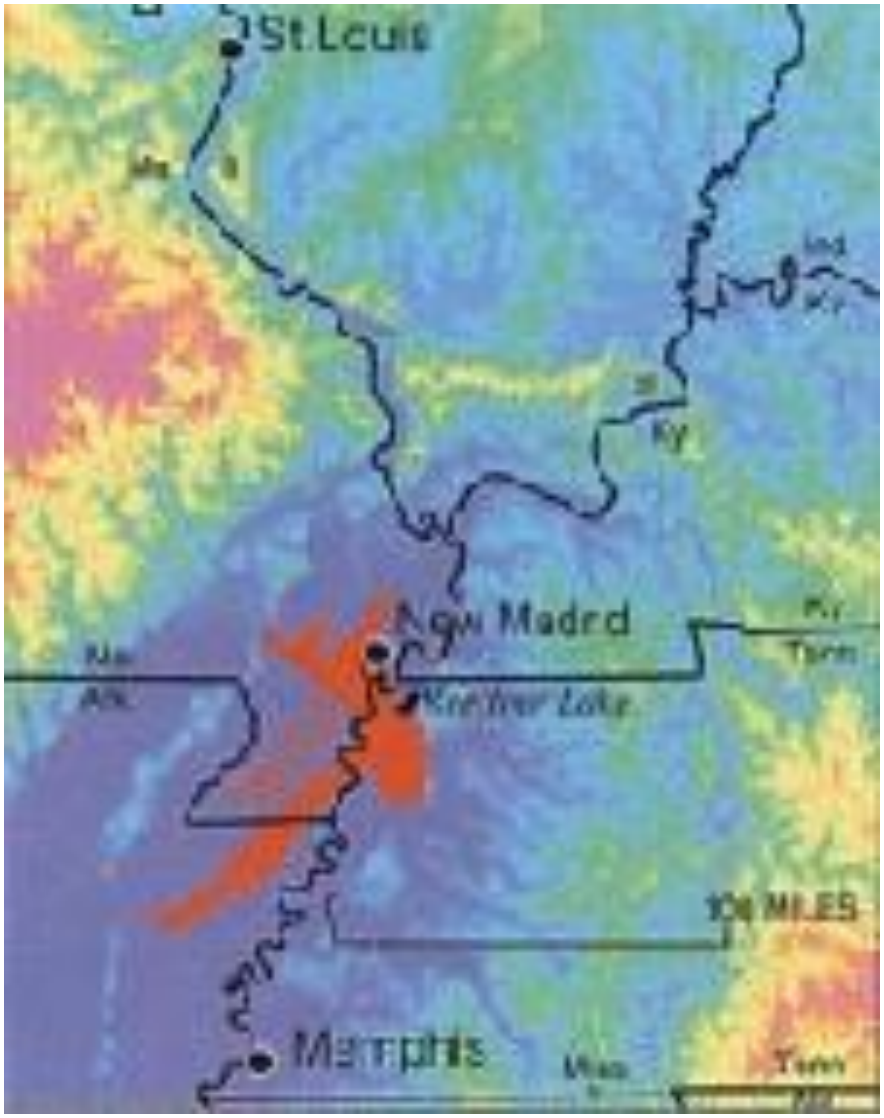

STRANGE HAPPENINGS

The New Madrid earthquakes were the biggest earthquakes in American history. They occurred in the central Mississippi Valley, but were felt as far away as New York City, Boston, Montreal, and Washington D.C. President James Madison and his wife Dolly felt them in the White House. Church bells rang in Boston. From December 16, 1811 through March of 1812 there were over 2,000 earthquakes in the central Midwest, and between 6,000-10,000

earthquakes in the Bootheel of Missouri where New Madrid is located near the junction of the Ohio and Mississippi Rivers.

In the known history of the world, no other earthquakes have lasted so long or produced so much evidence of damage as the New Madrid earthquakes. Three of the earthquakes are on the list of America's top earthquakes: the first one on December 16, 1811, a magnitude of 8.1 on the Richter scale; the second on January 23, 1812, at 7.8; and the third on February 7, 1812, at as much as 8.8 magnitude.

THE MISSISSIPPI RAN BACKWARDS

After the February 7 earthquake, boatmen reported that the Mississippi actually ran backwards for several hours. The force of the land upheaval 15 miles south of New Madrid created Reelfoot Lake, drowned the inhabitants of an Indian village; turned the river against itself to flow backwards; devastated thousands of acres of virgin forest; and created two temporary waterfalls in the Mississippi. Boatmen on flatboats actually survived this experience and lived to tell the tale.

GETTING OVER CRACKS

As the general area experienced more than 2,000 earthquakes in five months, people discovered that most of crevices opening up during an earthquake ran from north to south, and when the earth began moving, they would chop down trees in an east- west direction and hold on using the tree as a bridge. There were "missing people" who were most likely swallowed up by the earth. Some earthquake fissures were as long as five miles.

EARTHQUAKE PHENOMENA

Sand Boils

The world's largest sand boil was created by the New Madrid earthquake. It is 1.4 miles long and 136 acres in extent, located in the Bootheel of Missouri, about eight miles west of Hayti, Missouri. Locals call it "The Beach." Other, much smaller, sand boils are found throughout the area.

Seismic Tar Balls

Small pellets up to golf ball sized tar balls are found in sand boils and fissures. They are petroleum that has been solidified, or "petroliferous nodules."

Earthquake Lights

Lights flashed from the ground, caused by quartz crystals being squeezed. The phenomena is called "seismoluminescence."

Warm Water

Water thrown up by an earthquake was lukewarm. It is speculated that the shaking caused the water to heat up and/or quartz light heated the water.

Earthquake Smog

The skies turned dark during the earthquakes, so dark that lighted lamps didn't help. The air

smelled bad, and it was hard to breathe. It is speculated that it was smog containing dust particles caused by the eruption of warm water into cold air.

Loud Thunder
Sounds of distant thunder and loud explosions accompanied the earthquakes.

Animal Warnings
People reported strange behavior by animals before the earthquakes. They were nervous and excited. Domestic animals became wild, and wild animals became tame. Snakes came out of the ground from hibernation. Flocks of ducks and geese landed near people.

TECUMSEH'S COMET AND THE BATTLE OF TIPPECANOE

The earthquakes were preceded by the appearance of a great comet, which was visible around the globe for seventeen months, and was at its brightest during the earthquakes. The comet, with an orbit of 3,065 years, was last seen during the time of Ramses II in Egypt. In 1811-1812, it was called "Tecumseh's Comet" (or "Napoleon's Comet" in Europe). Tecumseh was a Shawnee Indian leader whose name meant "Shooting Star" or "He who walks across the sky." He was given this name at birth. A great orator and military leader, Tecumseh organized a confederation of Indian tribes to oppose the takeover of three million acres of Indian lands, which were obtained by the Treaty of Fort Wayne in 1809. His brother, a religious leader called "The Prophet," had gained fame when he foretold the total eclipse of the sun on June 16, 1806. (They had learned about it in advance from a team of visiting astronomers.) During this time, the Governor of Indiana Territory William Henry Harrison--worried about The Prophet's popularity--had challenged him to produce a miracle. After the day of the "Black Sun" the brothers had no trouble attracting followers. A Black Sun was said to predict a future war. On September 17, 1811 there was another solar eclipse—which, again, was predicted by The Prophet. The brothers' center of operations was at Prophet's Town, located near the junction of the Wabash and Tippecanoe Rivers in northern Indiana. Tecumseh was traveling and recruiting warriors among the southeastern tribes, when Governor Harrison attacked Prophet's Town with over a 1,000 men on November 6, 1811, a pre-emptive strike by the U. S., which marked the beginning of "Tecumseh's War." On December 16, when the earthquakes began, Tecumseh was at the Shawnee and Delaware Indian villages near Cape Girardeau, 50 miles north of the epicenter at New Madrid.

The earthquakes continued as he traveled back to Prophet's Town, arriving there in February, 1812. Tecumseh's followers lost the Battle of Tippecanoe, but they continued to fight as allies of the British during the War of 1812 between the United States and Great Britain. Tecumseh was killed in battle in Canada in 1813. He is honored as one of the greatest of Indian leaders, both in the United States, and in Canada, where he is considered a national hero.

THE FIRST STEAMBOAT ON THE WESTERN WATERS SURVIVED THE EARTHQUAKES

The first steamboat travel on the Ohio and Mississippi Rivers took place during the New Madrid earthquakes. The New Orleans set out from Pittsburgh on October 20, 1811, bound for New Orleans. Captain Nicholas Roosevelt had brought along his young wife, their two year old daughter, and a Labrador dog. Ten days after leaving Pittsburgh, his wife Lydia gave birth to a son in Louisville, Kentucky. They waited a while for her to recover, and for the water to rise prior to crossing the dangerous waters and coral reef at the Falls of the Ohio. On the night before the day of the earthquake, December 16, the steamboat was anchored near Owensboro, Kentucky, about 200 miles east of New Madrid, Missouri. Their dog, Tiger, insisted on staying in the cabin with them instead of sleeping on the deck.

Without realizing it, they were heading straight towards the epicenter of the greatest earthquake in American history. Their steamboat, intended to be an advertisement for steam travel, was thought instead to be the cause of the earthquake by many who saw it. At Henderson, Kentucky, where no chimneys were left standing, they stopped to visit their friends, the painter John James Audubon and his wife Lucy. Floating in the middle of the Ohio River they were protected from the earthquake tremors shaking the land, but not from the hazards of falling trees, disappearing islands, and collapsing river banks. After entering Indian Territory on December 18th, they were chased by Indians who figured the "fire canoe" had caused the earthquake, but they managed to escape capture by outrunning them. They even had a small cabin fire that night which they managed to put out.

Thousands of trees were floating on the waters of the Mississippi as they approached New Madrid on December 19th, three days after the earthquake. They found that the town of New Madrid had been destroyed. They didn't dare to stop and pick up a few survivors, for fear of being overrun, and they were without supplies. Most alarming was the fact that they had not seen a boat ascending the river in three days. They saw wrecked and abandoned boats. It was undoubtedly a miracle that they survived and kept on going. They tied up at one island, and the island sank during the night. Their dog, Tiger, alerted them to oncoming tremors. On December 22, they encountered the British naturalist John Bradbury on a boat at the mouth of the St. Francis River, who told them the town of Big Prairie was gone.

They arrived at Natchez, Mississippi on December 30 and celebrated the first marriage aboard a steamboat on December 31st, when the steamboat engineer married Lydia's maid. They arrived at New Orleans on January 10, 1812, safe and sound, after traveling 1,900 miles from Pittsburgh on the first steamboat to travel the western waters.

ESSAYS ON GLOBAL TECTONICS

ESSAY #4 EARTHQUAKES: ANALYSIS & PREDICTION

P.M. JAMES

There is a long history of fanciful origins for Earthquakes. In the Caucasus, the Earth was believed to be supported on bovine horns and earthquakes occurred when the bull shook its head. In Mexico, a jaguar got the blame. In Ancient Greece earthquakes and volcanoes occurred when the Titans – who had been imprisoned underground by the father of Zeus – became restless and breathed out fire. Poseidon was also called the Earth Shaker, probably because events in his domain produced tsunamis.

Such ideas have not been easily dispelled. In post-Renaissance times, the earthquake that levelled much of Lisbon in 1755 was claimed to be the deity's punishment for the sin and wickedness in that city, even though it occurred on a Holy Day so that most of the "executed" were worshippers in the Destroyer's Houses of Worship - a bit inconsiderate. In today's world, fanciful causes of this type are still alive and well, particularly in the area of earthquake prediction where even earth scientists have been known to put their money on things like the behaviour of chooks and dogs. Music hall actors might have warned them that reliance on animals, on the stage, usually resulted in downfalls and the same would probably apply in the case of earthquake predictions. Although animals might register something unusual, they are unable to relay to humans the epicentre, depth, and magnitude of an imminent event. More recently, electromagnetic responses have been studied with some correlations looking promising. But, again, there is often a lack of consistency in relation to the time, the depth and the magnitude of the coming event. Which is the sort of thing the public would obviously like to know.

This all led Charles Richter to state in the 1980s, that only fools and charlatans try to predict earthquakes. Well, as shall be outlined below, this is no longer necessarily the situation and so what might change in the Richter statement is that the fools and charlatans are those seeking solutions in erudite or disparate correlations, and hoping to get lucky. I say this because most failures in nature provide some form of early warning behaviour. It would therefore appear to be vital to understand, first and foremost, the mechanisms of earthquakes if one is to develop any realistic prognosis regarding the time of shallow failures, which are the most damaging.

As a starting point, we might look at the patterns exhibited by earthquakes at all depths in the oceanic regimes around the Pacific margin. **Figure** 1 provides the common pattern. The deepest activity on record is at around the 600 to 700 km mark, roughly commencing at what has been defined as the boundary between the Lower Mantle and Upper Mantle. Events follow in the Upper Mantle with a vertical orientation and, incidentally, one that indicates evidence of structure at these deep levels. Further illustrations of this are given a little later. Above the deep earthquake zone(s) there is sometimes an aseismic zone, this zone generally spanning the 400 km depth range and if anyone could explain this, it would be a great achievement. Proceeding further upwards, the next onset of activity is to be found along the Benioff- Watada Zones.

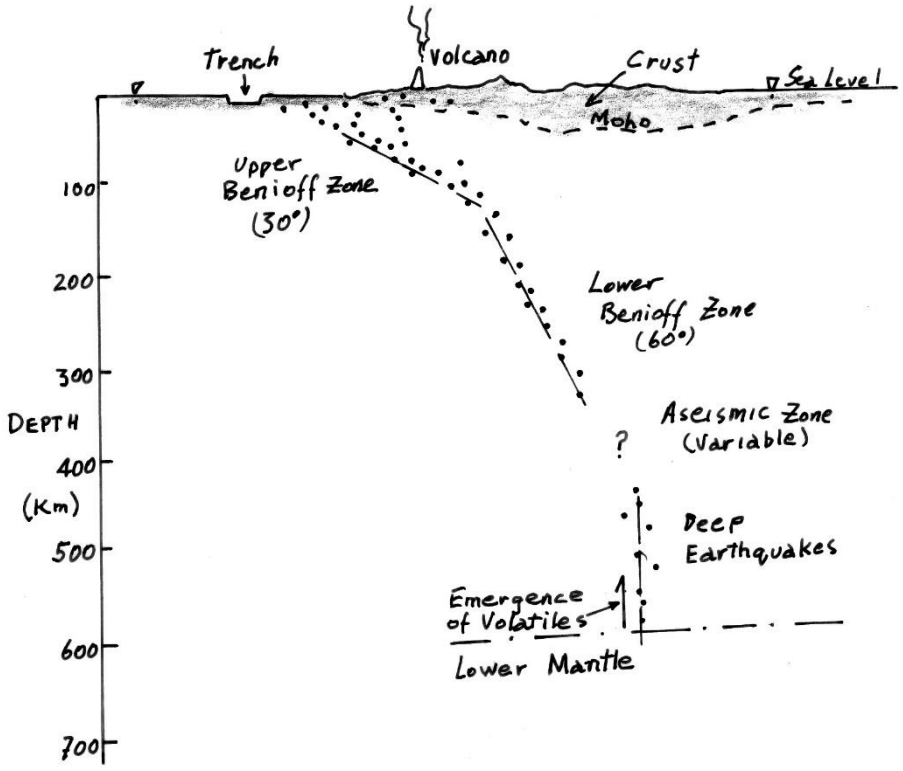

Figure 1. Pattern of the full earthquake occurrence often found in the Pacific

The deep end of the lower Benioff Zone is met at around 350 km depth and, typically, activity at this lower end begins close to a vertical location above the vertical patterns in the Upper Mantle. This is so even where an aseismic gap separates the two zones. Activity in the lower Benioff Zone then continues up to about 150-200 km depth. The interesting thing here is that this zone is inclined at around 60 degrees to the horizontal, an inclination typical of failures under tensile conditions. There is sometimes another gap between the top of the lower Benioff Zone and the bottom end of the upper Benioff Zone, just another gap in the mobilist model of subduction. In the upper Benioff Zone earthquake events typically occur along an inclination of 27 to 30 degrees to the horizontal, an inclination that is found in failures under compression, such as thrust faults. This, of course, suggests a different origin for each Benioff Zone, which is what Benioff also suggested.

The upper Benioff-Watada Zone extends from approximately 125-150 km depth up to around 50 km depth, when busy earthquake conditions generally mask any further patterns that might exist. However, there would appear to be no reason to assume the truncation of either of the Benioff Zone at these shallow levels, just because their definition is lost. For instance, extrapolation upwards of the lower Benioff alignment to the surface will often intersect the line of volcanoes.

The mechanisms of earthquakes along these various depths can be inferred to some degree. Starting with the deeper events of the Upper mantle, the idea of a simple shear failure – as occurs in shallow earthquakes - would not apply. A more likely mechanism in the Upper Mantle would be related to the release of high temperature, high pressure, volatiles from the Lower Mantle, such an action producing some form of the hydraulic fracture – now called fracking in the mining world. As the volatile migration continues its upward journey, it would encounter a drop in the ambient stress and further events of a hydraulic-fracture-nature can occur in the Upper Mantle. These events often define vertical orientations that would, in turn, indicate the Upper Mantle is not just mobile jelly but has semi-permanent structures

which are at odds with the mobilist subduction alignments, **Figures 1** and **2**. This is just another factor nullifying the concept of subduction.

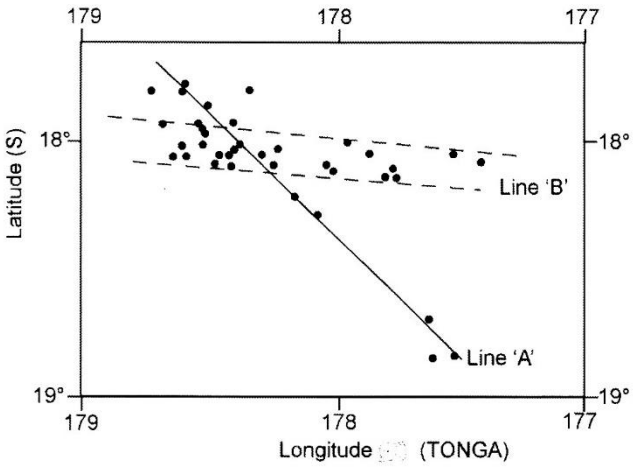

Figure 1a. Deep earthquakes occur along line B; line A is the alleged subduction zone.

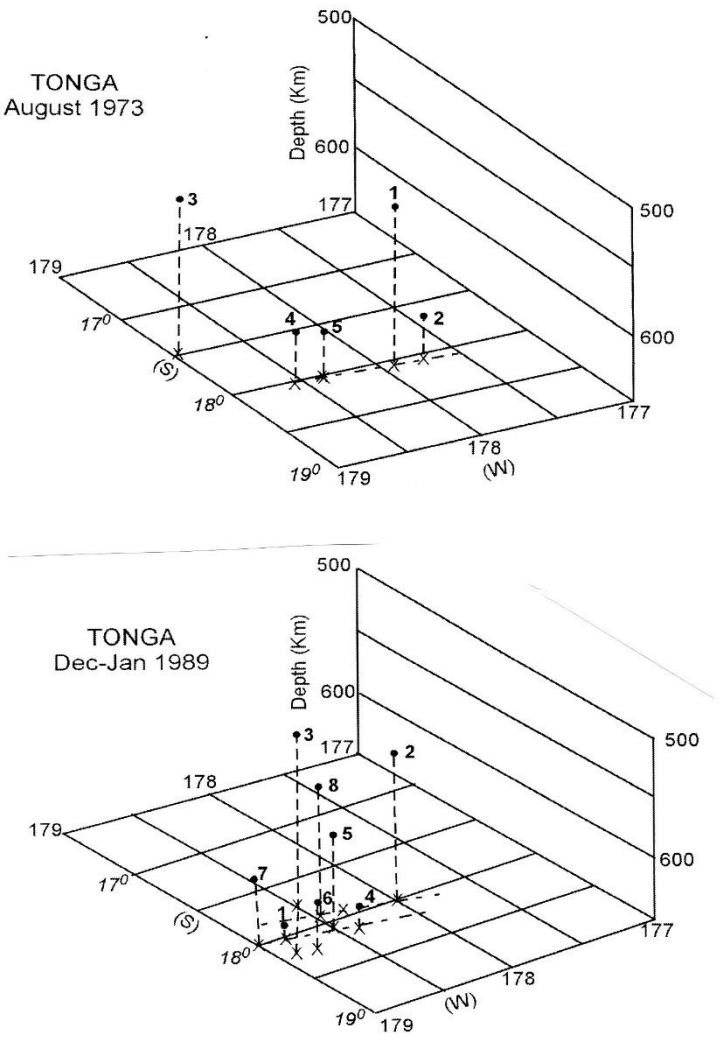

Figure 2a. Vertical structures in the Tonga region.

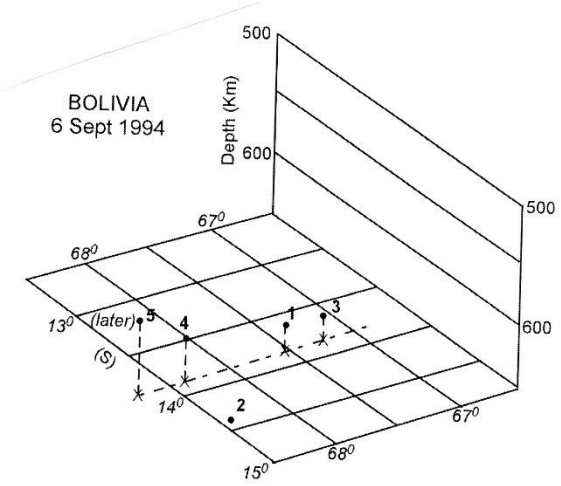

Figure 2b Bolivia, again with vertical structure close to right angles with the alleged subduction line.

After leaving the Upper mantle, the high temperature, high pressure volatiles would continue their vertical journeys, sometimes passing through an aseismic zone of presently unknown nature, before reaching the base of the Lower Benioff Zone. This, as mentioned above, is usually located almost vertically above the vertical paths in the Upper Mantle. There is a time lap in this journey, one that is often diagnostic of the region.

In the Benioff Zones themselves, an analysis using the Mohr Circle approach shows that shear failure is just possible under maximum geoid stresses - when combined with maximum uplift pressures of the volatiles: that is, uplifts almost equal to the loading of the super incumbent layers at any depth. The principal is shown in **Figure 3.**

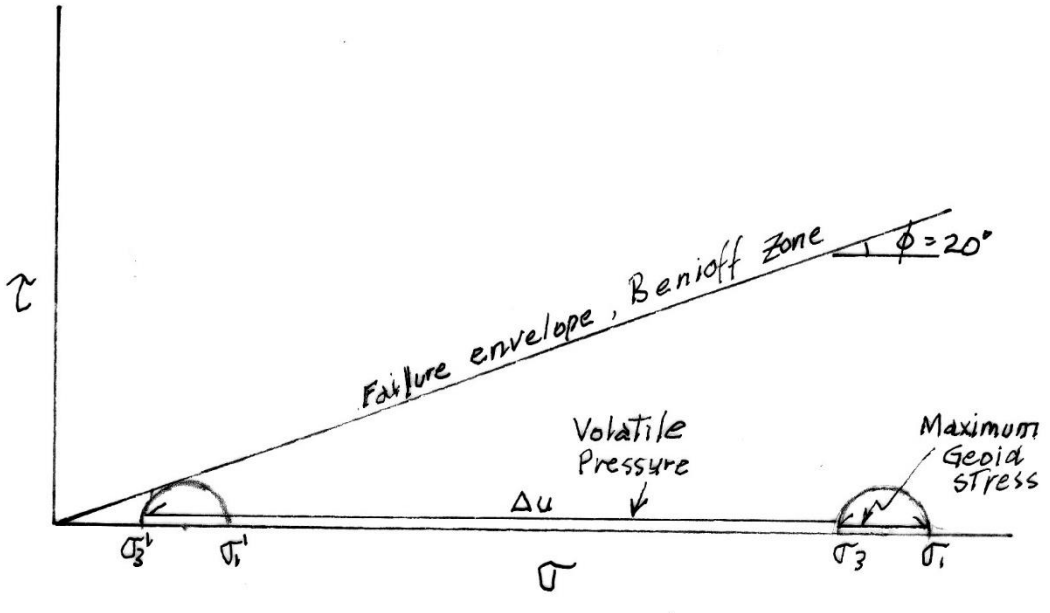

Figure 3 Effect of high volatile pressures on displacement of Mohr Circle

An analysis I once did revealed that this form of tensile shear failure is possible to the deepest level of the lower Benioff Zone, 350 km depth. Under the same criterion, compressive shear failure becomes

difficult to justify at anything deeper than the base of the upper Benioff Zone, around 125 - 150 km depth. In view of this coincidence, it is a guess that the Benioff Zones are probably pre-existing features that could well date back to the Pre-Cambrian. As an aside, these indications of variable horizontal stresses at depth puts paid to the old Heim's Rule that stresses should tend to equalise at depth. If there were no stress differentials, of course, earthquakes would be very difficult to explain.

Finally, there is a mass of shallow earthquakes, 50 km depth and above. A similar Mohr Circle approach to these shallow earthquakes can be made, again using maximum geoid stresses. If pore pressure conditions are assumed to be no more than hydrostatic, then the use of typical shear strengths along faults and/or major discontinuities leads to a limitation on depths: around 7km for failures under conditions of compression and a little more than double this under conditions of tension. Obviously, such depth limitations do not apply in practice. For a shallow earthquake zone to extend down to some 50 km depth, one would need some changes in the parameters involved. Shear strengths along rock mass discontinuities are variable but do not change much with time, except perhaps by weathering. Geoid shear stresses have a maximum value as already discussed. Thus, the only parameter capable of major changes is the pore (or volatile) pressure, this being provided by the upward migration of high temperature/high pressure volatiles originating from the Lower Mantle. Volcanoes are the visual evidence of this upward migration of volatiles from depth and it might be noted that volcanoes are, with few exceptions, not commonly found on continental crust or shields. In addition, earthquakes seldom occur below about 200 km depth in continental areas and this also suggests that the difference between the continental sections of the Earth and the oceanic regions might extend well below the Moho. Some seismological information by Dr Dong Choi suggests that such differences could well extend to 1,000km depth. If so, the onion skin structure of the upper Earth might not be ubiquitous?

To understand shallow earthquake mechanisms a little better, some guidance is given by the findings of reservoir induced seismicity.

Reservoir Induced Seismicity

Over seventy case histories are cited by Gupta in his 1992 Elsevier publication. Magnitudes up to M6 are not uncommon and the induced earthquakes range from very shallow, 1 - 2 km depth, with a majority falling within the 4 - 6 km range - which depth, incidentally, is about that when deep drilling first encounters problems of hole distortion – that is, stress levels able to deform the insitu rocks. (On this point, it has been noted in tunnels that the stresses around a tunnel's periphery can exceed the ambient stresses by a factor of two, so a similar situation is possible with drill holes.)

In a majority of cases, RIS commences at around full reservoir supply level, **Figure 4a**. Very occasionally, seismic activity has been known to commence some years after the reservoir has been in operation: three years after the completion of impounding behind the high Aswan Dam (Egypt); twelve years after the completion of the Oroville Dam (USA); and forty years after the commissioning of the Hoover Dam (USA) – if, indeed, this last could be reservoir induced and not natural. In such instances the delayed seismic activity typically takes place at some distance from the reservoir and the delay is likely to be associated with the time needed for the imposed high pore pressures to migrate laterally from beneath the reservoir. Which brings us to the cause of RIS.

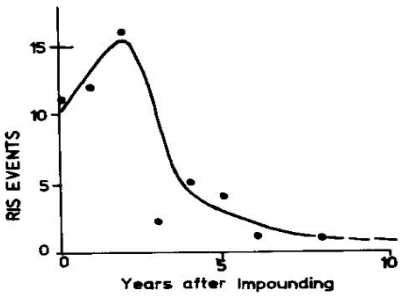

Figure 4a Timing of RIS events

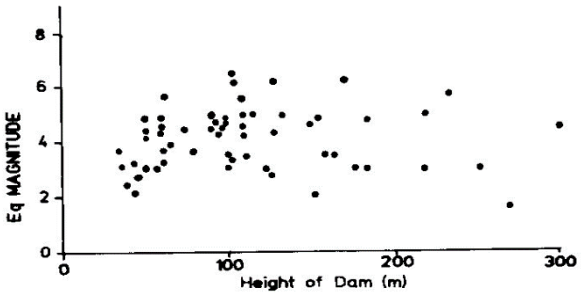

Figure 4b Earthquake Magnitude vs reservoir "load"

There has been some reluctance in the literature to identify any single major cause. Most texts give the reader a choice: the simple loading effects of the reservoir mass as if the reservoir behaved as an enormous, filled, bathtub; the possibility of "lubrication" on underlying faults/joints by the raised water level in the reservoir; the effect of a raised ground water level on the insitu effective stress condition in the ambient rock mass.

With regard to the first choice, it might be stated that a reservoir, even acting as a filled bathtub, replaces only a fraction of the load that has been removed by valley erosion. As can be inferred from **Figure 4b**, the magnitude of RIS does not have any consistent trend relating to the dam height (reservoir load), hence "simple loading" may be deleted from the discussion. Which is logical since, during impounding, the effects of the rising water level in the reservoir are transmitted immediately to the underlying ground water table to produce a quasi-immediate rise in ambient pore pressures beneath the reservoir and, by lateral migration, to just outside it. Increased pore pressures reduce the effective stresses, which means that impounding would cause a drop in the normal effective stresses acting across discontinuities in the rock mass. This, in turn, reduces the frictional strength of thee rock's discontinuities, making them more susceptible to shear failure in a crust that is under high (or low) horizontal stresses.

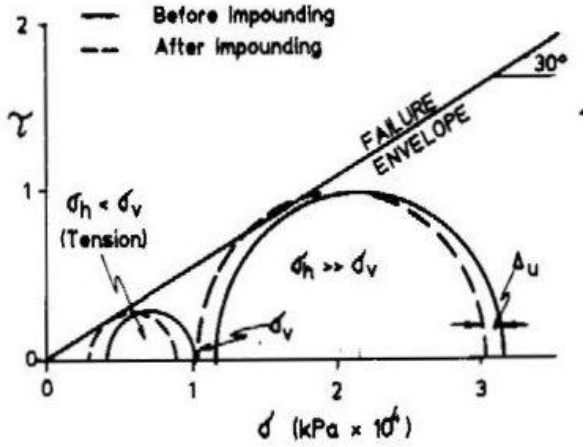

Figure 5 Shallow RIS conditions

This has an important codicil. If the applied loading – at least for dams above about 30 m high - has no recognisable effect on the magnitude of RIS, then it means that a reservoir induced earthquake must be largely dependent on the state of stress in the underlying crust. As demonstrated by **Figure 5,** the Earth's crust must be in a natural state that is close to incipient failure, if it is going to be susceptible to RIS.

Indeed, variable horizontal stresses up to 6 or more times the vertical stress are often recorded in shallow rock masses, even in horizontally bedded sedimentary rocks like the Hawkesbury Sandstone and the

Bowen Basin beds. It can be quite simply demonstrated that these high shear stresses are not the result of an erosion cycle, as suggested in many textbooks. They have to be tectonic in origin. Similarly, low horizontal stresses of half the vertical stress are also recorded and these are certainly not the result of erosion. What this small diversion means, then, is that RIS occurs only when the subsurface rocks are already stressed to a state close to failure, which failures would most likely occur on weaknesses, or discontinuities, in the rock mass. In turn, this would suggest that such an area would be likely to exhibit micro seismic activity in the pre-reservoir period. In fact, work at the University of Texas some forty years ago indicated that RIS was likely to occur only when such micro seismic activity was in progress prior to construction. No one took much notice of it. But the measurement of insitu stresses at a dam/reservoir site, prior to the start of construction, would thus be an important factor in predicting RIS.

RIS, once begun beneath or close to the reservoir, sometimes tends to migrate around, affecting a whole series of discontinuities in the rock mass(es), over time. What might be deduced from this is that a single RIS event relieves the stress only locally and that a wider area must be in a close-to-critical insitu stress condition.

Another cause of artificially induced earthquakes can be large scale mining. For instance, the excavation of a large open cut mine will reduce the vertical loading at the floor of the mine, while the horizontal stresses at that level – or just below it - are unlikely to be greatly changed.

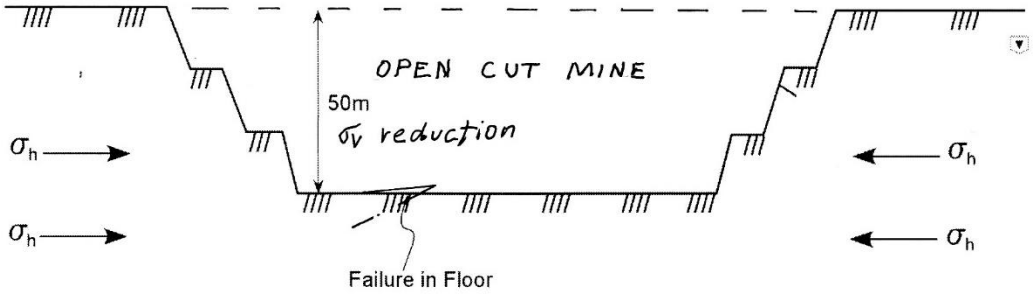

Figure 6 Open cut mine with floor heave at a moderate depth

This means that, under ambient compressive conditions, the shear stresses increase on excavation and, if adequate, can cause failure on a suitably orientated discontinuity. **Figure 6** illustrates the situation of a deep open cut in a highly stressed environment and the analysis of the situation is shown in terms of Mohr Circles, **Figure 7**.

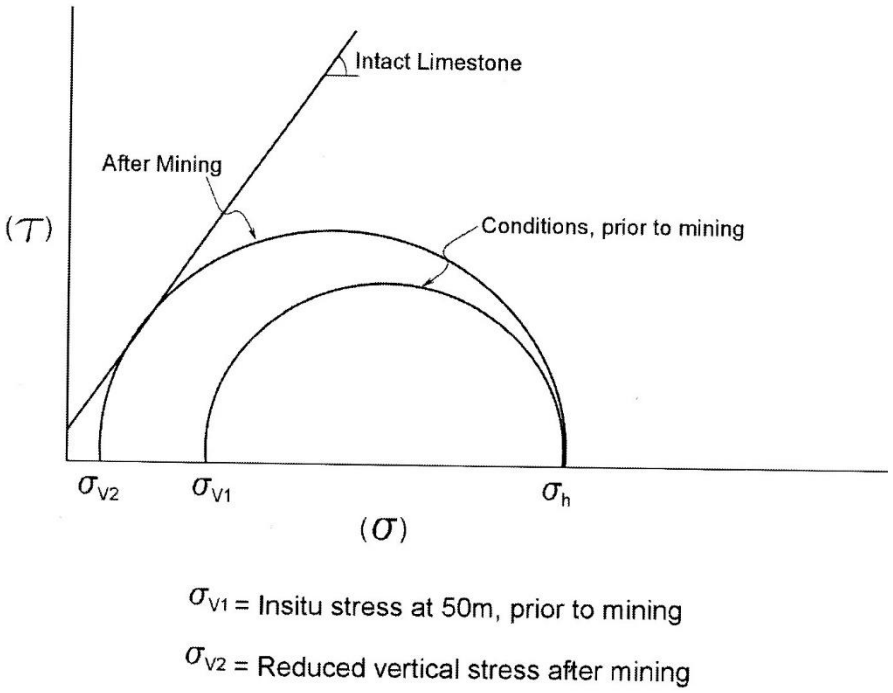

Figure 7 Reduction of vertical stress below the mine floor, as a result of the excavation, increases the shear stresses beneath the floor of the mine.

An interesting case history of this type is given by Hilleard (1993), in the *Case Studies in Engineering Geology*, Volume 2. In this, a railway viaduct crossing a wide and deep gorge in the Hawkesbury Sandstone was intended to be protected from coal mining and underground workings were therefore restricted to a safe horizontal distance from the viaduct. Despite this normally adequate safety measure, failure occurred in the base of the valley, disrupting the viaduct. The failure, a small thrust fault, was not caused by mining subsidence but by compressive failure in the sandstone beds at the base of the valley.

It thus seemed that the removal of the coal seam, even at what should have been a safe distance from the viaduct, nonetheless reduced the lateral strutting effect that the full coal seam would have applied. High horizontal stresses have been recorded in the Hawkesbury Sandstone, and so the most vulnerable zone, the base of the wide valley, suffered.

Regarding Prediction

A main purpose behind the study of earthquakes is obviously to discover a reliable method of prediction, particularly for the occurrence of shallow earthquakes which cause the havoc. In order to predict such a natural phenomenon, a first requirement is to understand the mechanisms that are involved in shallow earthquakes. If one works on wrong assumptions, then the conclusions one reaches are also liable to be in error. For example, the present plate tectonics explanation for some earthquakes is that subduction drags down a juxtaposed crust, until this crust realises what the subduction is up to and it springs back like a rat trap to produce an earthquake and tsunami. This probably takes the cake as an erroneous mechanism and hence is an irrational hindrance to any analysis on prediction. There have also been lots

of recent publications on the prediction of earthquakes, with an even greater catalogue of indicators, ranging from tides, astronomical effects, electrochemical effects, cloud jets, the behaviour of chooks...

Let us look at one historical approach to this matter that was touched on in the previous Essay. After a catastrophic volcanic eruption in the New Hebrides in the early 1960s, the English and French Residents held a meeting with their geophysicists to find out why such a catastrophic event had not been predicted, particularly when new seismological instruments had recently been installed. As already mentioned in the earlier Essay, Claude Blot, the French seismologist, took up the challenge of prediction and in quite a short time discovered that earthquake events fell into a definite pattern with the migration of seismic energy unquestionably upwards, from the deepest levels to the surface. That is, the patterns indicated the complete opposite of the subduction hypothesis. By then, of course, subduction was coming into general favour. Blot also discovered that the rates of upward migration were consistent in any one region and, on this basis, he began to predict both earthquakes and volcanoes with surprising accuracy, months – even a year or two – ahead of the events.

The evidence was published in French journals and apparently did not cross their language borders – at least in published form. Thus, Claude Blot was not acknowledged for his successes, let alone not nominated for a Nobel Prize. Instead, he was transferred by the French Government to an area of West Africa, one without any earthquakes, without any volcanoes. That stopped his anti-subduction nonsense and, indeed, his work might have remained buried to this day had it not been for the Australian resident geologist in the south west Pacific, John Grover by name. Grover had worked with Blot and, on retirement, wrote his autobiography which also included most if not all of Blot's calculations and results. This autobiography might never have found the light of day either, if international main-stream publications were relied on. However, it was published in Brisbane by Copyright Publications, in 1998. Which was how this author got to read the book and do a review of the methods used. This review was read by the editor of what was to become the *New Concepts in Global Tectonics Journal*, in Canberra: seismologist Dr Dong Choi. He took on the theme, initially with cooperation by the aging Claude Blot, and demonstrated its validity. As a result – well, after more than a decade - an International Earthquake and Volcanic Prediction Centre (IEVPC) was established in Florida in 2012, with research under the directorship of Dr Choi. At the time of preparing this Talk a number of recent hindsight connections have been established by the Prediction Centre, together with several successful predictions made of coming events. And all this by using Blot's model. A simplified basis of the model is shown in **Figure 8**.

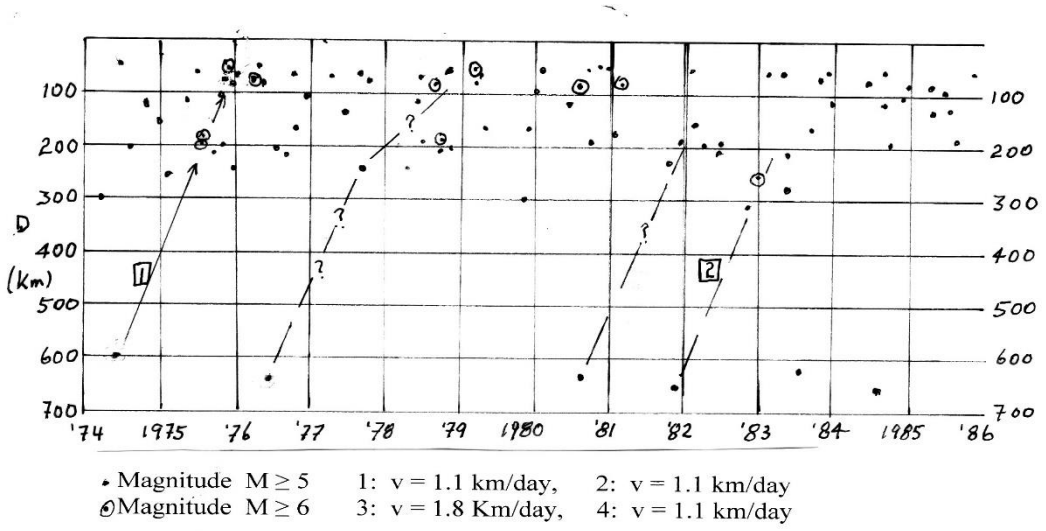

Figure 8. Rates of upward migration of seismic energy (after Blot)

A final point on some historical seismological evidence. Back in the 1960s, seismologist Nick Ambrayseys, who ran the course in Engineering Seismology at Imperial College, did some historical studies of earthquakes in the Middle East and found that, in Biblical times, the line of earthquakes, representing the plate boundary, was in quite a different location from the position of the line today. So, had we lived in those times, we might have defined our lithospheric plates quite differently from today's. One might ask: How can that be possible if the lithospheric plates are declared to be unbreakable?

Should one wish to follow up on any of this, worldwide earthquake data from the early 1970s are available on **http://neic.usgs.gov**. Reference to the *New Concepts in Global Tectonics* will provide all the present-day lines of thought one could need.

REFERENCES

Enever, J.R. and Lee, M.F., 2000. On the prediction of rock stress. *GeoEng 2000,* IEA, Melbourne.

Fell R., MacGregor P. and Stapledon D. (1992). *Geotechnical Engineering of Embankment Dams.* Balkema, Rotterdam

Gay, N.C. and Wainwright, E.M., Ed., 1984. *Rockbursts and Seismicity in Mines.* Sth Afr. Inst. Mining & Metallurgy, Symposium Series 6.

Grover J.C. (1998). *Volcanic Eruptions and Great Earthquakes*. Copyright Publ., Brisbane

Gupta, H.K. (1992). *Reservoir Induced Earthquakes.* Elsevier, Amsterdam.

Hilleard, P.R. (1993). Bedrock movements and failure of the Stanwell Park Railway viaduct. *Collected Case Studies in Engineering geology,* (G. McNalley Ed.), v. 2, GSA.

James, P.M., 2000. On the state of stress in the Earth's crust: inferences from RIS. *NCGT Newsletter,* no. 17, p. 9-10

James, P.M., 2007. On the origin and implications of high horizontal stress variations in the Earth's crust. AAPG Conf., Athens (Extended Abstract)

ELECTROMAGNETIC MONITORING OF THE NEW MADRID FAULT US AREA WITH THE RDF SYSTEM - RADIO DIRECTION FINDING OF THE RADIO EMISSIONS PROJECT

Valentino Straser[1], Daniele Cataldi[2], Gabriele Cataldi[3]

[1]Department of Science and Environment UPKL Brussels (B). valentino.straser@gmail.com

[2]Radio Emissions Project, Rome (I). daniele77c@gmail.com

[3]Radio Emissions Project, Rome (I). ltpaobserverproject@gmail.com

Abstract: The study presents the monitoring data of the pre-seismic signals, detected with the RDF System, of the New Madrid Fault. The experimentation was carried out in 2018 and concerned 57 earthquakes of M2.5 + magnitude of the Richter scale, including earthquakes of magnitude 3.3 and 4.4 occurred in the New Madrid area in December 2018. The earthquakes analyzed in the course of the experimentation were preceded by electromagnetic frequencies between 1000 Hz and 32000 Hz, appeared a few hours to a few days before earthquakes. Thanks to this new technology, developed in Rome by Daniele and Gabriele Cataldi, thanks to the use of a radio receiver designed for the amplification of low-frequency electromagnetic signals (between the SELF band and the VLF band, 0-32000 Hz) it is possible to identify the origin of the electromagnetic signals and to identify, with the triangulation method, the future epicentral area. The development of the RDF methodology, applicable to all areas of the Earth Globe, will contribute to a greater understanding of the crustal diagnosis of a potentially high-risk seismic zone, as evidenced by the violent earthquakes in New Madrid in 1811 and 1812.

Keywords: RDF system, earthquake prediction, SELF-VLF, New Madrid fault.

INTRODUCTION

The RDF - Radio Direction Finding system of the Radio Emissions Project - is a electromagnetic detection system that covers the entire terrestrial surface. This coverage is subdivided into colorimetric areas to which very precise azimuths are associated. The first monitoring station was built in Lariano (Rome, Italy), and was created by the LTPA Observer Project and the Radio Emissions Project and allows monitoring of "crust diagnosis" in real time, on a global scale (Straser et al., 2018).

During the experimentation of the Radio Emissions Project it was possible to detect strong and precise radio emissions to precede destructive earthquakes worldwide (Straser et al., 2015; Straser et al., 2016; Cataldi et al., 2017). Given these results, it was necessary to develop a system capable of detecting the position or azimuth of origin of these electromagnetic signals to better understand the evolution and nature of the electromagnetic signals. Against this need, the RDF monitoring technique was developed (Straser et al., 2018).

Between February 2, 2018 and November 30, 2018, the Radio Emissions Project monitored the area of North America, characterized by the Fault of New Madrid, long indicated as a dangerous seismic area subject to destructive earthquakes (Fig. 4) (Choi et al., 2018). This study served to understand if the monitoring technique developed by the Radio Emissions Project, by means of the RDF - Radio Direction Finding system, was able to ascertain a relationship between electromagnetic emissions and the occurrence of earthquakes.

The Fault of New Madrid, after the very strong earthquakes of 1811 and 1812, is one of the areas subject to monitoring, as early as the first half of the seventies of the last century. The succession of

jolts felt and recorded by seismic networks, generally of low magnitude, testify to the tectonic vivacity of the area that stretches from New Madrid, in the north-west of Arkansas, southwest of Kentucky, southeast of Missouri and northwest of Tennessee. It is an intraplate type seismicity and the seismic hazard in the Mississippi area is well known to American geologists, who expect new important events in the coming decades. In 1968 the last major earthquake occurred at Illinois with magnitude 5.4 Richter. If, on the one hand, an interpretation of the current tectonic activity is associated with the seismic tail of the earthquakes of the winter of 1811 and 1812 (Morgan and Hough, 2014) that had caused extensive damage along the Mississippi, on the other, seismic sequences could be a prelude to a new crisis with the fear of destructive events deemed, not wrongly, a Big One, aggravated by the anthropization that was not present more than two centuries ago. The areas located along the Fault of New Madrid could also be involved in land liquefaction processes, as revealed by the data on paleoseismology. The new technologies, such as the RDF System, made in Italy in Rome by Gabriele and Daniele Cataldi, allow to detect in real time, 24/7, the electromagnetic activity of the areas subjected to tectonic stress, with indication of the provenance of electromagnetic anomalies. Thanks to the triangulation method, having multiple monitoring stations, it is possible to approximate the future epicentral area with sufficient approximation. In this context, given the importance of monitoring potentially high-seismic areas, the New Madrid area was chosen to add new data and information useful for monitoring crustal stress and, in perspective, the forecast of destructive seismic events.

1. The RDF Network

Starting from the use of a first radio reception station RDF (Straser et al., 2018), experimented in 2018, the Radio Emissions Project, has started to install other stations equipped with the "Radio Direction Finding" technology, thus creating the network monitoring called "Radio Emissions Project Network". The Radio Direction Finding (RDF) Network, developed by the Radio Emissions Project is based on technology that evolved starting from the late 1800s thanks to the studies of Heinrich Hertz, who discovered the directionality of an open loop of wire used as an antenna. Compared to other electromagnetic monitoring systems employed within the scope of scientific research to forecast potentially destructive earthquakes (MW=6+), the RDF system allows 24/7 monitoring of a wide bandwidth of the Earth’s background electromagnetic emissions to trace radio anomalies in seismically active areas of the terrestrial surface.

1.1 The World Mapping

The Radio Direction Finding (RDF) system developed by the Radio Emissions Project, is a electromagnetic detection system that covers the entire surface of the Earth. This coverage is divided into colorimetric areas to which very specific azimuths are associated (Fig. 1).

In 2017, the Radio Emissions Project created an interactive world map, divided into colored spatial axes that identify the azimuth of origin of the electromagnetic signals (Fig. 1) with respect to the detection station (positioned at the center of this mapping). This map represents a zoonization of the entire terrestrial surface, from which the detected electromagnetic signals can come, identifying in this way the geographical area of origin of the signals.

To understand the operation of the RDF system it’s necessary to assume that the receiving system is able to provide a stereo signal coming from the antennas, arranged orthogonally and oriented towards the cardinal points. The flow of radio signals coming from the antennas is subdivided into "colors" to which a forward direction is then associated.

According to the colorimetric scheme used by the RDF station, the cardinal points and the goniometric values associated with the individual composing this scheme, indicate geographic areas (near or far) radially displaced with respect to the position of the monitoring station.

The result is a subdivision into "strips" all having the same length (about 20.000 km) that start from the geographic position where the station is located and all join at the "antipodal point" of the station itself.

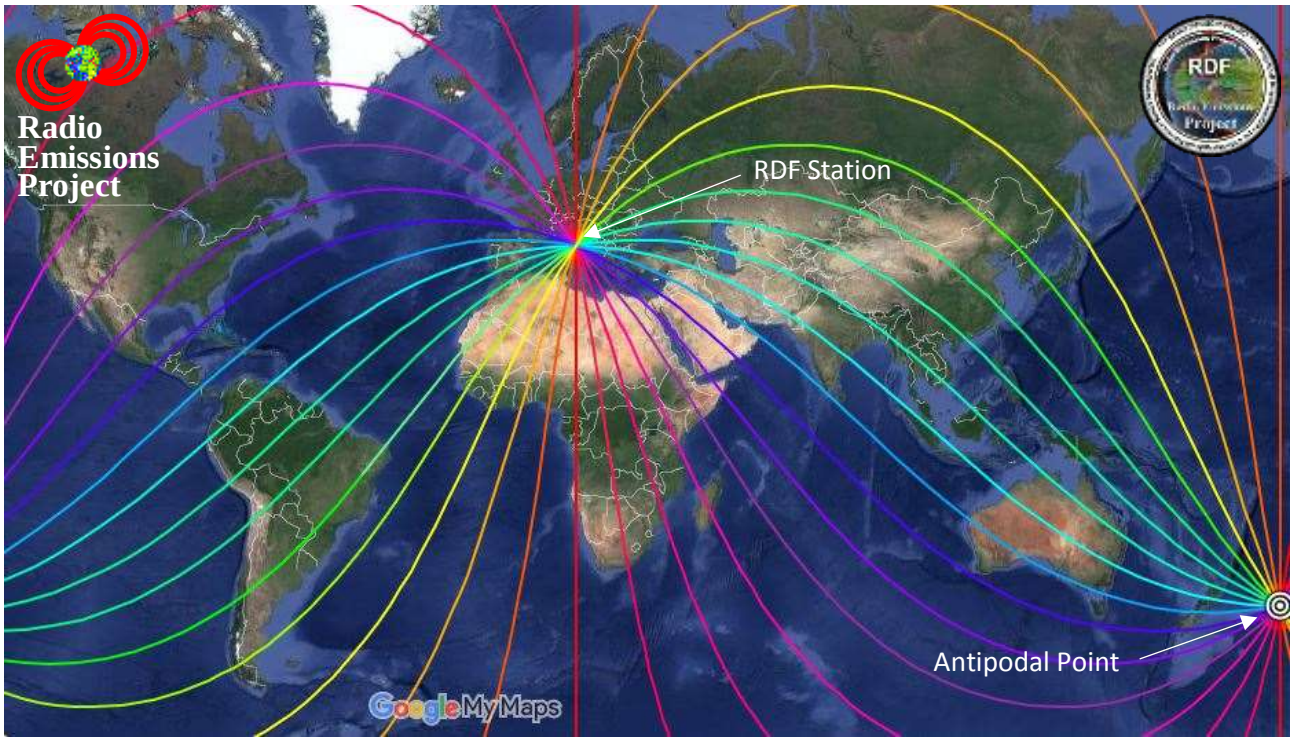

Fig. 1 - World Mapping of the RDF system, developed by the Radio Emissions Project, located in Lariano (Rome, Italy).

2 The Study

On 2 February 2018 the electromagnetic monitoring of the US area began in the area of New Madrid, as shown in Fig. 2.
This electromagnetic monitoring was made possible thanks to the RDF - Radio Direction Finding station of the electromagnetic detection system developed by the Radio Emissions Project, installed in Lariano, (Rome, Italy). The station began to provide the first data on the origin of electromagnetic signals in March 2017 (Straser et al., 2018), while the monitoring of the New Madrid Fault began almost a year later.
The geographical area examined for this study has an extension of approximately 266.851 million square kilometers, and a perimeter of 1.917 kilometers. The area covers 7 US states in North America:

1. Illinois
2. Indiana
3. Kentucky
4. Tennessee
5. Mississippi
6. Arkansas
7. Missouri

North American area

The extension of this area confirms the high degree of seismic hazard of the fault, as it is able to generate intense earthquakes as occurred in the past (Choi et al., 2018): as already mentioned, the most intense seismic events recorded in the New Madrid Fault began between 1811 and 1812 with an initial earthquake of magnitude Mw 7.5-7.9 of 16 December 1811, followed by an earthquake of magnitude Mw 7.4 (aftershock) on the same day. These remain the most powerful earthquakes that have ever hit the United States east of the Rocky Mountains in US history (source: USGS).

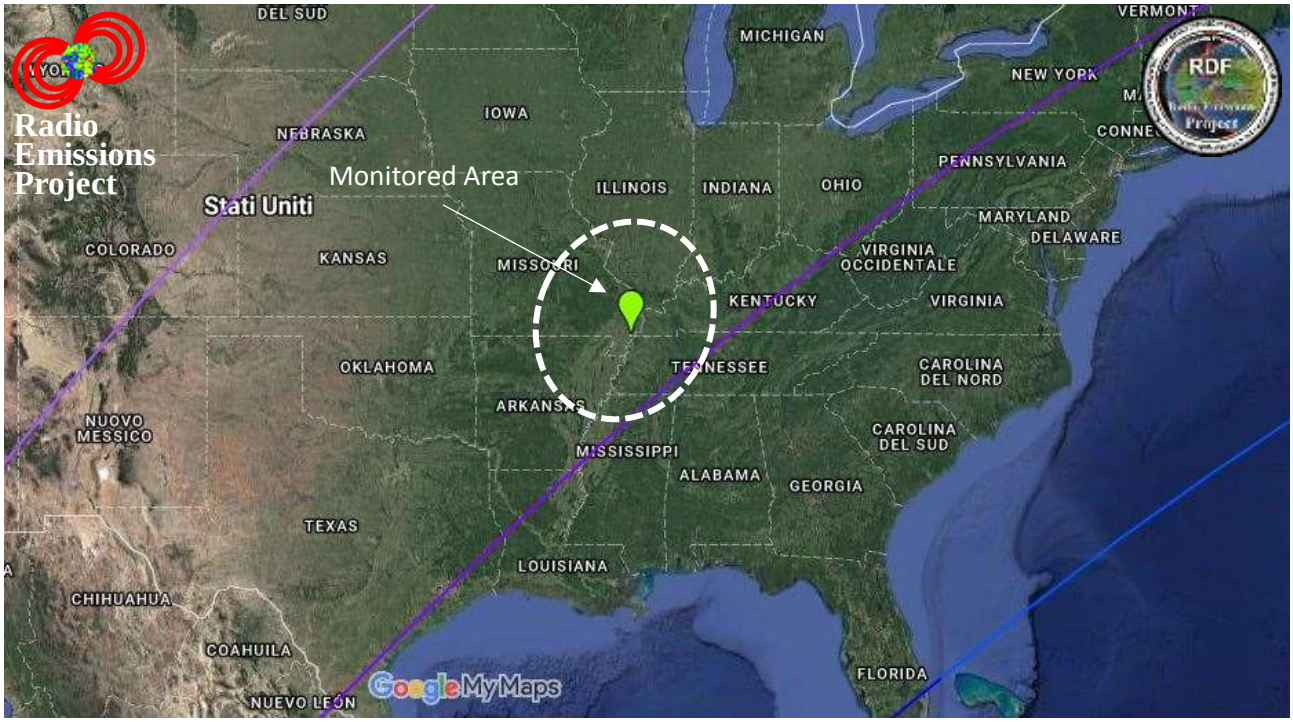

Fig. 2 - Mapping of the RDF system developed by the Radio Emissions Project, with reference to the area of North America (Fault of New Madrid) under monitoring.

The experimentation study, in relation to the results obtained by the Radio Emissions Project (Straser et al., 2018), took place in this area, to test the RDF monitoring system of the Radio Emissions Project and to find information and results useful for understanding the nature of the electromagnetic emissions recorded by the monitoring system if there were earthquakes of a certain intensity.

In this case the azimuth that the Radio Emissions Project has kept under strict control was the "dark purple" (as seen in Fig. 3 and Fig. 4), in the proper direction of the United States where the New Madrid Fault is present. . This monitoring had to monitor the possible appearance of signals having this origin azimuth, compared to the position of the receiving station, located in Lariano, Rome, Italy.

The experimentation was able to record numerous signals coming from the area, first identifying their azimuthal origin in the direction of the US area, discarding all the others accordingly, then checking their electromagnetic frequency, the time of appearance and the bandwidth. (average of the width) of the same.

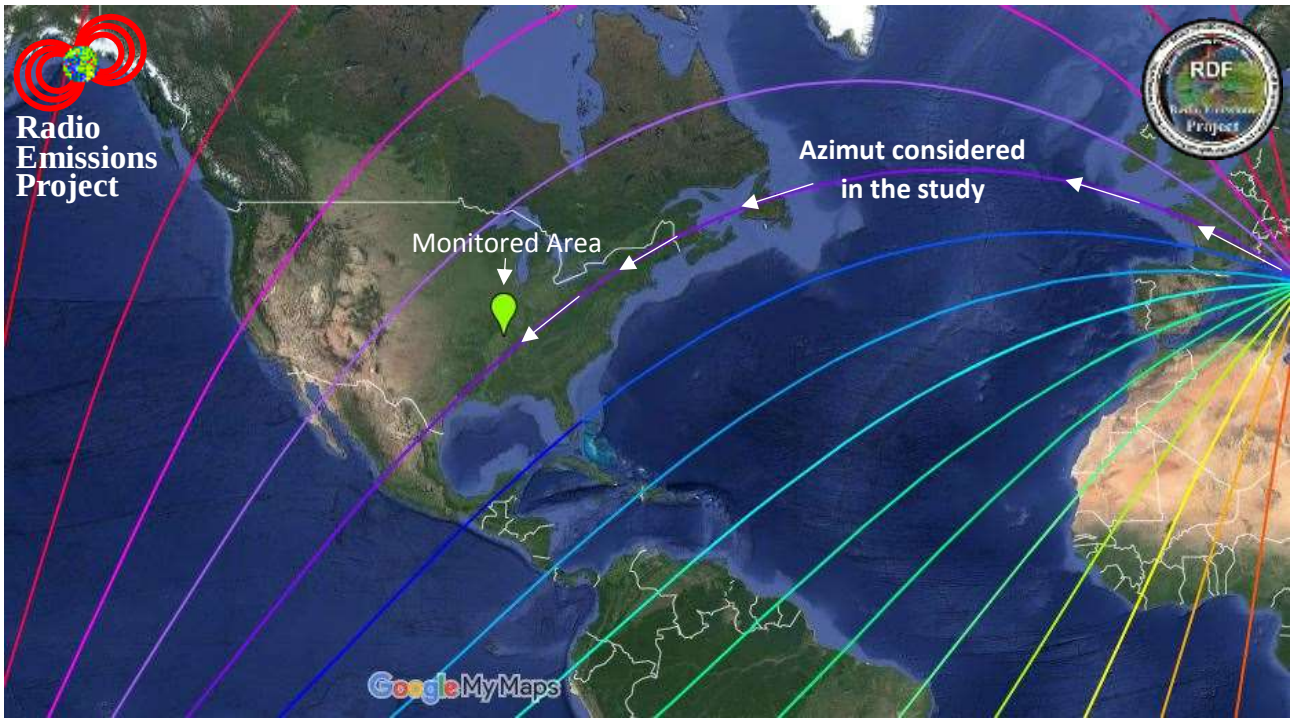

Fig. 3 - Mapping of the RDF system developed by the Radio Emissions Project, with reference to the area of North America (Fault of New Madrid) - View of part of the world mapping of the oceanic area, with reference to the dark violet azimuth examined.

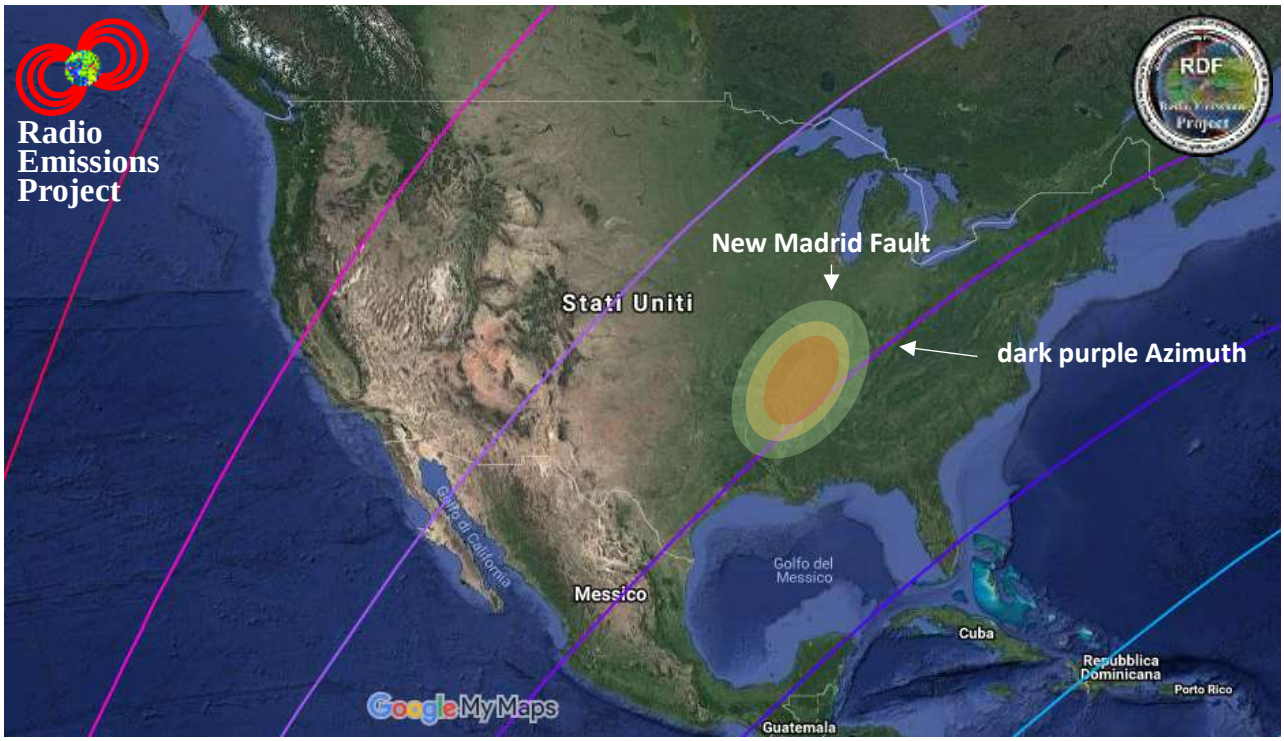

Fig. 4 - Area of the New Madrid Fault - Source: Radio Emissions Project. The map indicates the seismic hazard of the area, which is monitored by the RDF system of the Radio Emissions Project.

The area examined was identified by means of the global mapping of the RDF system. It is located in correspondence of the dark violet azimuth (as already mentioned), or on the N-W - S-E axis (direction N-W) with respect to the Lariano station (Rome, Italy). This area (Faglia di New Madrid) is about 8,500 km away from the monitoring station (Fig. 5).

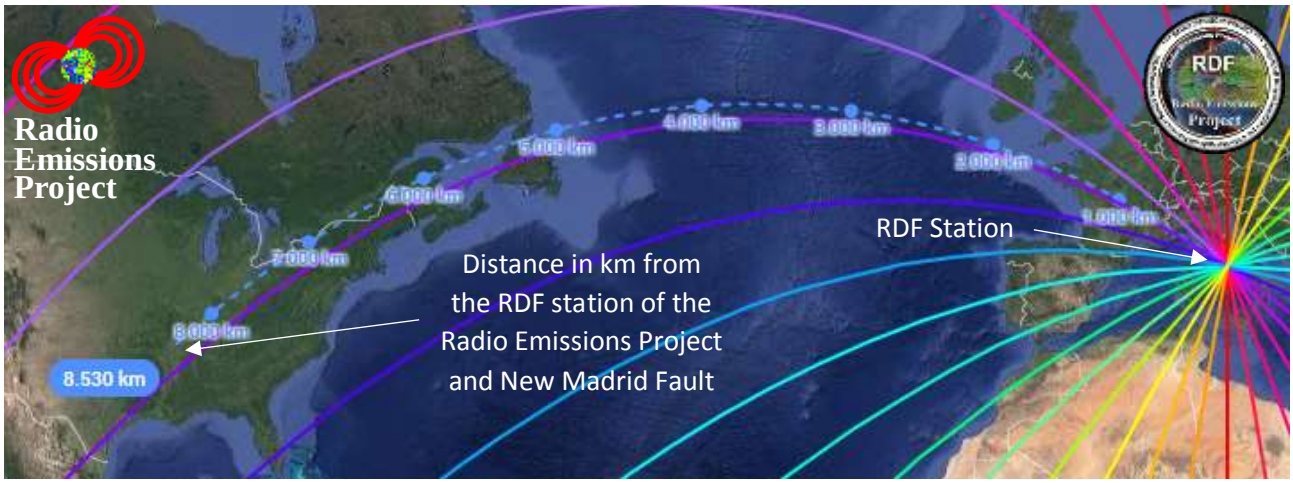

Fig. 5 – World mapping of the RDF system of the Radio Emissions Project - Distance of the New Madrid Fault area compared to the RDF monitoring station, ot 8500 km in the direction of N-W from Lariano (Rome, Italy). In this image the violet azimuth on which the area is located is visible. Source: Google Maps. Source: Google Maps.

During the study, there were 57 M2.5 + seismic events on the Richter scale, all preceded by intense radio emissions; the RDF - Radio Direction Finding system has been able to provide important indications on the origin azimuth of electromagnetic signals, on their temporal behavior, on their frequency variation, on the intensity and on their morphological behavior: data that allowed to improve the reliability of the RDF monitoring system and confirm, also in this case, the existence of important radio broadcasts (with wide bandwidth) that appeared before non-underestimable seismic events.

3 The data

The data of the study realized through the recordings made by the RDF station of Lariano (Rome, Italy) have confirmed the existence of electromagnetic signals with wide bandwidth related to the azimuth of the New Madrid Fault. The characteristics of these electromagnetic signals are listed below.

3.1 Frequency of electromagnetic signals

The electromagnetic signals having the area of the New Madrid Fault as azimuth of origin, have shown a reduction in their frequency of emission with respect to the period considered (2 February 2018 - 30 November 2018) as shown in Fig. 6.

The study of the emission frequency of these signals appears important if the data on the reduction of solar activity (solar minimum) are considered, confirming the previous studies of the Radio Emissions Project.

In fact, Fig. 6 confirms that the average frequency of radio emissions detected by the RDF system of the Radio Emissions Project follows the trend of solar activity, which in recent months is being reduced due to the approach to the "Solar Minimum", as shown in Fig. 7.

This indicates that the Lariano RDF detection system (Rome, Italy) has detected electromagnetic phenomena influenced by geomagnetic activity, ie linked to solar activity, having a precise azimuth.

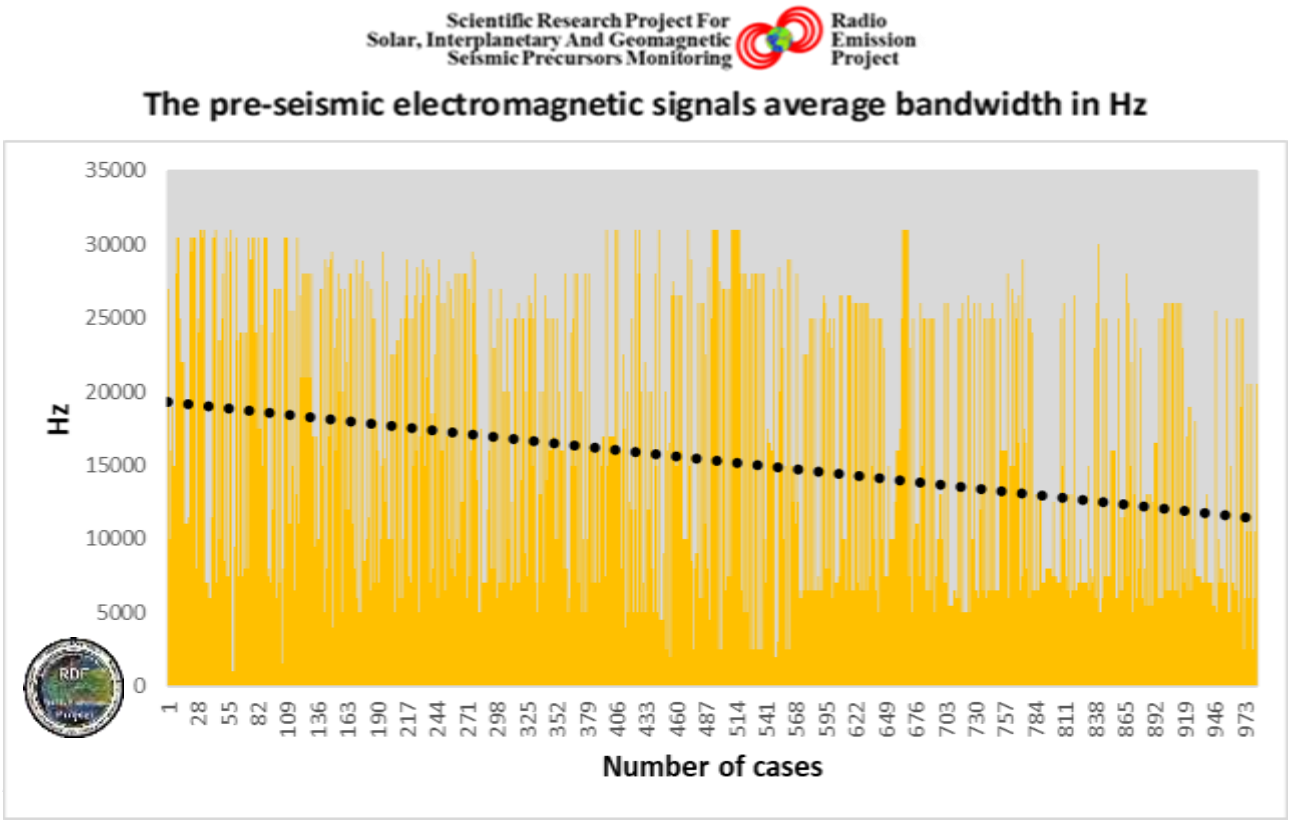

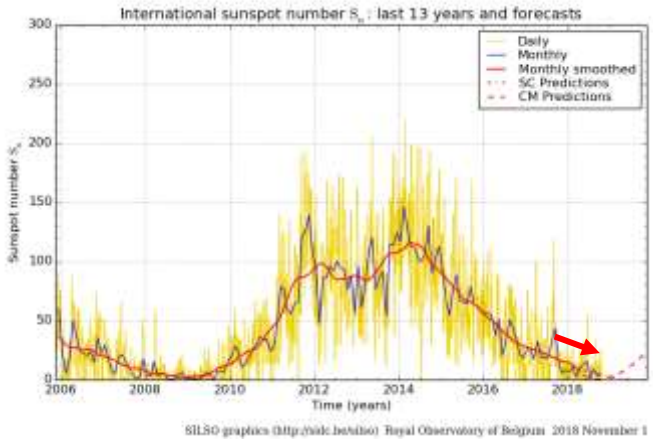

Figura 7 - Andamento dell'attività solare (sunspot number).

The solar minimum, is the period of lower activity of the Sun in the solar cycle; during this period, the activity of sunspots and flares tends to decrease, until it becomes almost absent for several consecutive days.

According to recent studies the solar minimum period coincides statistically with the greatest disasters occurred on a global scale, due to the energy release accumulated during the period before the solar minimum itself (Choi and Casey, 2015).

The RDF system, as already mentioned, has detected a decrease in the electromagnetic frequency of the natural signals in the direction of the monitored area, which follows the same trend of the solar cycle, it is indeed possible that solar activity influences our planet and with it also the natural electromagnetic emissions generated by this interaction.

3.2 Time of Occurrence

Analyzing the time at which these signals appeared, it was discovered that the greatest number of radio emissions are concentrated in the daytime hours, that is at times when there was solar lighting in the Italian geographical area where the monitoring station is located. . It can be deduced that this factor has influenced the detection of electromagnetic signals in general; after which the number of recorded radio signals is reduced by 50%.

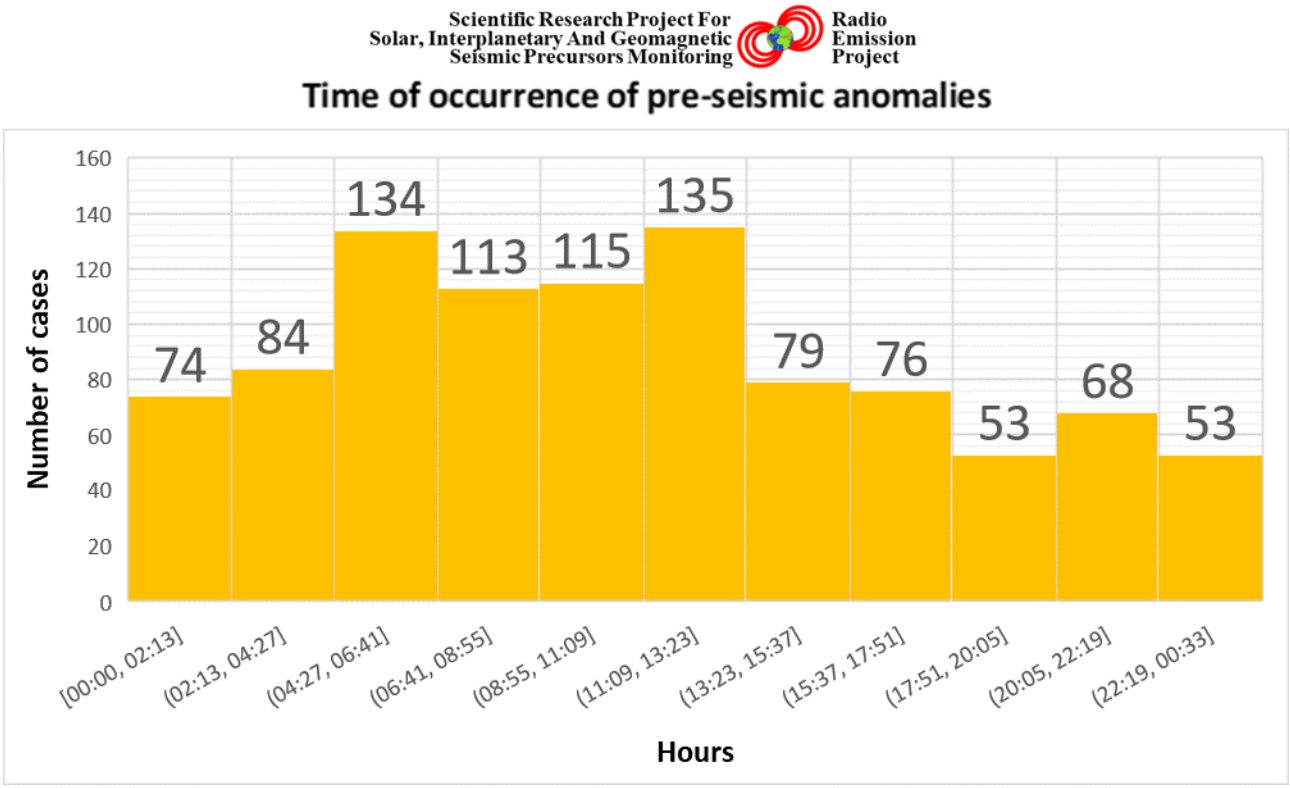

Fig. 8 - Time of occurrence of the geomagnetic signals with the azimuth of New Madrid as the arrival direction.

This data shows that the solar interaction with the magnetosphere and the ionosphere is one of the factors influencing the radio emissions recorded by the RDF system (Fig. 8). It is evident that on the detection capacity of the RDF system, especially for the areas very far from the detection station, ionospheric phenomena induced by solar activity can influence which can interact with the propagation of long distance ionospheric signals (Appearance and disappearance of ionospheric Layers). In this context, the experimentation of the monitoring system highlighted this important data.

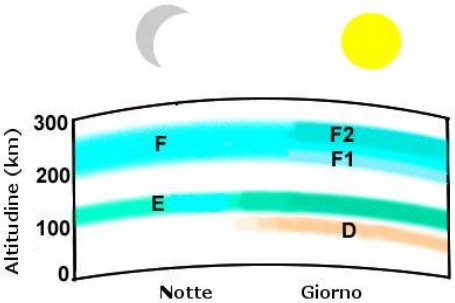

Fig. 8b – Schematization of the number and type of ionospheric Layers between the day and night hours. The modification of these Layers is determined by solar irradiation.

3.3 Number of radio-anomalies

Also the number of radio-anomalies is extremely important compared to their appearance. The highest concentration of recorded signals, whose direction is the azimuth of the New Madrid Fault (azimuth of dark purple color), appear to be those visible in Fig. 10.

- A first peak of concentration of radio signals appeared between 22 February 2018 and 21 May 2018.

- A second peak of concentration of radio signals appeared instead between June 12, 2018 and November 30, 2018.

Analyzing this graph shows how the number of electromagnetic emissions is inversely proportional to the Sunspot Number, or the index of solar activity in the period considered by this study (Fig. 9). The average frequency of emissions seems to be again influenced by the trend of solar activity, and the number of daily emissions seems to follow this index (Sunspot Number) in an inversely proportional way.

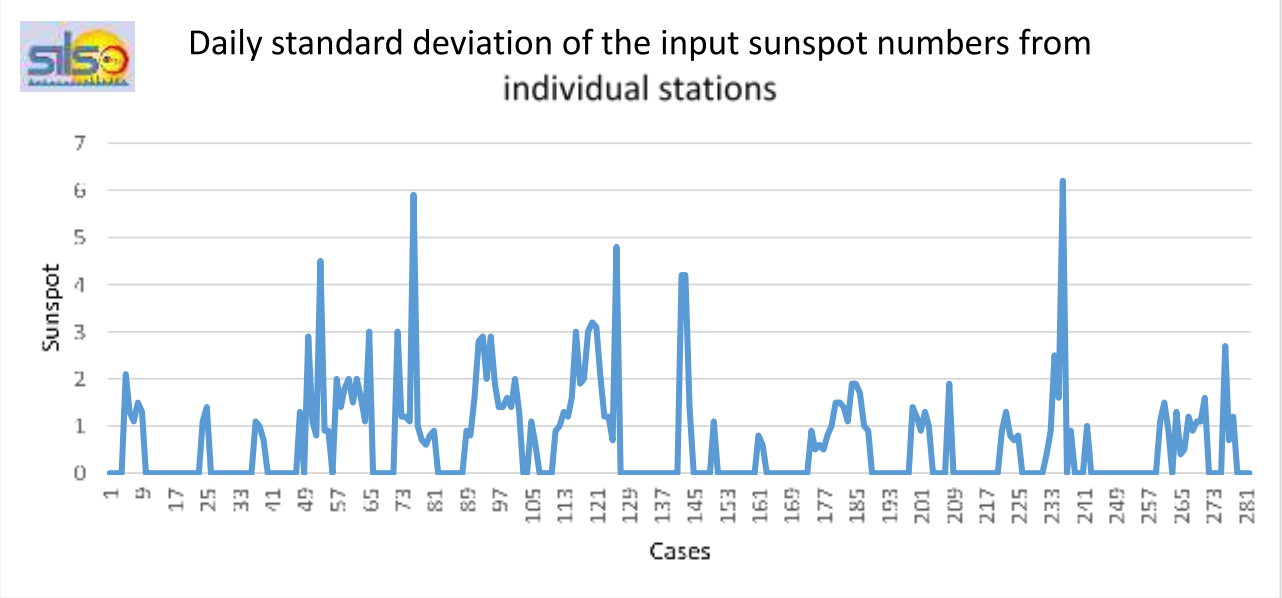

Fig. 9 - Sunspot Number - Source: http://www.sidc.be.

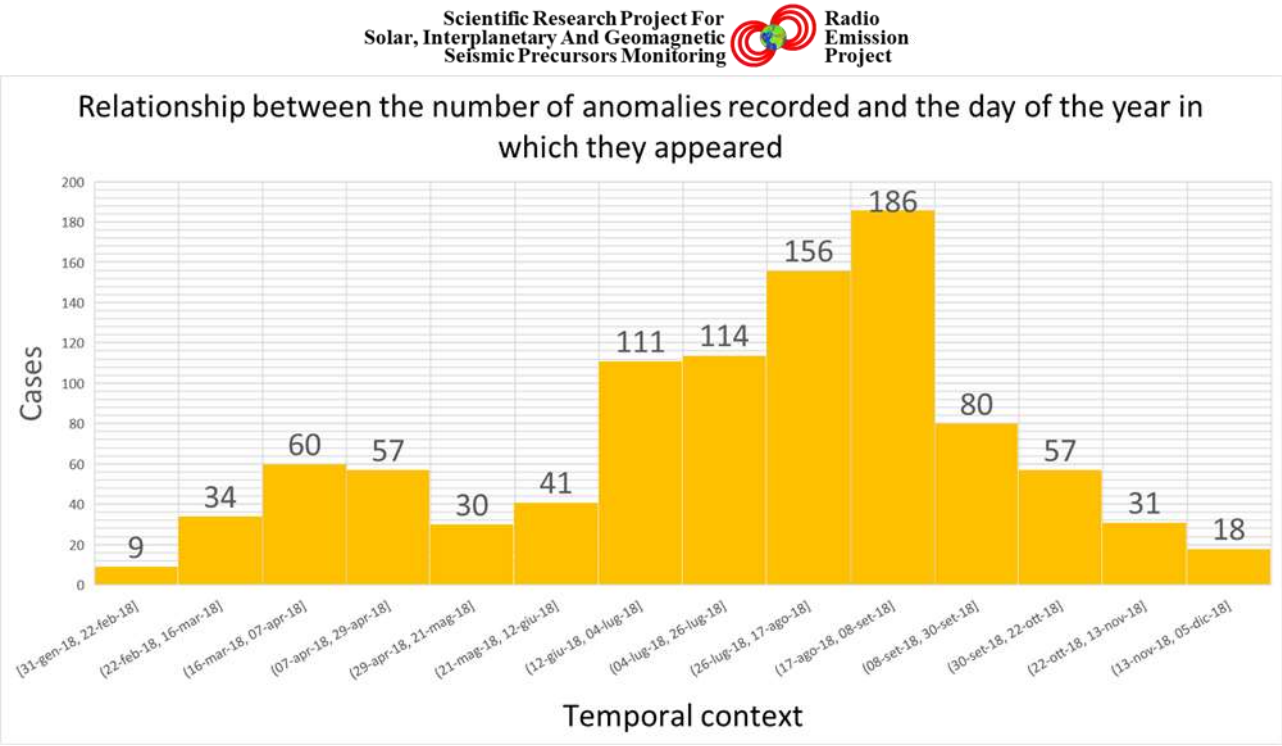

Fig. 10 - Number of radio-anomalies with respect to the temporal context. They follow inversely proportional the number of sunspots, or the number of sunspots that appeared on the Sun's chromosphere.

3.4 Frequency of the radio-anomalies

Very important data appear to be the frequency of the radio-anomalies appeared on a total of 984. As shown in Fig. 11, the highest number of radio-anomalies, as many as 259 (26.32%) were observed with a frequency included between 4.1 and 7.2 kHz. Then there were 151 radio-anomalies (15.35%), with a frequency of three 7.2 and 10.3 kHz. A third grouping of radio-anomalies concerns signals with a frequency included: between 25.8 and 28.9 kHz (132 cases - 13.41%).
Also in this context the rest of the other radio emissions decrease considerably in frequency, except for the range between 13.4 and 16.5 kHz (98 cases - 9.96%) which represents a fourth grouping of important radio emissions.

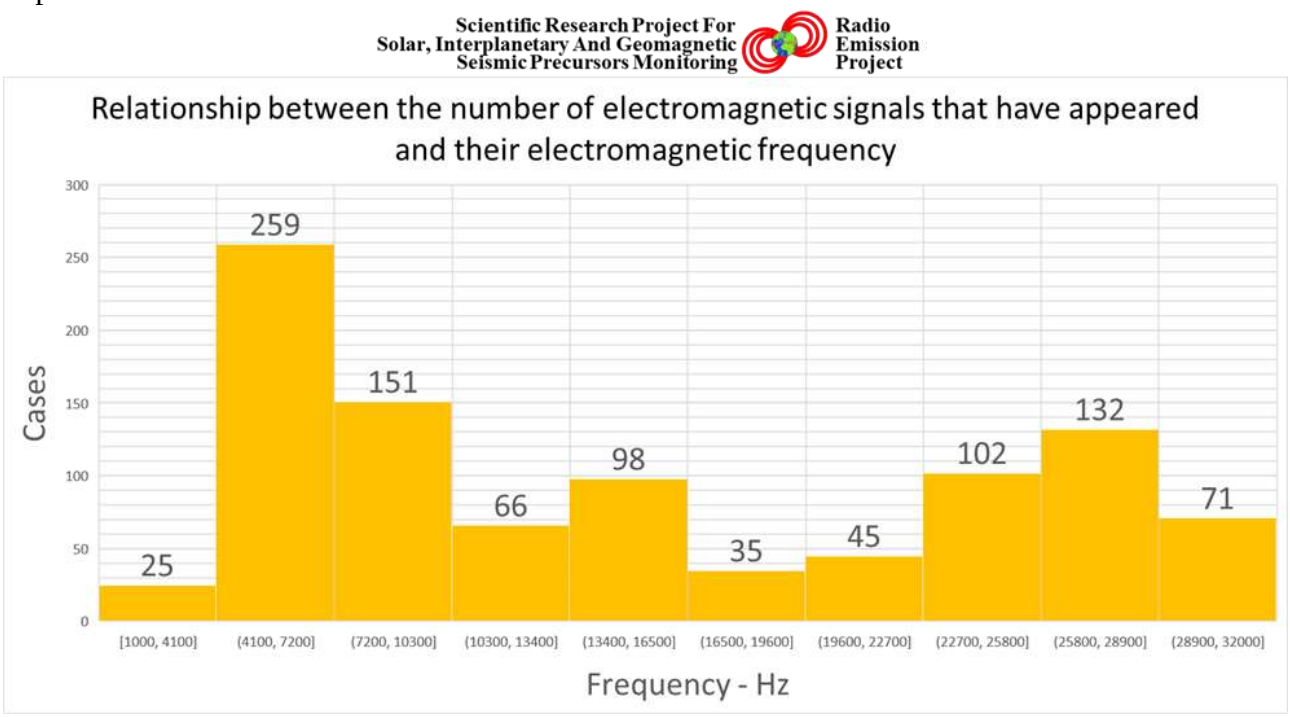

Fig. 11 - Frequency range of registered radio-anomalies and their grouping.

The graph confirms the principle of attenuation of radio wave propagation, given that the highest number of radioanomalies that have come to Italy, where the monitoring station is present, has exhibited a lower electromagnetic frequency.

Low-frequency electromagnetic signals are able to reach farther due to the reduced resentment of "Static Fading" due to absorption by oxygen and atmospheric water vapor (mostly at certain absorption peaks) and for effect of the "Reflection Fading" of the ground that produces reflected waves that are added, with different phases, to the direct wave creating interference and evanescence aleatory and not least due to the "Fading for Diffraction" due to the presence of physical obstacles. A higher frequency means a greater number of oscillations of the sinus wave that produces a greater effect of Fading on such frequencies.

The evidence of the experimentation of the RDF system in this area of the United States poses an obvious result already known by the mechanics of the physics of the propagation of electromagnetic waves. Given the distance, in fact, the type of ionospheric propagation is the propagation of radio waves that exploits electromagnetic reflection by the ionized atmospheric layer (conductor which is the ionosphere) allowing its propagation beyond the simple optical range between natural carrier and receiver, or beyond the limits imposed by terrestrial curvature. This is precisely the case with the monitoring of the New Madrid Fault.

3.5 Distribution of radio-anomalies

Interesting seems to be the distribution of radio-anomalies (with a total of 984 radio-emissions detected during the study) compared to the time of day, as shown in Fig. 11 and 12. They seem to be distributed mainly between 5 and 10 kHz and above 25 kHz. In many cases the radio anomalies were presented in broad band (those always indicated in Fig. 12 with frequency at 31 kHz), which appeared above all in the night time and in the time of maximum solar illumination.

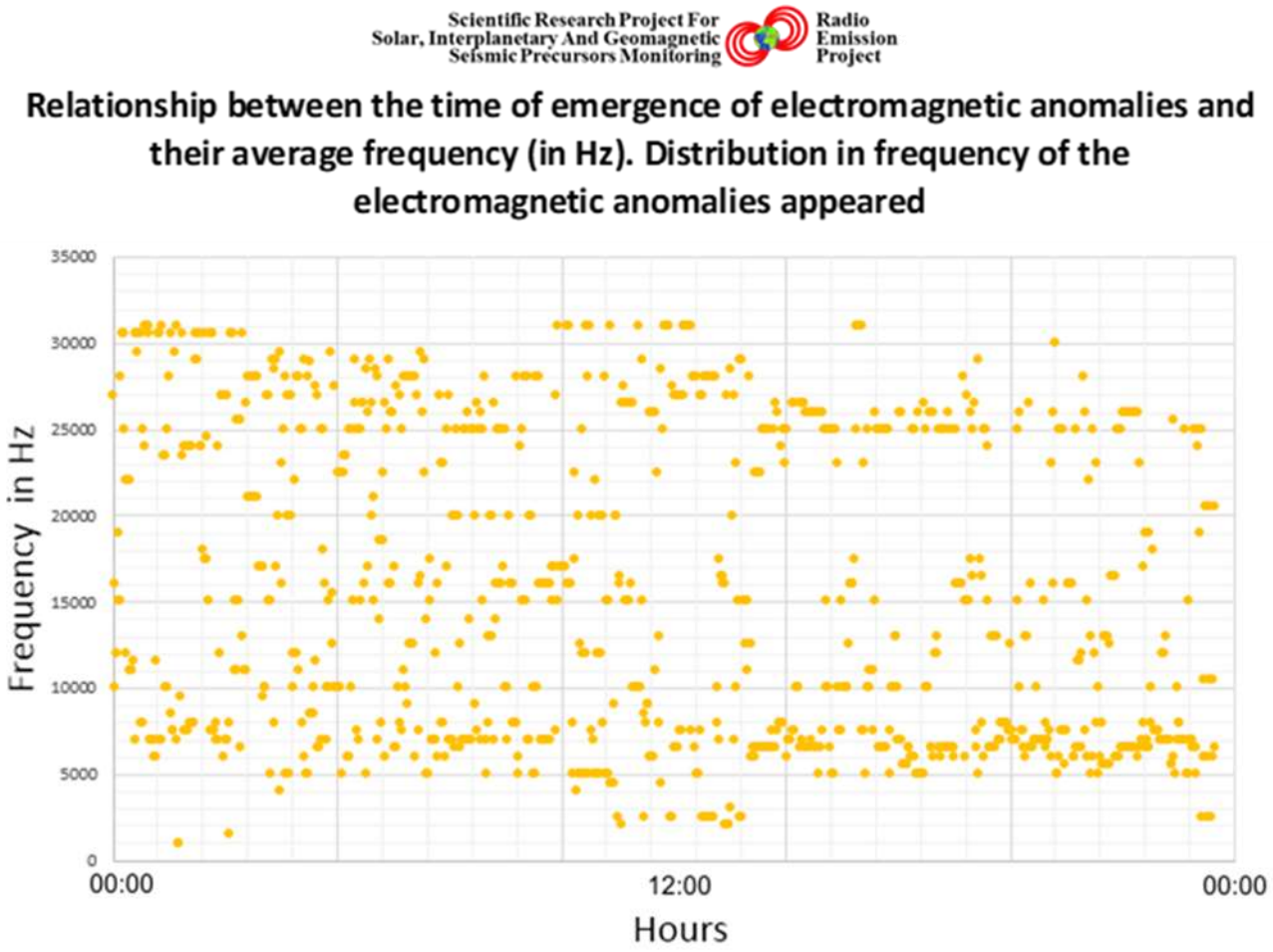

Fig. 12 - Distribution of radio-anomalies with respect to the hours of the day.

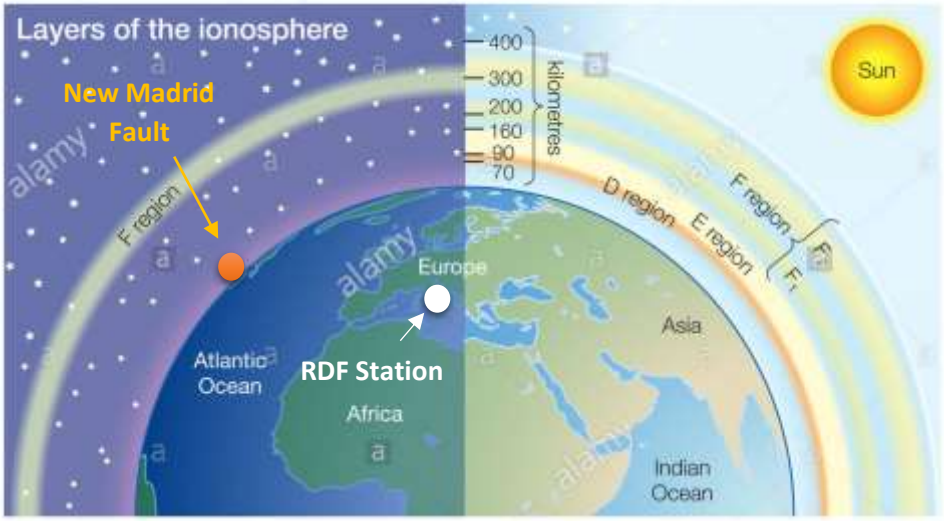

Fig. 13b – Schematic representation between the effect of solar irradiation and the formation of ionospheric Layers.

The variation of the ionospheric layers in relation to the signals received by the RDF system may have certainly influenced the recording of radio signals, coming from the US area under monitoring, on their frequency distribution and their number, with respect to the time of appearance.

3.6 Distribution of the rafio-anomalies respect to the months considered

Following are the graphs related to the study, which incorporate the data relating to electromagnetic signals (number of radio-anomalies and their frequency) and the appearance of earthquakes in the period considered.

Graph 1

Scientific Research Project For Solar, Interplanetary And Geomagnetic Seismic Precursors Monitoring — Radio Emission Project

Monthly

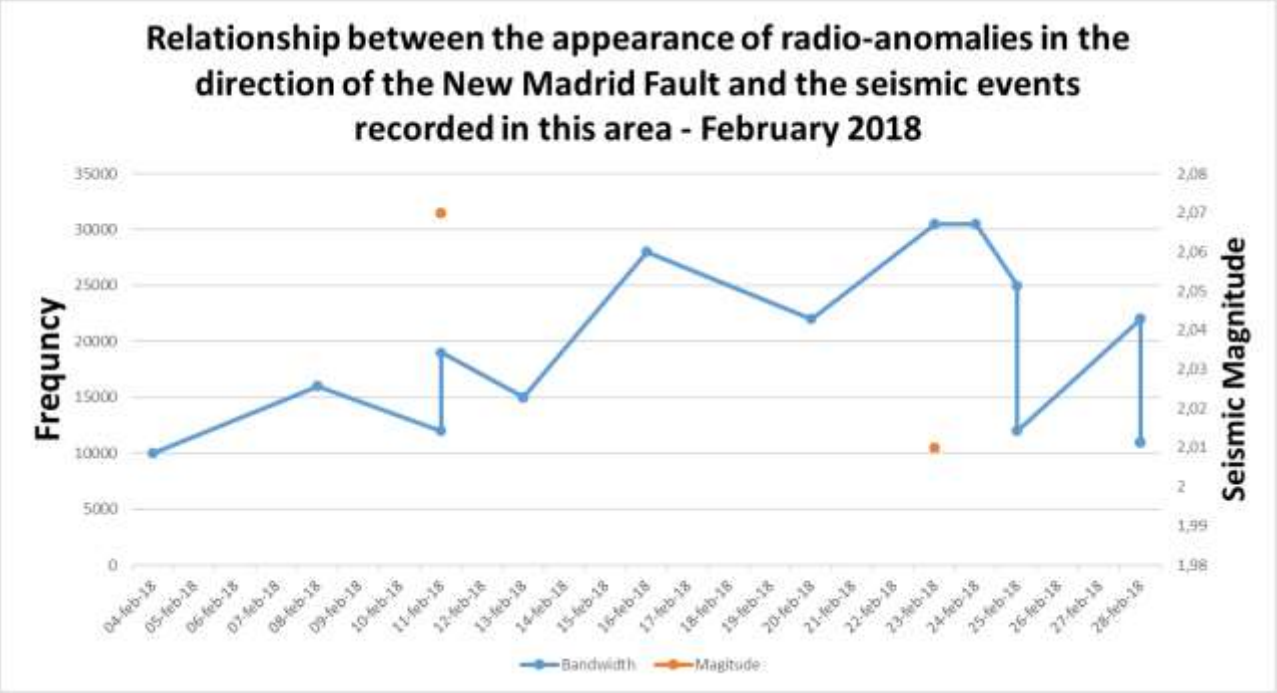

Graph 2

Scientific Research Project For Solar, Interplanetary And Geomagnetic Seismic Precursors Monitoring — Radio Emission Project

Monthly

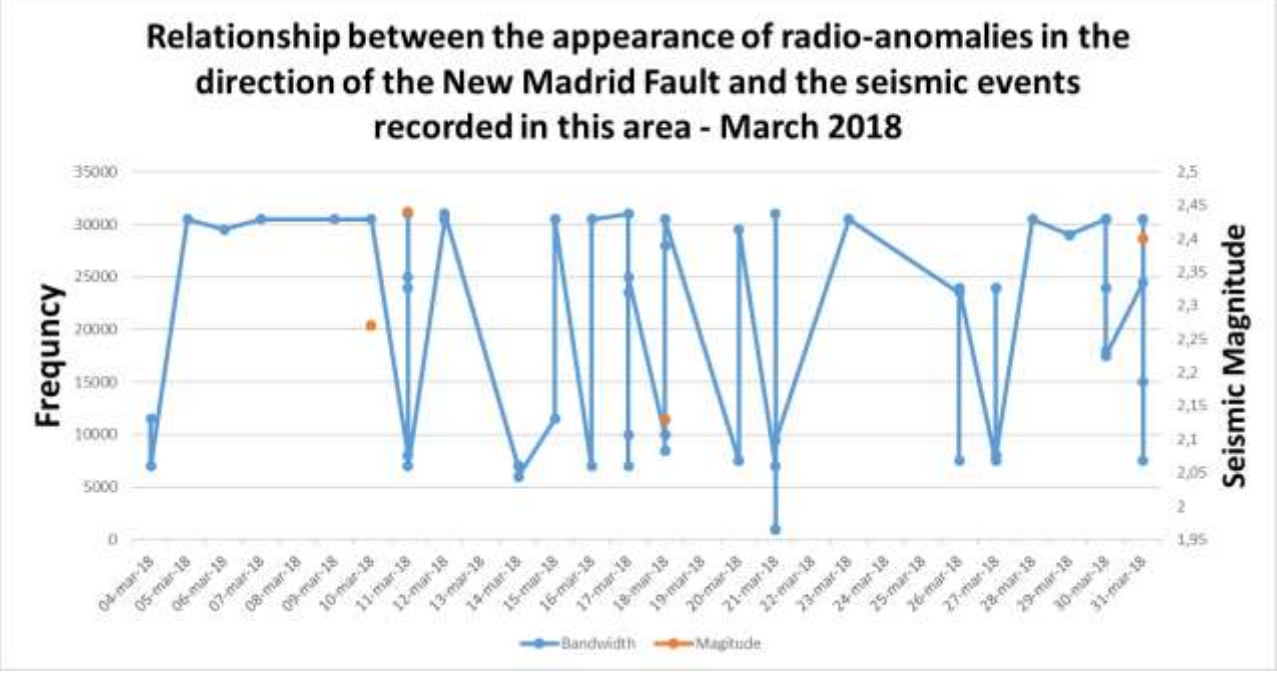

Graph 3

Scientific Research Project For Solar, Interplanetary And Geomagnetic Seismic Precursors Monitoring — Radio Emission Project

Monthly

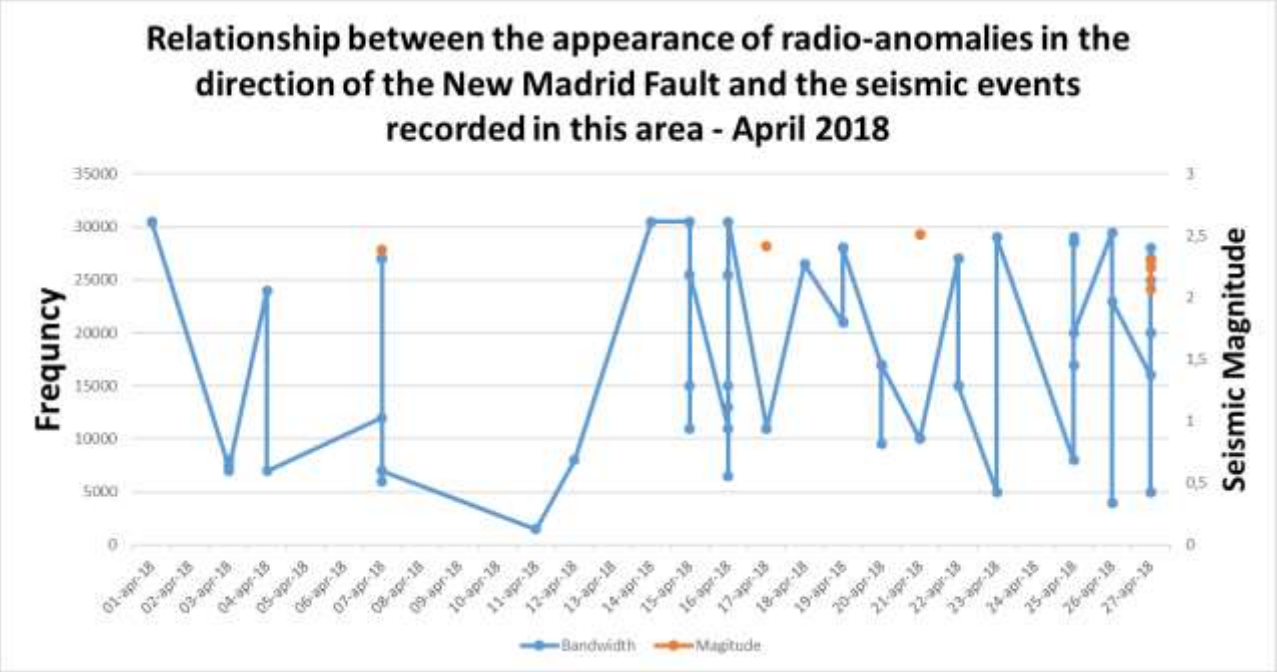

Graph 4

Scientific Research Project For Solar, Interplanetary And Geomagnetic Seismic Precursors Monitoring — Radio Emission Project

Monthly

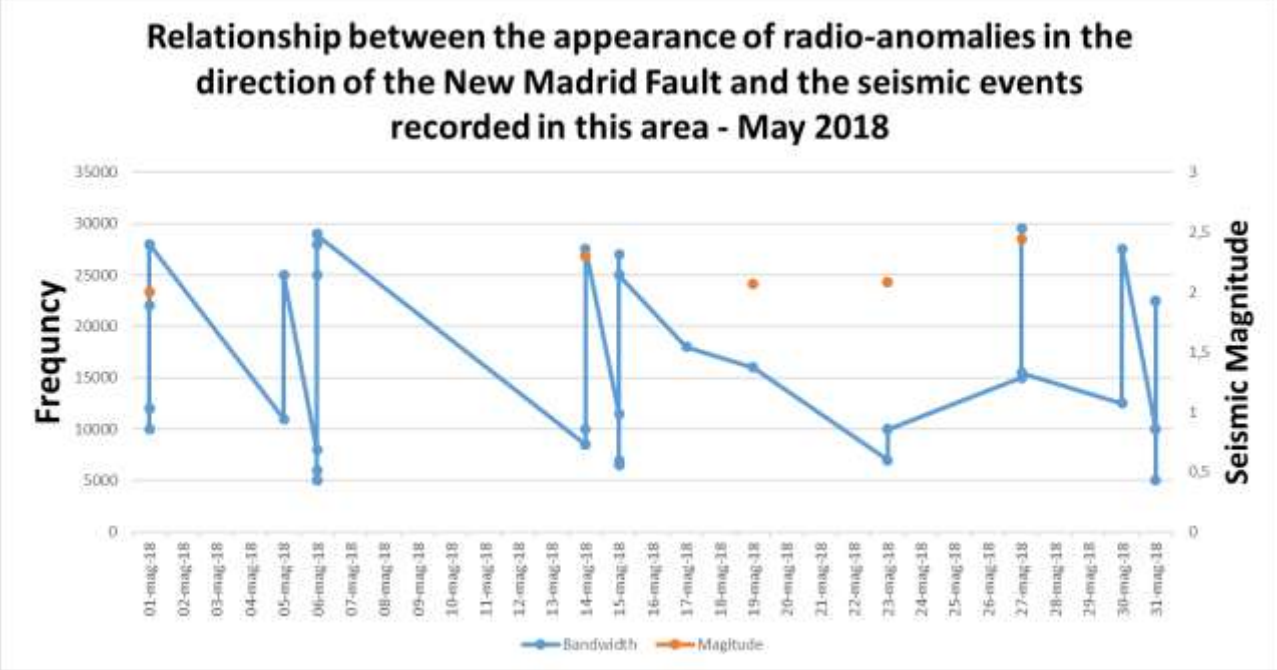

Graph 5

Scientific Research Project For Solar, Interplanetary And Geomagnetic Seismic Precursors Monitoring

Radio Emission Project

Monthly

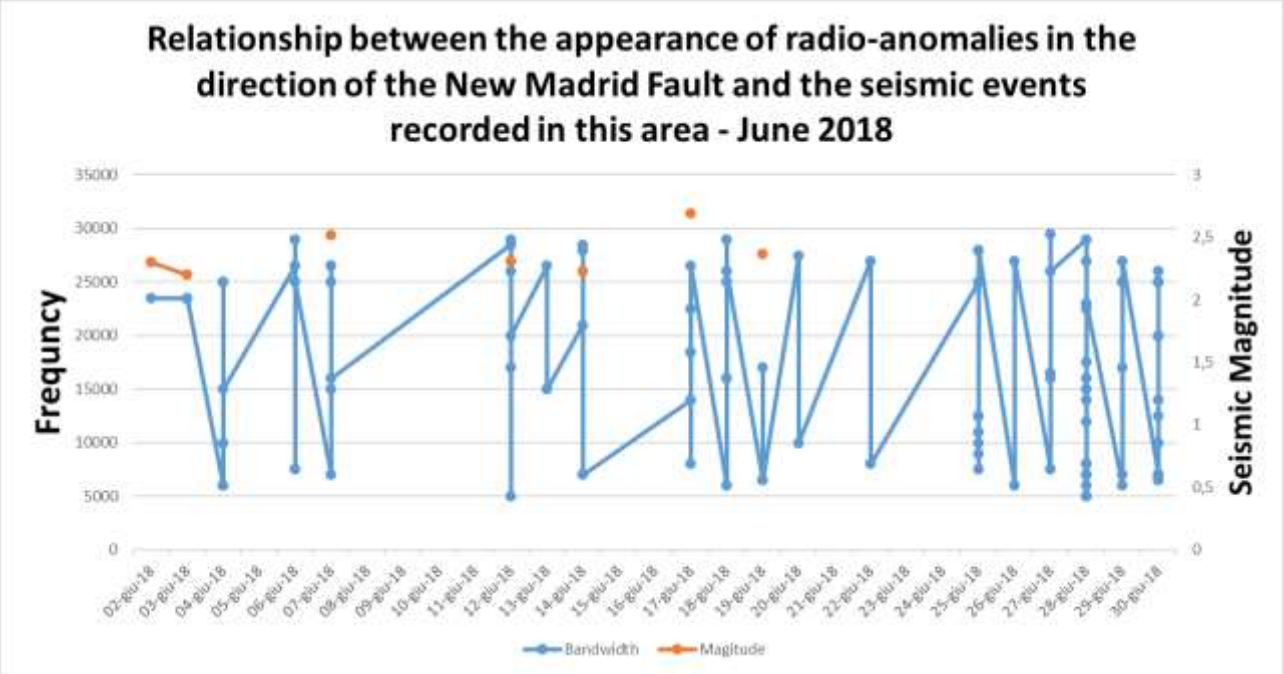

Graph 6

Scientific Research Project For Solar, Interplanetary And Geomagnetic Seismic Precursors Monitoring

Radio Emission Project

Monthly

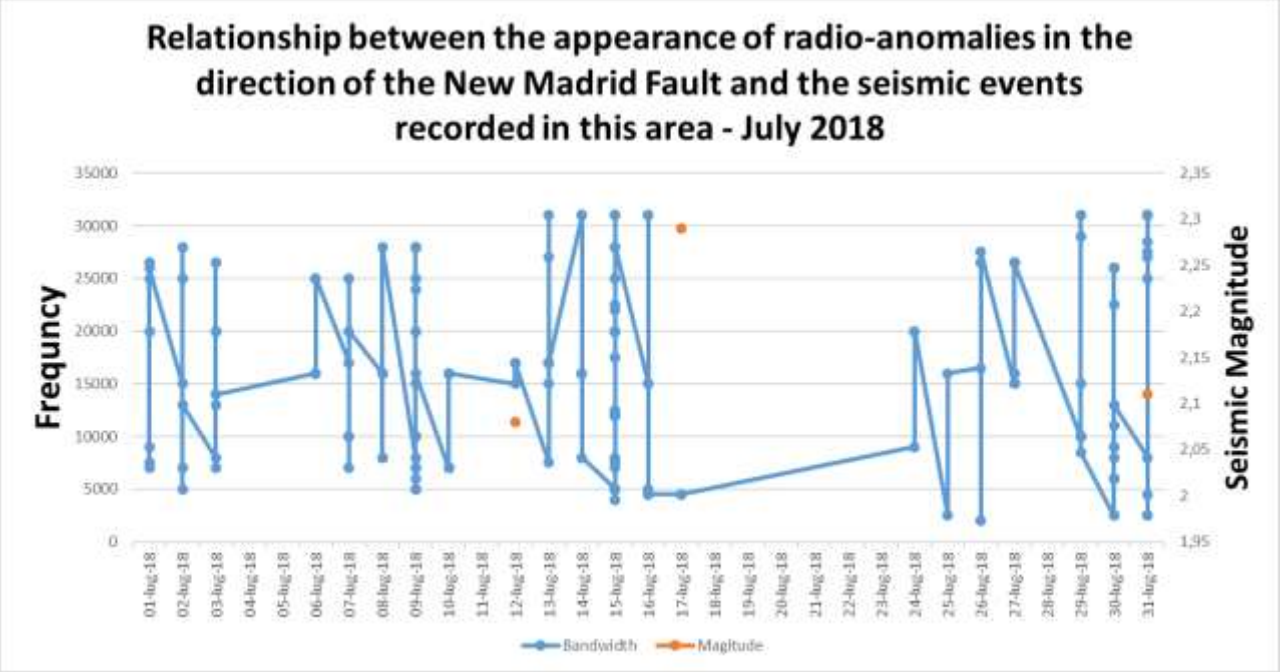

Graph 7

Scientific Research Project For Solar, Interplanetary And Geomagnetic Seismic Precursors Monitoring — Radio Emission Project

Monthly

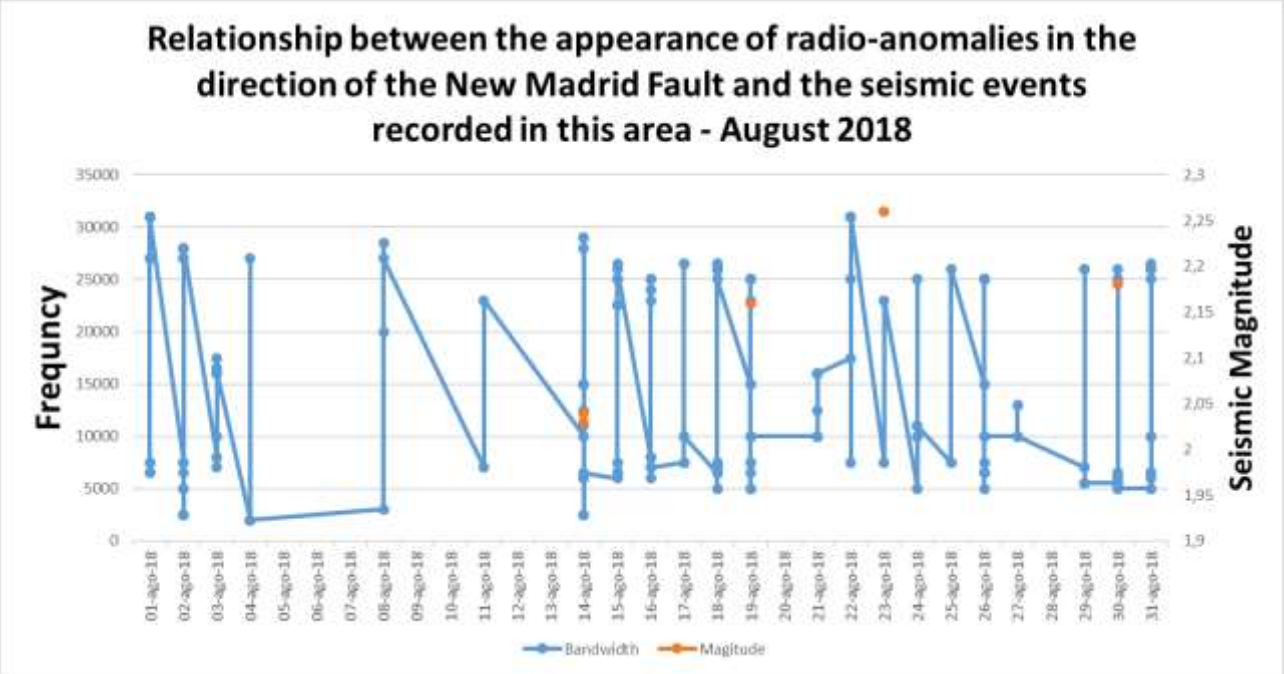

Graph 8

Scientific Research Project For Solar, Interplanetary And Geomagnetic Seismic Precursors Monitoring — Radio Emission Project

Monthly

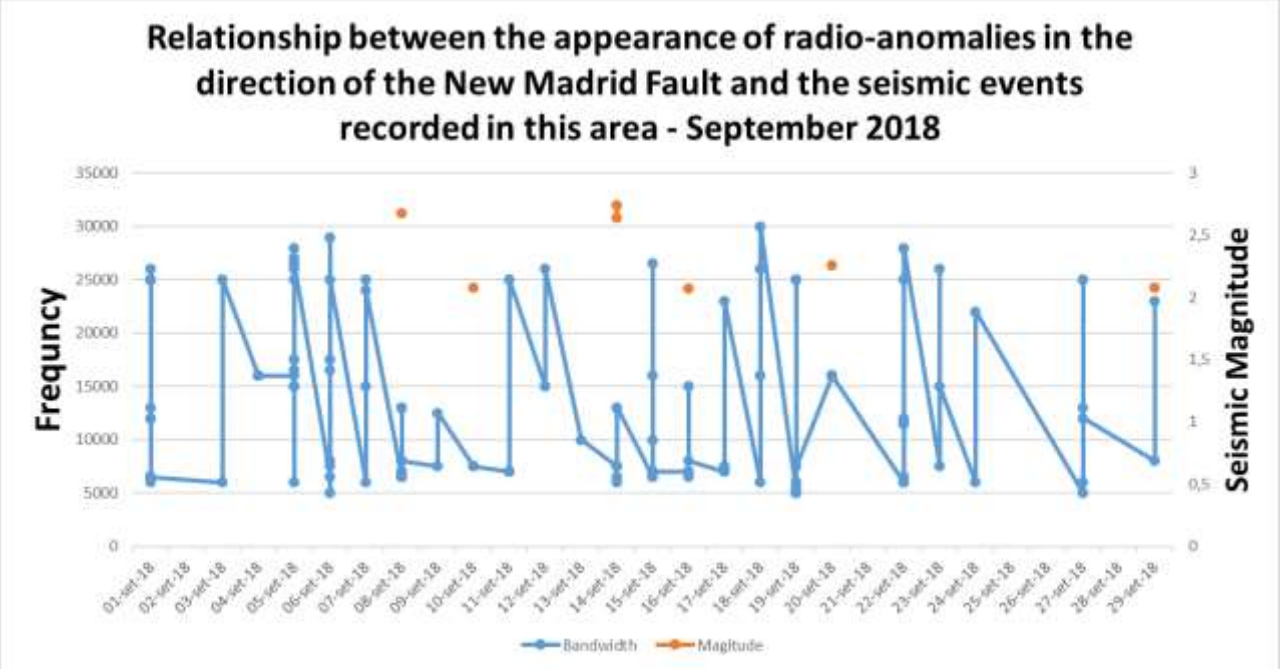

Graph 9

Scientific Research Project For Solar, Interplanetary And Geomagnetic Seismic Precursors Monitoring

Radio Emission Project

Monthly

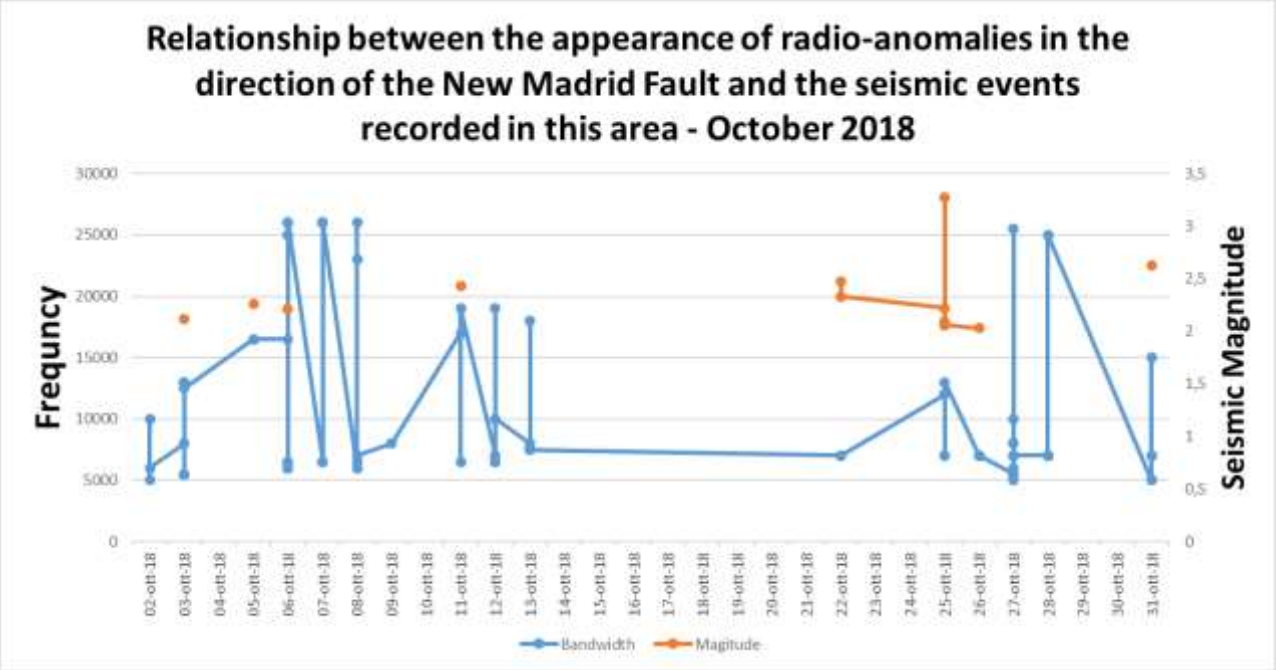

Graph 10

Scientific Research Project For Solar, Interplanetary And Geomagnetic Seismic Precursors Monitoring

Radio Emission Project

Monthly

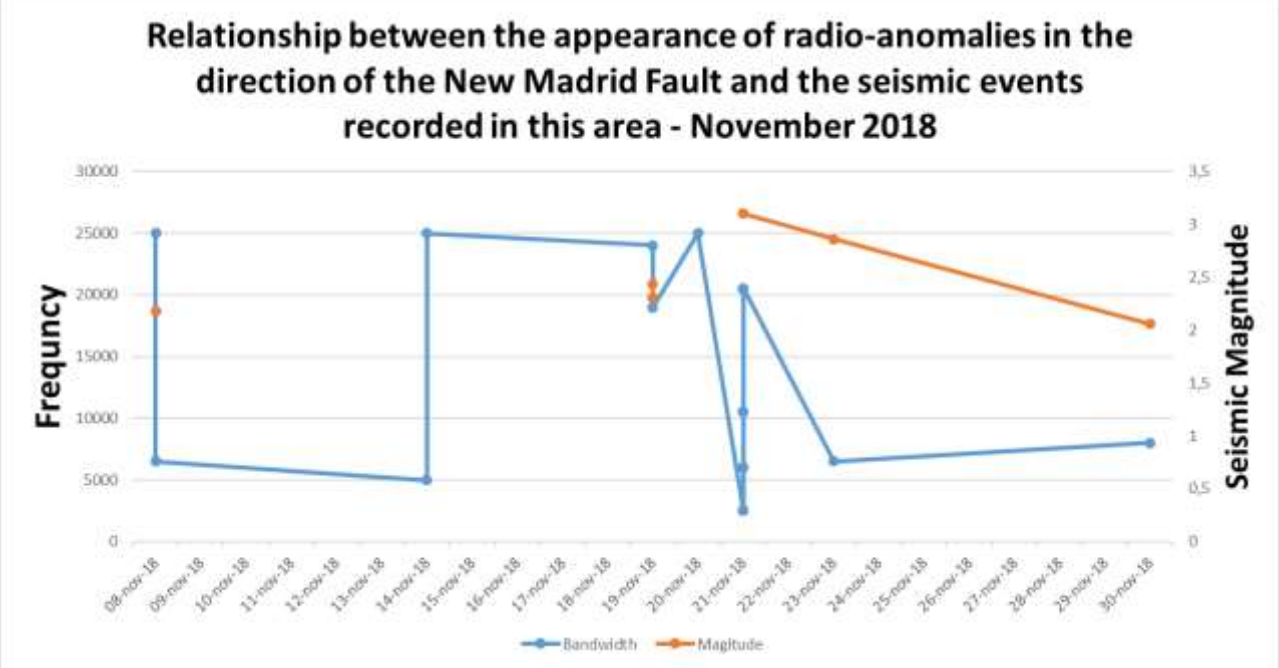

Graph 11

Scientific Research Project For Solar, Interplanetary And Geomagnetic Seismic Precursors Monitoring

Radio Emission Project

Monthly

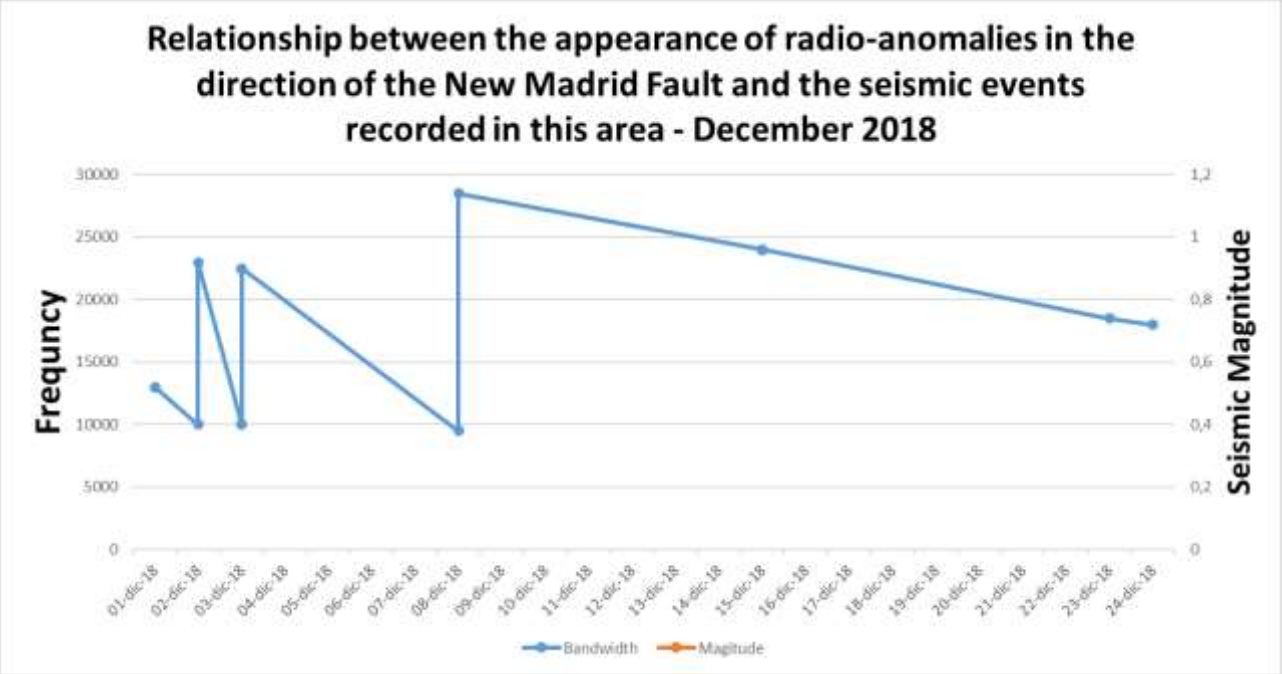

The monitoring of the New Madrid Fault area, clearly shows on the monthly charts, a close relationship between the increase in the number of radio-anomalies and the occurrence of more or less intense seismic events with magnitude M2.5 + of the Richter scale.

This indicates that the electromagnetic signals recorded by the RDF system are interesting, if we consider the seismic trend of the area, and this from a detection distance of more than 8500 km away.

4 Relationship between monitoring data and seismic events

Between February 2, 2018 and November 29, 2018, 57 Mw2.5 + magnitude earthquakes of the Richter scale were recorded in the area of the New Madrid Fault, in the same period of time during which the electromagnetic monitoring of the area from part of the RDF station in Lariano (Rome, Italy).

The data considered in this area concerned the magnitude and depth of earthquakes (Fig. 13), compared with the electromagnetic monitoring data of the Italian RDF station.

The aim was to understand whether there was a direct correlation between the observation and the appearance of radio-anomalies, their characteristics and the occurrence of such earthquakes.

The observation of these data (visible in Fig. 13) shows how the appearance of radio-anomalies and the occurrence of geophysical phenomena has a link. The data show that earthquakes of greater magnitude, are preceded by radio-anomalies that possess a lower electromagnetic frequency and vice versa, the lower magnitude earthquakes, are preceded by higher-frequency geomagnetic increments.

This evidence demonstrates that there are indeed phenomena of interaction between the geomagnetic variations recorded by the RDF system and the seismic events.

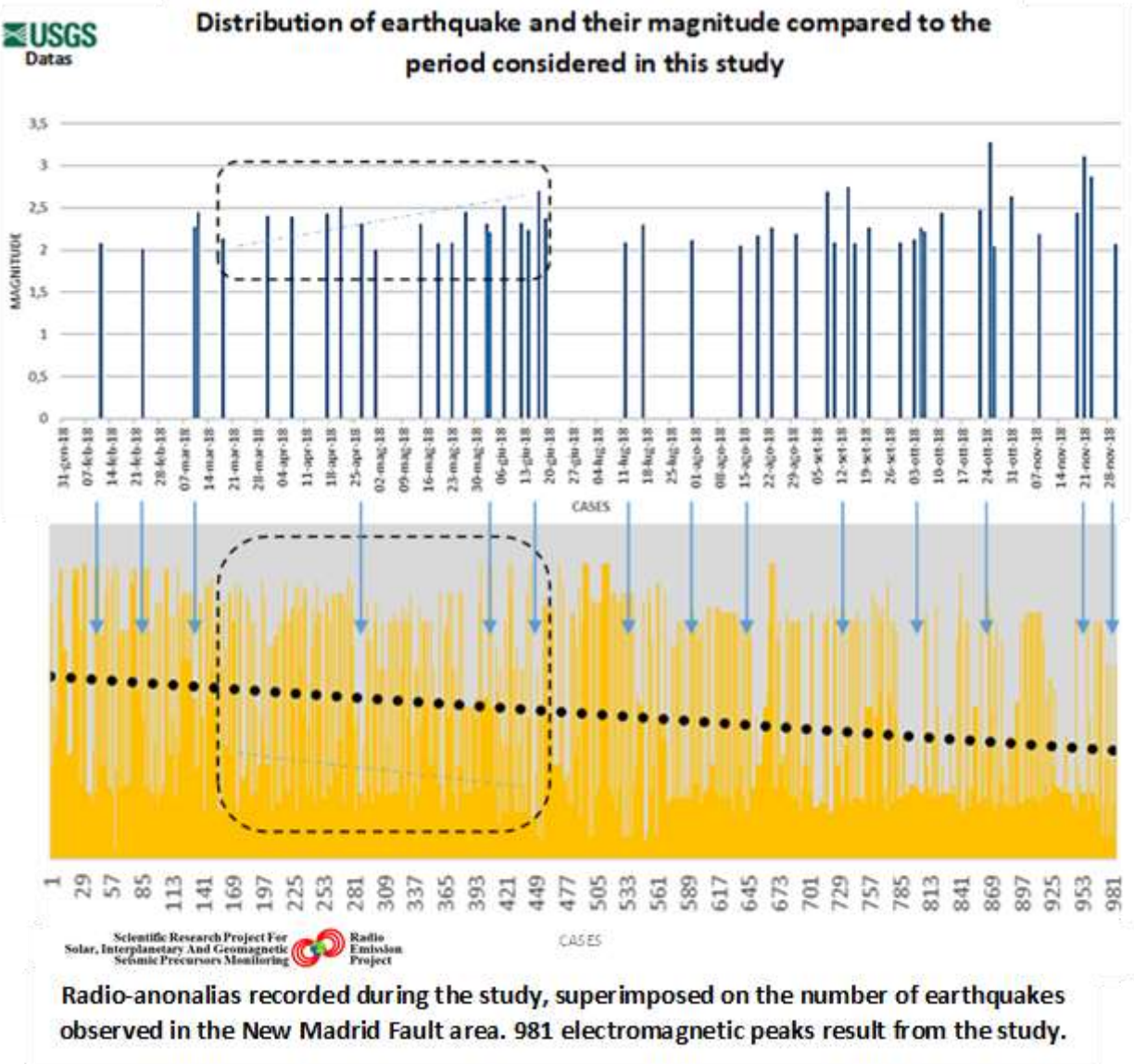

Fig. 14 - Correlation between the appearance of radio-anomalies, their frequency and the seismic events occurring in the New Madrid Fault.

The total of the signals recorded by the RDF system consists of 984 radio-anomalies (as already mentioned) that appeared during the study. The results are as follows:

- Groups of single signals or single very intense signals preceded the occurrence of earthquakes.

- Another important fact, emerged from the study, is that the impulsive appearance of electromagnetic phenomena was then followed by alternating seismic intensities, or by earthquakes with a magnitude that has changed little (see Fig. 13b). This last evidence could indicate impulsive accumulations of mechanical energy at the crustal level, which in a cadenced manner is released, giving rise to earthquakes having a similar magnitude.

- The data thus indicate a close influence between the electromagnetic frequency of the radio emissions detected by the Radio Emissions Project, preceding the low-intensity earthquakes detected in the same geographical area.

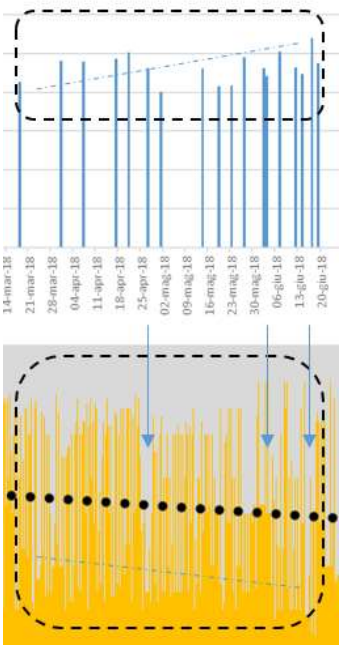

Fig. 13b - Impulsive signals with significant frequency variation and little temporal variation, precede magnitude of seismic events with low variations.

- The periods of considerable frequency variation of the electromagnetic signals always precede earthquakes of strong magnitude, this could always depend on the accumulation of mechanical energy at the crustal level which emits radio frequency. This high number of signals would in fact indicate a certain amount of energy in the lithosphere that within a certain time is then able to free itself giving rise to more intense earthquakes.

The evidence of this morphological behavior of radio-emissions, is for the first time visible thanks to the RDF system, which is able to filter all the signals that are polarized with the azimuth considered.

5 Conclusions

It is evident that the RDF system developed by the Radio Emissions Project has detected electromagnetic increments preceding low-magnitude telluric events in the same area of origin of the signals (dark violet azimuth). The data indicate that electromagnetic monitoring in this context is important for understanding the azimuth of origin of the pre-seismic signals and thus identifying the probable seismic epicenter.

This suggests that it is necessary and important to use two or more electromagnetic monitoring stations equipped with RDF technology in order to triangulate the epicentral emission source in a precise and global way. The study demonstrates how the frequency of radio-anomalies is associated with the seismic magnitude, such as its decrease or increase inversely proportional to the average electromagnetic frequency of the signals themselves. The periods in which there are many electromagnetic emissions always precedes earthquakes of a strong or greater intensity than the average of the period (see Fig. 13 and Fig. 13b).

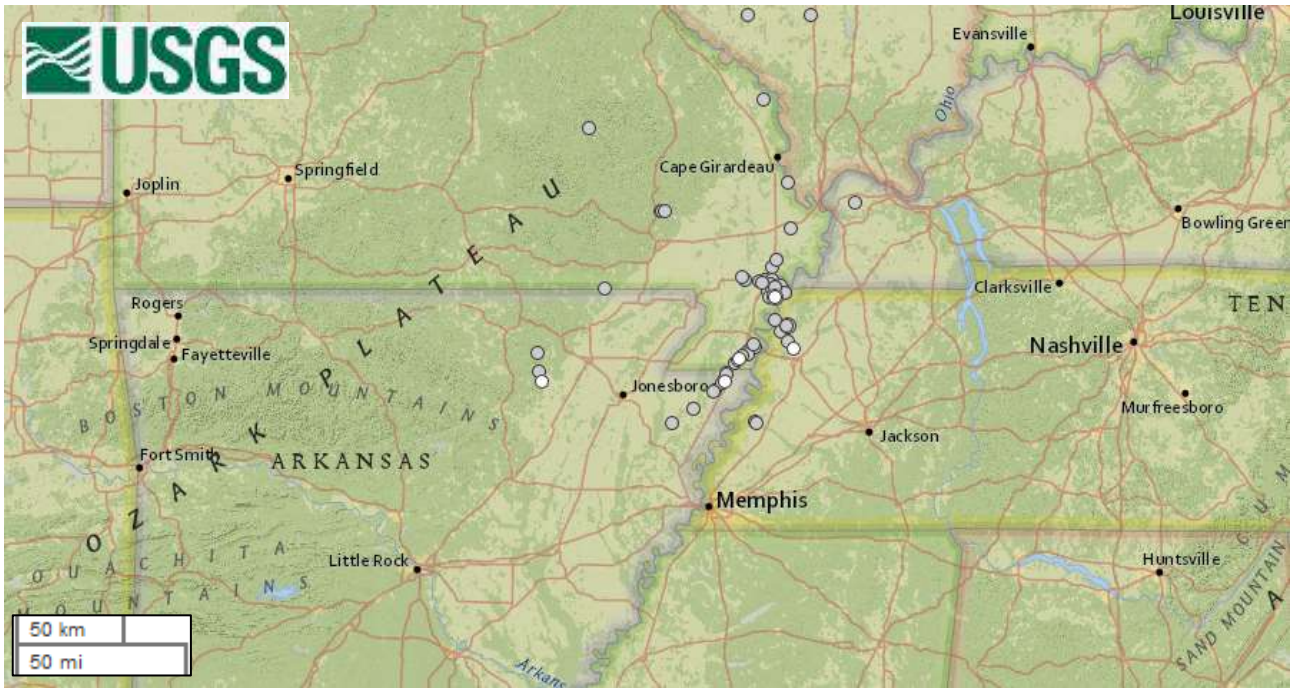

Figura 15 - Map of the North America relating to the New Madrid Fault, with its 57 earthquakes greater than Mw 2.5. Source: USGS.

It is also evident that solar activity has an important influence on the electromagnetic emissions detected with the RDF system. The study in this case has found that these emissions (their concentration in a given period of time) follow the Sunspot Number inversely proportionally, ie solar activity (Fig. 9 and Fig. 10).

References

- Cataldi, D., Cataldi, G. and Straser, V., 2017. SELF and VLF electromagnetic emissions which preceded the M6.2 Central Italy earthquake that occurred on August 24, 2016. European Geosciences Union (EGU), General Assembly 2017. Seismology (SM1.2)/Natural Hazards (NH4.7)/Tectonics & Structural Geology (TS5.5). The 2016 Central Italy Seismic sequence: overview of data analyses and source models. Geophysical Research Abstracts Vol. 19, EGU2017-3675.
- Cataldi, G., Cataldi, D. and Straser, V., 2017. Solar and Geomagnetic Activity Variations Correlated to Italian M6+ Earthquakes that Occurred in 2016. European Geosciences Union (EGU), General Assembly 2017. Geophysical Research Abstracts, vol. 19, EGU2017-3681. Seismology (SM1.2)/Natural Hazards (NH4.7)/Tectonics & Structural Geology (TS5.5) The 2016 Central Italy Seismic sequence: overview of data analyses and source models.
- Cataldi, G., Cataldi, D., Rossi, R. and Straser, V., 2016. SELF-ELF Electromagnetic signals correlated to M5+ Italian Earthquakes that occurred on August 24, 2016 and January 18, 2017. NCGT Journal, vol. 5, no. 1, p. 134-143.
- Straser, V., Cataldi, G. and Cataldi, D., 2015. Radio-anomalies: a tool for earthquake and tsunami forecasts. European Geosciences Union (EGU) General Assembly 2015, Natural Hazard Section (NH5.1), Sea & Ocean Hazard - Tsunami, Geophysical Research Abstract, vol. 17, Vienna, Austria. Harvard-Smithsonian Center for Astrophysics, High Energy Astrophysics Division, SAO/NASA Astrophysics Data System.
- Straser, V., Cataldi, G. and Cataldi, D., 2016. SELF and VLF electromagnetic signal variations that preceded the Central Italy earthquake on August 24, 2016. NCGT Journal, vol. 4, no. 3, p. 473-477. Harvard-Smithsonian Center for Astrophysics, High Energy Astrophysics Division, SAO/NASA Astrophysics Data System.
- Straser, V., Cataldi, G. and Cataldi, D., 2017. Seismic signals detected in Italy before the Nikol'skoye (off Kamchatka) earthquake in July 2017. NCGT Journal, vol. 5, no. 3, p. 391-396.
- Straser V., Cataldi D., Cataldi G., Radio Direction Finding System, a new perspective for global crust diagnosis. New Concepts in Global Tectonics Journal, v.6, no. 2, June 2018, p. 203-211.
- Choi, D.R., Casey, J.L., Leybourne, B. and Gregori, G.P., The January 2018 M7.5 offshore North Honduras earthquake: its possible energy link to the New Madrid Seismic Zone, Mississippi Valley. NCGT Journal, 2018, v. 6, no. 1, p. 21-36.
- Choi, D.R. and Casey, J.L., New Madrid Seismic Zone, central USA: the great 1811-12 earthquakes, their relationship to solar cycles, and tectonic settings. Global Climate Status Report, 1-2015. Space and Science Research Corporation.
- Morgan T. Page and Susan E. Hough, The New Madrid Seismic Zone: Not Dead Yet. Science 2014, vol. 343, Issue 6172, pp. 762-764. DOI: 10.1126/science.1248215

The Potential of Biotic and Abiotic Hydrocarbons in Karakoram, Pakistan

Haleem Zaman Magsi
ORIC, Karakoram International University, Gilgit 15100, Pakistan
Corresponding author: e-mail: zamanhaleemmagsi@gmail.com

Abstract:

The Karakoram is a zone of Alpine -Karakoram Folded System and covers area between Eastern Hindu Kush, Pamir, Qiangtang Terrane and Kohistan-Ladakh Arc. Karakoram composed of sedimentary and crystalline complex from Precambrian to Pliocene age. The assessment of formation indicates the presence of geosyncline in Ordovician. Where occur weak Hurricane orogeny and develop rift in the Carboniferous - Permian time. This rift converts into Cimmerian Folded System which move towards Kirthar –Suleiman geosyncline. Therefore, Karakoram linked with Alpine-Himalayan folded Belt and experienced block fault tectonic processes. The presence of the coal, carboniferous shale, carbonate and clastic rocks in Northern Sedimentary Zone and crystallization and recrystallization processes in the Axial and the Southern zone allows to envisage potential of biotic and abiotic hydrocarbon in Karakoram. The palaeotectonic condition of development of Karakoram illustrates presence favourable environment of biotic and abiotic hydrocarbons in Karakoram. The sedimentary layers are source of biotic hydrocarbons. The abiotic hydrocarbons are result of geodynamic processes in upper mantle and upper crust. The semi –graben and graben structures can be a potential Oil and Gas Reservoirs. However geochemical studies will determine the total organic carbon, a factor to evaluate the volume of biotic hydrocarbons. The survey of zones of the crystalline and recrystallize rocks will elucidate the volume of the abiotic hydrocarbons in Karakoram.

Keywords: *Biotic and Abiotic Hydrocarbons, Microbiological Fractionation, Kinetic Fractionation, Graben, Reservoirs, Source of Hydrocarbon*.

Introduction:

Hydrocarbon reservoirs form the basis of socio-economic stability of a country. Therefore, every country searches for additional hydrocarbons reservoirs within its national borders. Both biotic and abiotic sourced hydrocarbons form the target of petroleum exploration surveys over the world. Despite abiotic hydrocarbons, including methane hydrates, forming the sources of many of the commercial oil and gas fields in the world, petroleum exploration in Pakistan still only focuses on biotic hydrocarbons in previously recognized sedimentary basins (Bender and Raza 1995, Kadri 1995, Kazmi and Jan 1997 and Hasany et al., 2007). The specialists even inadequately address exploration of biotic hydrocarbons beyond the already established producing basins despite the outcrops of sedimentary sequence of Karakoram resembling the oil and gas source rocks in the Alpine - Himalayan Fold System part of Pakistan (Magsi 2018). Areshev (1992), Breshkuntsov (2011), Dmitriyesvskii (1993), Kalan (1994), Muslimov et al., (2004), Plotnikova (2006), and Schuster and Punanova (2014) evaluate crystalline basement reservoirs as producing Oil and Gas in the world, (Figure 1a and b).

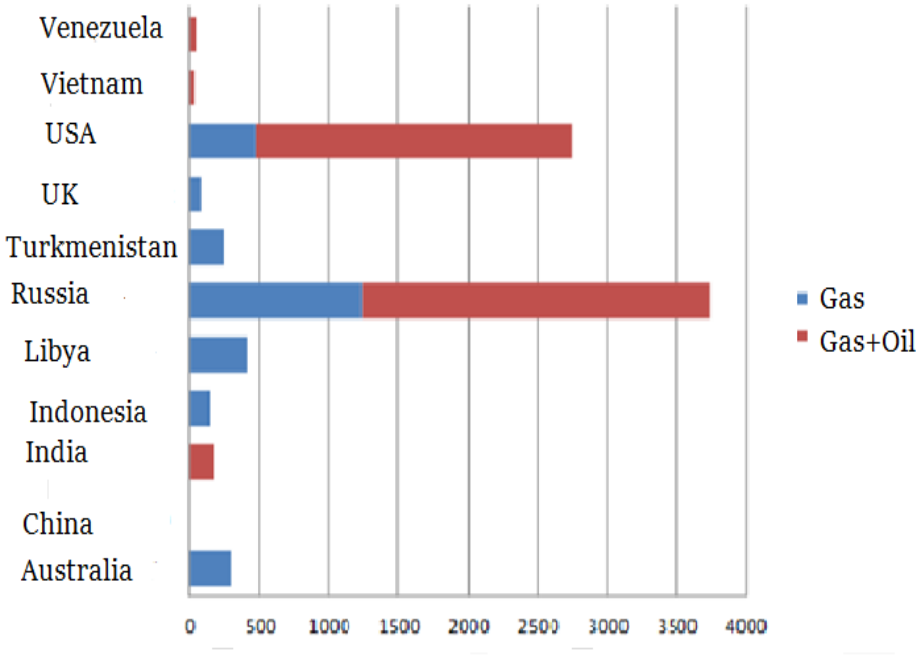

Figure 1 a. Gas Producing Crystalline Reserviors

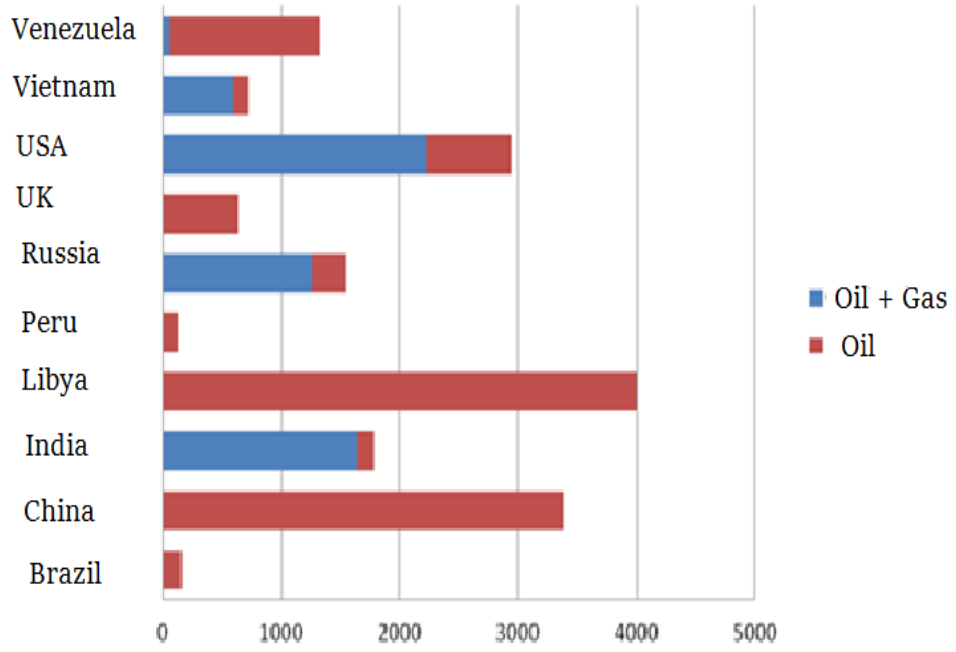

Figure 1. b. Oil Producing Crystalline Reserviors

Perhaps doubt in the concept of crystalline rocks as biotic hydrocarbon reservoirs, and deep geodynamics processes as source of abiotic hydrocarbon is temporizing exploration of additional reservoirs in Pakistan. Muslimov et al., (2004), Plotnikova (2006), Shuster and Punanova (2014) appraise the role of sedimentary cover in generation and accumulation of biotic hydrocarbons in the crystalline basement in Russia. According to Muslimov (2004), Plotnikova (2006) vertical migration

of hydrocarbons form petroleum pools in sedimentary and crystalline basement reservoirs. Halimov (2012) elucidates various geological characteristics of some famous crystalline basement hydrocarbon reservoirs and assumes the possibility of biotic origin hydrocarbons and also refers to the presence of the abiotic hydrocarbons.

McCollom (2013) define sources of the abiotic hydrocarbons in the earth's crust which migrate from deep sources of earth's crust through different channels. The deep-seated faults (Belousov 1976) which disturb the Moho-Discontinuity (Belousov et al., 1979) could be a possible channel of migration of methane. Yue (2013) also postulates the presence of methane gas in the upper mantle, which initially accumulates at the Moho-Discontinuity and migrates upwards to secondary reservoirs in the earth's crust. Sephton and Hazen (2013) base their conclusions on experimental, theoretical and field evidence supporting an abiotic origin of deep hydrocarbon deposits. The inorganic reduction of the carbon probably occurs during granitization and metamorphism processes (McCollom 2013) during endogenic processes of earth's crust formation (Dedeev and Kulikov 1980). In opinion of Yiwen et al., (2015) the unconventional (abiotic) oil deposit is approximately 6200 X 10^8 tonnes and gas deposit is 4000 x 10^{12} m^3 in the world.

The assessment of the available literature on biotic and abiotic hydrocarbons encourages the evaluation of the possibility of biotic and abiotic hydrocarbons occurring in the Karakoram Cimmerian Mega-anticlinorium, comprised of a Precambrian – Pliocene sedimentary - crystalline complex (Desio 1979, Faisal et al., 2015, Gansser 1964, Heuberger 2004, LeFort et al., 1994, Kravchenko 1979, Searle 1992, 1999, Searle and Philips 2007, Ronald et al., 2002, Zanchi and Gaetani 1996,2011). The correlation of the palaeotectonic conditions of deposition of the hydrocarbon producing sedimentary rocks of the Alpine- Himalayan folded system of Pakistan with the Karakoram zone of the Alpine-Karakoram Folded System (Desio 1979, Gattinger 1961, Schneider 1959,1960, Magsi 1983) and consideration of the geodynamics processes of Karakoram zone, allows the possible presence of biotic and abiotic hydrocarbons in the Karakoram zone. However, the determination of the total organic carbon requires the calculation of the volume of possible hydrocarbons in sedimentary sequence and in addition the measurement of the emission of methane in corresponding structures, for the estimation of total volume of potential abiotic hydrocarbon volumes in the Karakoram Zone.

Tectonics of the Karakoram Zone:

The Karakoram Cimmerian Mega-anticlinorium, (Khain et al., 1973, Zanchi and Gaetani 2011), is a zone of the Alpine-Karakoram folded system (Desio 1979, Gattinger 1961, Schneider 1959,1960 and Magsi 1983). The concave shape of the Karakoram Cimmerian Mega-anticlinorium stretches between Eastern Hindu Kush, Pamir, Qiangtang Terrane and Kohistan -Ladakh Arc (Fig.2) where the Tirich Boundary Zone, Kilik Thrust Fault, the Karakoram dextral Strike-slip fault and the Karakoram-Kohistan Suture Zones serve as the boundary between the Karakoram and adjoining tectonic elements respectively (Desio 1979, Faisal et al., 2015, Gansser 1964, Heuberger 2004, LeFort et al., 1994, Kravchenko 1979, Searle 1992, 1999, Searle and Philips 2007, Zanchi and Gaetani 1996,2011). The author still considers the Karakoram as a zone of Alpine – Karakoram folded system (Desio 1979, Schneider 1959,1960, Magsi 1983). The detail reasons for such a link will be evaluated elsewhere in the article The Fault Tectonics of Karakoram (in preparation).

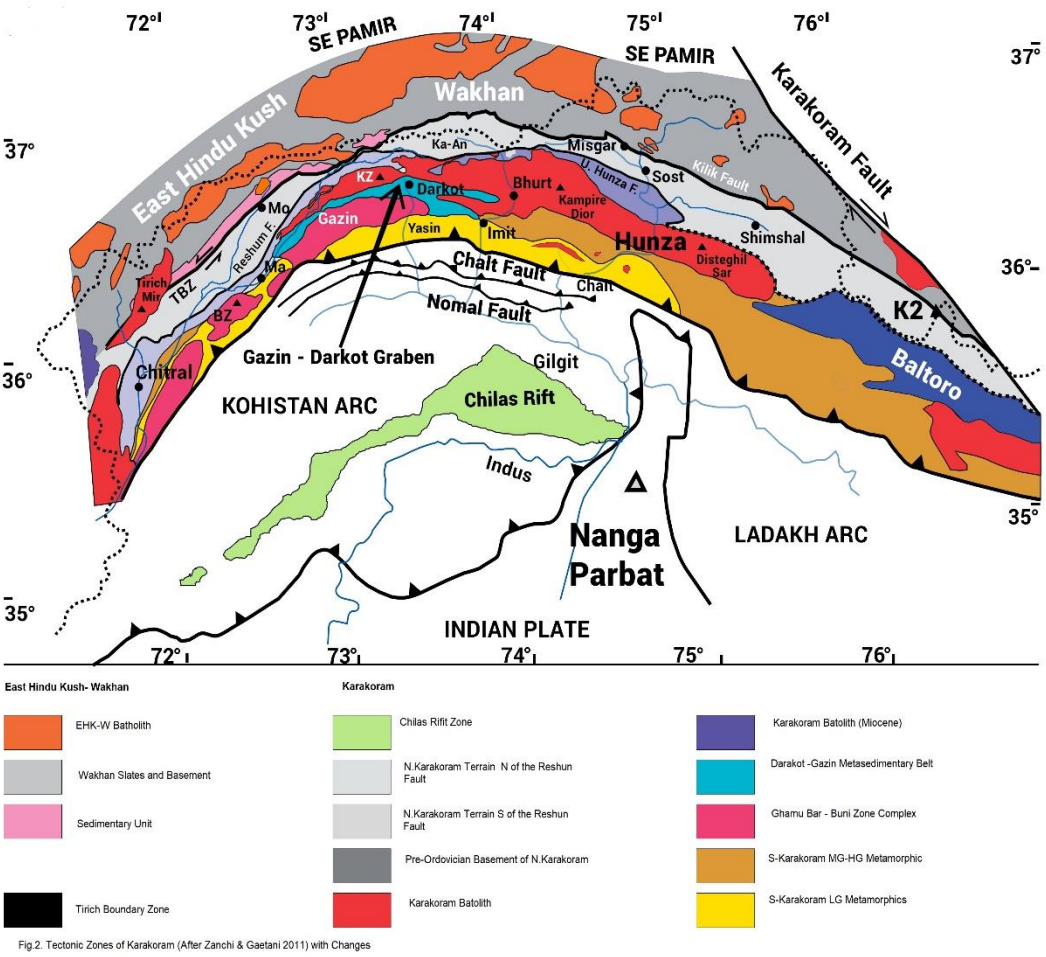

Fig.2. Tectonic Zones of Karakoram (After Zanchi & Gaetani 2011) with Changes

Figure 2 Tectonic map of Karakoram (after Zanchi and Gaetani 2011 with changes

Gansser (1964) and Desio (1979) divided the Karakoram Cimmerian Mega-anticlinorium into three zones: (a) Northern Sedimentary Zone (b) Axial (batholithic) Zone and (c) Southern Metasedimentary Zone. While Zanchi and Gaetani (2011) split the axial zone into a Karakoram batholithic unit and Ghamu Bar unit, where the Ishkoman graben divides the axial zone (Gaetani (2015). Whereas the Southern Metasedimentary Zone is divided into the Darakot -Gazin metasedimentary zone and the Southern Metamorphic zones. The Reshun – Upper Hunza fault (Zanchi and Gaetani 2011) is also an important tectonic element which controls the tectonic activity of the Northern Sedimentary Zone and Axial (batholithic) Zone of the Karakoram.

The northern sedimentary zone is composed of clastic and carbonate including coal, with minor magmatic rocks of Ordovician to Cretaceous age (Gaetani et al., 1997, Gaetani et al., 1996, Pudsey et al., 1985, Tahirkheli et al., 1990, Zanchi and Gaetani 1996, 2011). The axial zone and southern metasedimentary zone consist of Precambrian basement, Cambrian – Pliocene plutonic, metamorphic and metasedimentary rocks and Cambrian - Ordovician Sedimentary rocks (Gaetani 1997, LeFort et al., 1994, Palin et al., 2012, Ronallad et al., 2002, Searle et al., 1992, 1999, Tahirkheli et al., 1990, Zanchi and Gaetani 1996,2011). According to Le Fort et al., (1994), sediment deposition starts with a relatively shallow sea facies of Ordovician and part of Silurian in Karakoram, that successively changes to deep sea facies with the accumulation of bathyal deposits during the Carboniferous in the Karakoram (Khain and Limonov 2004). Kravchenko (1979) postulates the occurrence of significant subsidence in the Late

Carboniferous to form a miogeosyncline filled with volcanic and carbonate sediments and after a passage of time, clastic sediments. The new tectonic stage starts during the gradual transition from Permian to Triassic on the weak Henrician orogeny area (Khain and Limonov 2004), The Permian - Triassic complex is considered as a Cimmerian folded system (Khain 2000, Khain and Limonov 2004, Zanchi and Gaetani 2011). The platform carbonate conditions developed in the Upper Triassic and continued in some places during the Jurassic period (Khain 1979). While general uplift and flysch accumulation starts in the Jurassic period. Cretaceous - Paleogene sedimentation was completed by the Alpine orogeny with the intrusion of granitoid plutons and the metamorphism of the sediments in the Eocene – Miocene period. The Cretaceous period was represented by the intrusion of a giant batholith. The last orogeny started in Miocene to the present when the Karakoram was intensively uplifted. Gaetani (2015) and Zanchi and Gaetani (2011) link above-mentioned tectonic evolution of Karakoram as a Peri-Gondwana fragment, which separate from Gondwana and collided with Asian Plate. But paleotectonic condition (fig.3) of the Late Henrician – Early Gondwana phase (Khain 1979) and Proterozoic Era Structures around Karakoram (fig.4) covering Alpine – Himalaya Folded Belt (Arsentyev et al., 1978) illustrate Karakoram acritarch with Central Asia (Le Fort et al., 1994) before development of rift in Late Carboniferous -Triassic (Kravchenko 1979).

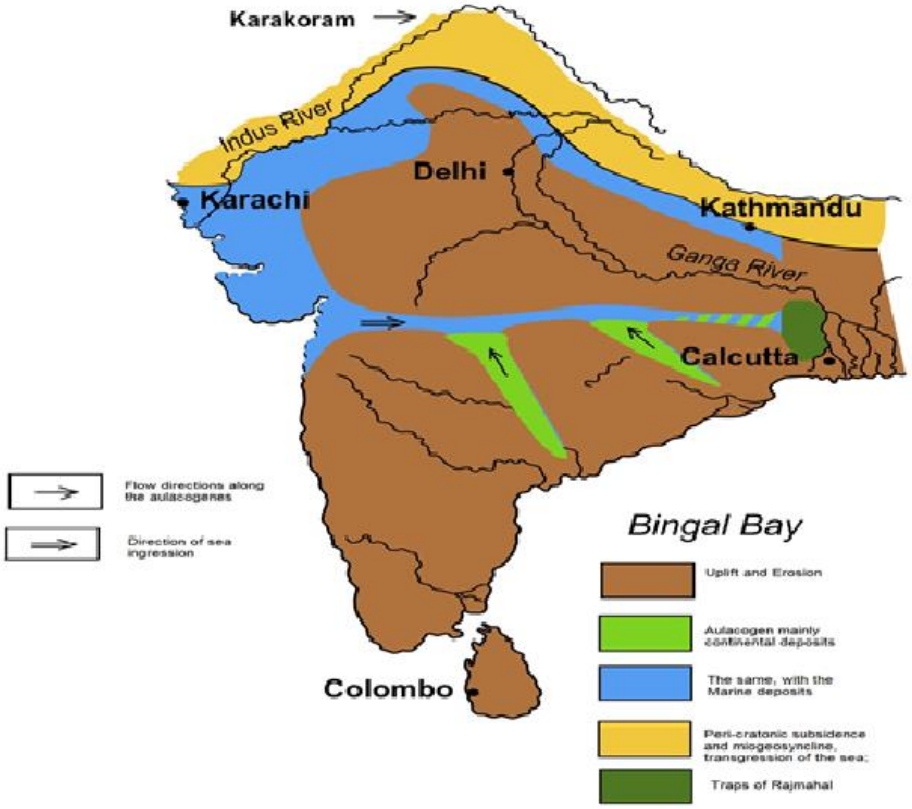

Figure 3 Paleotectonic Map of Pak-Indian Platform (after Khain 1979 with changes)

The massif experiences complex deformation (regeneration) phases since Neoproterozoic time (Arsentyev et al., 1978, Khain 2000, Khain and Limonov 2004). The concept of Pak – Indian Peninsular unit near to Asia (Crawford 1979), absence or shallow Tethys sea (Smoot 2007,2018) and opening of Indian ocean in Carboniferous-Early Permian (Leichenkov 2013) decline plate tectonic evaluation model of Karakoram as a Peri-Gondwana fragment (Gaetani 2015, Zanchi and Gaetani 2011). The

geosyncline model of tectonic development support possibility of biotic and abiotic hydrocarbons in Karakoram.

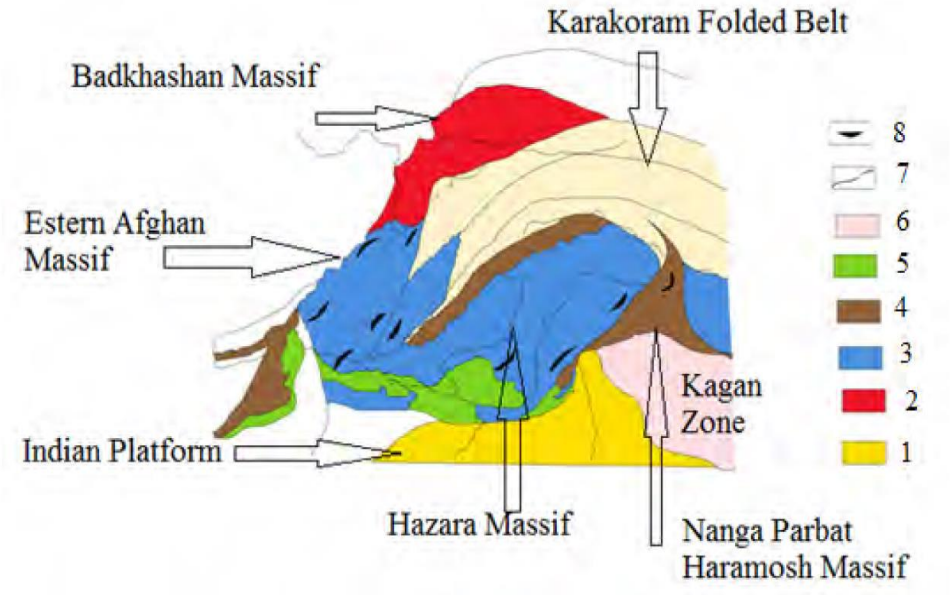

Figure 4. Proterozoic Era Structures around NPHM (after Arsentyev et al., 1978). 1. Indian Epimidproterozoic Platform, 2. Mesoproterozoic Central Massifs, 3. Early Neoproterozoic Central Massif, 4. Early Neoproterozoic Regenerated Central Massif, 5. Phanerozoic Sedimentary Cover, 6. Mesozoic- Tertiary Folded Belts, 7. Faults, 8. Axis of folded Structure.

Discussion and Conclusion:

The general concept describes hydrocarbon is of biotic origins. The sediments with organic material and atmosphere gases undergo biological, microbiological and kinetic fractionation and isotopic differentiation mechanism to produce the biotic and abiotic hydrocarbons (Galimov 1989). Figure (5) illustrates the distribution of the stable isotopes of biotic hydrocarbon at different level including exchange fractionation zone and abiogenic synthesis, the sources of abiotic hydrocarbons in deep earth's crust.

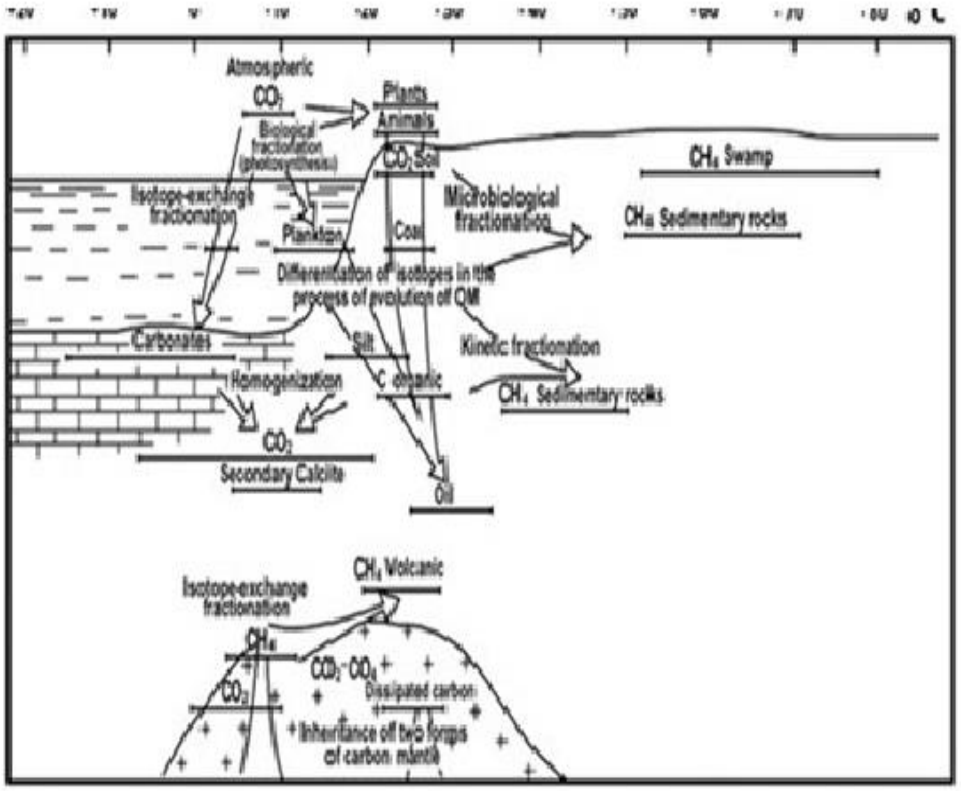

Figure 5. The Model of microbiological and Kinetic fractionation of sediments and geodynamic fractionation to produce biotic and abiotic hydrocarbons (after Galimov 1989)

The microbiological and kinetic fractionation and abiogenic synthesis allows the belief that sources of hydrocarbon in the earth are organic present remains in rocks (Kantorovich 1998) or polycondensation synthesis reactions occurring deep in the earth's crust, where carbon and hydrogen oxides are present in fluids and gases. Accordingly, a working hypothesis that hydrocarbons are a polygenic structure, and form from both biogenic and abiogenic generating mechanisms (Dmitriyesvskii et al., 1993). Shepton and Hazen (2013) also emphasize the need to conduct enhanced studies to elaborate the polarized abiotic origin of hydrocarbons. In the opinion of McCollom (2013), hydrocarbons migrate from deep sources (mantle) with different sources and secondary hydrocarbon can form within the Earth's crust through reduction of inorganic carbon sources. The Yue (2013) hypothesis involves the presence of Methane (CH_4) at the Moho-Discontinuity produced in upper mantle transfers upwards to a secondary reservoir in Earth's crust and enhances the presence of methane in the epicenter zone before earthquakes. The in-situ earth's crust generation of abiotic hydrocarbon can be explained with endogenous structure processes (Dedeev V. and Kulikov 1988) during the regional metamorphism and granitization of Earth's crust (Rosen O and Fedorovsky 2001). However, the mantle and earth's crustal environments are different for the formation of abiotic organic compounds (McCollom 2013). Farooqui et al., (2009) also report the presence of hydrocarbons in the volcanic rocks.

The author is considering both biotic and abiotic hydrocarbon sources to evaluate the possibility of oil and gas reservoirs in sedimentary and crystalline rocks of the Karakoram Cimmerian Mega-anticlinorium. Whereas present day exploration is limited to the clastic and carbonate reservoirs for biotic hydrocarbons in the conventional sedimentary basins in Pakistan. The conservatism in hydrocarbon exploration is temporizing even preliminary work to evaluate the possibility of

hydrocarbons in the Paleozoic – Mesozoic clastic and carbonate rocks of the Palaeozoic – Mesozoic of the Karakoram. The possible arguments for a lack of hydrocarbons in Karakoram are the intensive tectonic activity resulting in complex folding and faulting structures and loss of hydrocarbons in accordance with collision of Indian and Asian plates. This can be counter-argument with vertical migration of the biotic hydrocarbons (Muslimov et al., 2004), Plotnikova (2006), Yue (2013), where deep faults tap the upper mantle and control the accumulation of hydrocarbons and influence recent activity on surface. Such deep faults are reported in the Karakoram Cimmerian Mega-Anticlinorium (Zanchi and Gaetani 2011) and may play a facilitating role for the migration of the hydrocarbons into Karakoram region. The relation of occurrence of the fluid natural resources, including hydrocarbons with deep crust processes, make geodynamics criteria important as a preliminary parameter of exploration for hydrocarbons.

The correlation of the hydrocarbon producing clastic and carbonate horizons of the Indus Basin, Kohat - Potwar Basin, Balochistan Basin and offshore of Pakistan with clastic and carbonate rocks of the Karakoram Cimmerian Mega Anticlinorium illustrates the possibilities of biotic origin hydrocarbons in study area. The Gondwana phase palaeotectonic map (Fig.2) shows the deposition condition of the clastic and carbonate rocks during the Palaeozoic – Mesozoic epoch in hydrocarbon production and the Karakoram region.

The analysis of lithology of the world hydrocarbon producing reservoirs of crystalline basement and crystalline basement with sedimentary cover, where granites, granitoid, volcanic, serpentine granitic gneiss, tuffites, chlorotic quartzite, and shale or slate as basement rocks, sericitic/siliceous schists intercalated with fine sandstone, fine conglomerate, marble, are hydrocarbon reservoirs (Gutmanis 2013). The above-mentioned rocks are exposed in the Karakoram Cimmerian Mega-Anticlinorium and which can be potential reservoirs of hydrocarbons. The block folding Belousov (1976) characteristic for Alpine- Himalayan Folded Belt including Karakoram Cimmerian mega-Anticlinorium and normal faulting (Zanchi and Gaetani 2011) geodynamic and fluid dynamic processes, it is possible to form reservoirs in sedimentary, metamorphic and magmatic rocks (Nikonov 2004). The geological aspects of producing and accumulation of biotic and abiotic hydrocarbons allow the hypothesis of the presence of oil and gas in the Yasin and Chupersan Areas of Karakoram, where sedimentary rocks cover the crystalline fundament. The preliminary selection based on sources of formation of abiogenic and biogenic hydrocarbons are the transformations of sedimentary cover rocks and organic mineral substances in them in different forms (Nikonov 2004) and vertical migration of the hydrocarbons through active deep faults. However, geochemical aspects will confirm the hypothesis of presence of biotic and abiotic hydrocarbons in the Karakoram Region.

Acknowledgment: I thank anonymous reviewer for comments and Dr. Louis Hissink for editing of the paper. I also thank Iftikhar Magsi and Emilia Magsi for preparation of the Maps.

References:

1. Areshev E., Dong L., San N., and Shnip O, 1992 Reservoirs in Fractured Basement on the Continental Shelf of Southern Vietnam., Journal of Petroleum Geology, Vol. 15, pp. 451-464.
2. 2.Arsentev, I., Becker, R.V., Blagonravov, V., Wii, K.M.A.M., Votakh, O., Gintsipger A., Glukhov, G., Gusev, A., Dykopov, I., Zhabip, O, Zhero, V., Kiselev, V., Kpyazev, I., Lyubofeev, N., Makhlaev, L., Mokshaptsev, K., Mitrofapov, G., Mitrofapov, F., Mmorality, V., Mordovia, V. and Shpip, O., 1978. Precambrian of Continents: Folded regions and recent platforms of Eastern Europe and Asia. Academy of Sciences of the USSR, Siberian Branch Transaction of the Institute of the Geology and Geophysics (420), p. 322. (in Russian).
3. . Barenbaum A., and Abaya E., 2012 Proof of policonsolidation synthesis hydrocarbon Oil. Vestnik ONZ RAN, Vol. 4. (In Russian).
4. . Bath G., Craig J., Hafiz M., Hakhoo N., Thurow W., Thusu B., & Cozzi A. Geology and hydrocarbon potential of Neoproterozoic–Cambrian Basins in Asia: an introduction.

5. Bender F. and Raza H. 1995. Hydrocarbons. [ed.] and Raza H., Bender F. Berlin -Stuttgart: Gebruder Borntraeger, pp. 182-202.
6. Belousov, V., 1976. Geotectonics. M. Nedra, p.264 (in Russian).
7. Belousov, V.V., Belyavsky, N.A. and Borisov, A.A., 1979. The structure of the lithosphere the profile of deep seismic sounding of the Tien Shan, Pamir-Karakoram Himalaya. Sovetskaya Geology, no. S, p. 11-28. (In Russian).
8. . Blot, C. and Choi, D., 2005. Forerunners of the catastrophic Kashmir Earthquakes (8 October 2005) and their Geological significances. New Concepts in Global Tectonics Newsletter, no. 37, p. 4-16.
9. Breshkuntsov A., Monastyrev B., and Nesterov (Jr.) I. 2011. Distribution Patterns of oil and Gas Accumulation in West Siberia. Geology and Geophysics, Vol. 52, pp. 1001-1012.
10. Crawford A. 1979. Gondwanaland and the Pakistan Region. [ed.] & De Jong K., Farah A. Geodynamics of Pakistan. Geological Survey of Pakistan, Quetta pp. 103-110.
11. Desio, A., 1979. Geological Evolution of the Karakoram. In: Farah, A. and DeJong, K.A. (eds.), Geodynamics of Pakistan. Geol. Surv. Pak., Quetta, p. 111-124.
12. Dedeev, V. and Kulikov, P., 1988. Origin of the Earth's crust. Nedra, 364p. (In Russian).
13. Dmitriyesvskii A., Kireyev F., Bochko R., and Fedorova T. 1993. Hydrothermal Origin of Oil and Gas Reservoirs in Basement rocks of the South Vietnam Continental Shelf. International Geology Review, Vol. 35, pp. 621-630.
14. . Farooqui M., Hou H., Li G., Machin N., Nevile T., Pal A., Shrivastava C., Wang Y., Yang F., Yin C., Zhao J., and Yang X., 2009 Evaluating Volcanic Reservoirs. Oilfield Review Spring Vol.21 No.1pp.36-47
15. . Shah Faisal Larson K., Jess King, John M. Cottle d Faisal, S., et al., 2015. Rifting, subduction and collisional records from pluton petrogenesis and geochronology in the Hindu Kush, NW Pakistan, Gondwana Research http://dx.doi.org/10.1016/j.gr.2015.05.014.
16. Gaetani M 1997 The Karakorum Block in Central Asia, from Ordovician to Cretaceous.1997, Sedimentary Geology, Vol. 109, pp. 339-359.
17. Gaetani M. 2015. Blank on the Geological Map. Rendiconti Lincei. Scienze Fisiche e Naturali. DOI: 10.1007/s12210-015-0494-2
18. Gansser A., 1964. The Geology of Himalayas. John Wiley & Sons Ltd. pp. 289
19. Gattinger T., 1961. Geologischer Querschnitt des Karakorum vom Indus zum Shaksgam. Geologische Ergebnisse der Österreichischen Himalaya-Karakorum-Expedition 1956. JB. Geol. B. A. Sonderband 6 S 3—118.
20. Gavrilov V., Gulev V., Kireev F. 2010. Granitoid Reservoir and Oil and Gas potential of Southern Shelf Vietnam. Moscow: OOO Izdatelskiy dom Nedra p. 494 (In Russian).
21. Galimov E. Sources and mechanisms of formation of hydrocarbon gases in sedimentary rocks. Geochemistry, Vol. 2, pp. 163-180.
22. Gutmanis J., Batchelor T., Cotton L., Doe S., 2013 Hydrocarbons Production from fractured Basement Formations, Geoscience Limited, version 11
23. Hasany T., Ahmad N., and Mirza O. 2007. Identification of New Potential Source and Reservoir Rock of Early Jurassic Age supported with Basin Modelling. Islamabad: PAPG, 2007. PAPG Annual Technical Conference, March 27-28, 2007.
24. Halimov Yu. 2012. Petroleum Potential of Granitoid Basement Reservoirs. Neftegasovaa Geologia.Teoria I Practika (RUS) V.7 No. 4 URL: HTTP:// www.ngtp.ru. (In Russian).
25. Heuberger 2004. Kinematics of The Karakoram-Kohistan Suture Zone, Chitral, NW Pakistan. Dissertation of Doctor of Natural Sciences. pp.191.
26. Kadri I. 1995 Petroleum Geology of Pakistan. Karachi: Pakistan Petroleum Limited. p. 300.
27. Khain, V.E., 2000. Tectonics of continents and oceans. Moscow. 585p. (in Russian).
28. Khain, V.E., 1979. Regional Geotectonics of Asia and Australia M. Nedra. (in Russian).
29. Khain V., Limonov L. 2004. Regional Tectonics. 2004. (In Russian)
30. Kazmi H., And Jan M. Q. 1997 Geology and Tectonics of Pakistan. Karachi.
31. Kalan, T., Seterus, H.P., Eman, M 1994. Jatibarang Field, Geologic Study of Volcanic Reservoir for Horizontal Well Proposal. Jakarta, In: Proc. 23rd Ann. Convention, Indonesian Petroleum Assoc., pp. 229-244. Paper IPA94-1.1-186.

32. Kravchenko, K., 1979. Tectonic Evolution of the Tien Shan, Pamir, and the Karakorum. In: Farah, A., and DeJong, K.A., (eds.), Geodynamics
33. Krayushkin, V.A., Tchebanenko., Klochko., Dvoryanin, Ye. S., Kenny 1994. Recent Applications of the Modern Theory of Abiogenic Hydrocarbon Origins: Drilling & Development of Oil & Gas Fields in the Dnieper-Donets Basin. Santa Fe, New Mexico: In Proc. 7th Int. Symp. on the Observation of the Continental Crust Through Drilling. DOSECC.
34. Le Fort P., Tongiorgi M. & Gaetani M. 1994. Discovery of a crystalline basement and an Early Ordovician marine transgression in the Karakorum mountain range, Pakistan. Geology, Vol. 22, pp. 941-944.
35. Leichenkov G. 2013. The Crustal structure and the geological history of the sedimentary basins of the Indian Ocean: offshore Antarctic. The summary of thesis for the degree of Doctor of Geological and Mineralogical Sciences, Vol. MSU, pp. 1-42. (in Russian),
36. Magsi, H.Z., 1983. Seismotectonic of Pakistan. Ph. D. Thesis, p.155 (in Russian).
37. Magsi H.Z. 2018. The question of the oil and gas potential of western and central Karakorum, Pakistan. Proceedings of the International Geological and Geophysical Conference GeoEurasia 2018. Modern technologies of studying and development of Eurasian resources » pp.104-107
38. McCollom T. 2013. Laboratory Simulations of Abiotic Hydrocarbon Formation in Earth's Deep Subsurface. Reviews in Mineralogy & Geochemistry, Vol. 75, pp. 467- 494.
39. Muslimov R., Glumov I., Plotnikova I., Trifonov V., Nurgaliyev D., Oil and Gas Fields- Spontaneous and steadily renewable targets. 2004. Oil and Gas Geology. The material of the International Conference. pp. 43-49.
40. Nikonov A.I. 2006. The role of geodynamic processes in the formation of anisotropy of physical properties of the rocks of local uplifts. Geology, geophysics, and exploration of oil and gas fields. № 12. P. 23-33.
41. Palin M., Searle M., Waters I., Horstwood M., and Parrish R. 2012. Combined thermobarometry and geochronology of peraluminous metapelites from the Karakoram metamorphic complex, North Pakistan; New insight into the tectonothermal evolution of the Baltoro and Hunza Valley regions. J. Metamorphic Geology. Pp.1-29. doi:10.1111/j.1525-1314.2012. 00999.x
42. Plotnikova I. 2006. Nonconventional hydrocarbon targets in the crystalline basement, and the problem of the recent replenishment, of hydrocarbon reserves. Journal of Geochemical Exploration, Vol. 89, pp. 335–338.
43. Pudsey C., Coward M., Luff I., Shackleton R., Windley B., and Jan Q., 1985. Collision zone between the Kohistan arc and the Asian plate in NW Pakistan. Transactions of the Royal Society of Edinburgh: Earth Sciences, 76, 463-479.
44. Rosen, O.M., and Fedorovsky, V.S., 2001. Collision granites` and delimitation of the crust (examples Cenozoic, Paleozoic and Proterozoic collision systems). Tr. GIN RAS- M.: Scientific World, v. 545, 188p.
45. Rolland Y., Picard C., Pêcher A., Carrio E., Sheppard S, Oddone M., Villa I., 2002. Presence and geodynamic significance of Cambro-Ordovician series of SE Karakoram (N Pakistan). Geodinamica Acta I5 pp. 1-21.
46. Schneider H., 1957, Tektonik und Magmatismus im NW-Karakorum. Geol. Rdsch., 46,426-476.
47. Schneider H.,1960, Geosynklinale Entwicklung und Magmatismus an der Wende Palaozoikum-Mesozoikum im NWHimalaya und -Karakorum. Geol. Rdsch., 50, 334-352.
48. Searle M., Crawford M., Rex A., 1992. Field relations, geochemistry, origin and emplacement of the Baltoro granite, Central Karakoram. Transactions of the Royal Society of Edinburgh: Earth Sciences, 83, 519-538,
49. Searle M., Khan M., Frasera, J., Gough J.,1999. The tectonic evolution of the Kohistan-Karakoram collision belt along the Karakoram Highway transect, north Pakistan. Tectonics, vol. 18, No. 6, pages 929-949.
50. Searle M., and Philips R., 2007. Relationships between right-lateral shear along the Karakoram fault and metamorphism, magmatism, exhumation, and uplift: evidence from the K2–Gasherbrum–Pangong ranges, north Pakistan and Ladakh. Journal of the Geological Society, London, Vol. 164, pp. 439–450.

51. Sephton M., and Hazen R. 2013. On the Origins of Deep Hydrocarbons. Reviews in Mineralogy & Geochemistry, Vol. 75, pp. 449 - 465.
52. Shuster V., Punanova C., 2014. Development of Unconventional Hydrocarbon Sources in Western Siberia and Evaluation of Oil and Gas Prospects., Georesources, Vol. 4, pp. 53-58. (In Russian).
53. Smoot N., 2007. Wherefore the Tethys Sea(s)? New Concepts in Global Tectonics Newsletter, no. 45, pp.21-30.
54. Smoot N., 2018. Observations on the Southern and African plates. New Concepts in Global Tectonics Journal, v.6, no. 2, pp. 149-170 www.ncgtjournal.com.
55. Tahirkheli R., Dongli S., Yusheng P., Wangming D., Yuquan Z., Baqri S., and Dawood H.,1990. Review of Stratigraphy of the Upper Hunza Valley (UHV), NW Karakoram Pakistan. Geol. Bull. Uni. Peshawar, Vol. 23, pp. 203-214.
56. Voskresensky, I., Kravchenko, K., Movshovich, E. and Sokolov, B., 1971. Outline of Geology of Pakistan. M. Nedra, p. 166. (in Russian).
57. Yiwen J., Shuangfang L., Yan S., Fengqi T, Fengqi, Guochang W., Ku H., Yuan B., and Qingguang L., 2015. Nano-Geology and Unconventional Oil and Gas. Acta Geologica Sinica (English Edition), 89 (supp.): 192-193.
58. Yue Z. 2013 Why our Earth's crust not quiet? [ed.] Wu & Qi. Global View of Engineering Geology and the Environment, pp. 43- 50.
59. Zanchi A. & Gaetani M. 1994. Introduction to the Geological map of the Northern Karakoram Terrain, from Chapurson valley to Shimshal Pass. Riv. It. Paleont. Strat., 100(1), 125-136.
60. Zanchi, A. and Gaetani, M., 2011. The Geology of the Karakoram range, Pakistan: the new 1:100,000 geological map of Central –Western Karakoram. Ital. J. Geo.sci. (Boll. Soc. Geol. It.), v. 130, no. 2, p. 161-262, 91. DOI: 10.3301/IJG.2011.09.`

ABOUT THE NCGT JOURNAL

The New Concepts in Global Tectonics Newsletter, the predecessor of the current NCGT Journal, was initiated at the International Geological Congress in Beijing in August 1996. The name is taken from an earlier symposium held at the Smithsonian Institution, Washington, in association with the 28th International Geological Congress in Washington, D. C. in 1989. The NCGT Newsletter changed its name to NCGT Journal in 2013.

Aims include:

1. Providing an international forum for the open exchange of new ideas and approaches in the fields of geology, geophysics, solar and planetary physics, electric universe, cosmology, climatology, oceanography, electric Earth, and other fields that affect or are closely related to physical processes occurring on the Earth from its core to the top of its atmosphere.
2. Forming an organizational focus for creative ideas not fitting readily within the scope of dominant tectonic models.
3. 3. Forming the basis for the reproduction and publication of such work, especially where there has been censorships or discrimination.
4. Create a publication that can serve as an exchange of methods and concepts devoted to the prediction, well in advance, of catastrophic earthquakes. Establish a forum for discussion of such ideas and work which has been inhibited in existing channels.

APPENDIX

Electric Earth, third instalment: Michael Csuzdi.

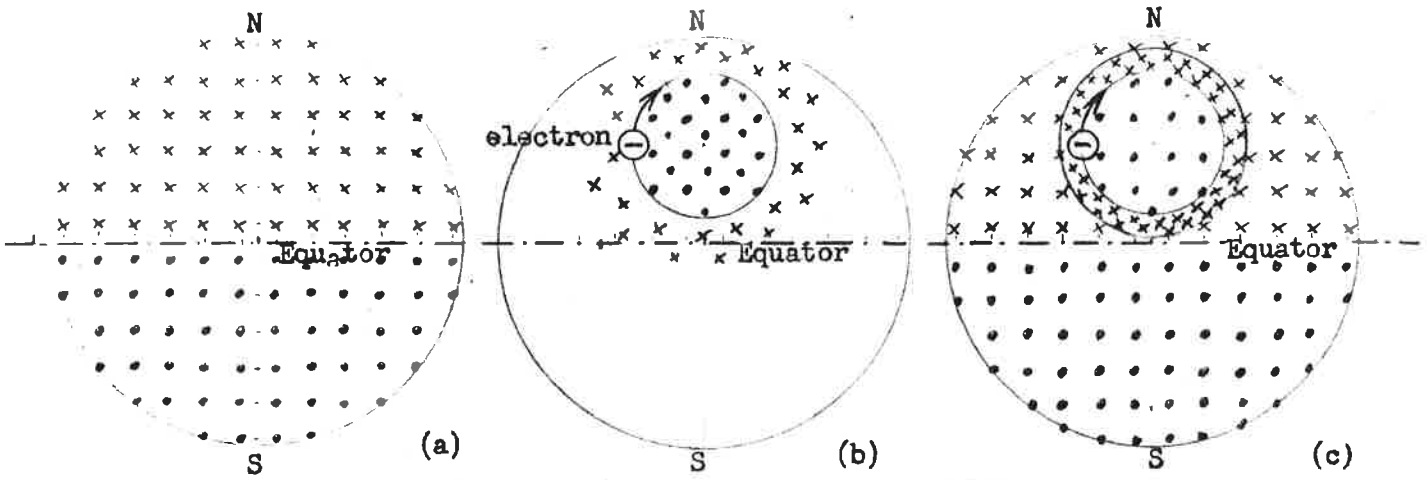

Figure 12-3

Figure 12-4

thus they also approach the ring (Figure 12-4).

In the Southern Hemisphere a symmetrically opposite rotation takes place. Figure 12-5 summarizes the rotations and the magnetic polari-

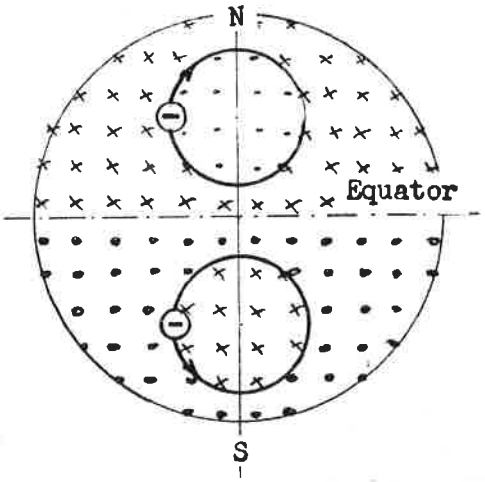

Figure 12-5

ties for both hemispheres.

The low pressure upward flowing interior air of the anticyclone clears away all positively charged clouds and deposits them outside the

ring in a mushroom-type flow. Inside the system the upward flow of electrons are deflected only around the horizontal axis, always and everywhere towards the east. All anticyclones drift towards the east on both hemispheres.

The clearing of the anticyclone's interior from positive charges and the concentration of emission electrons in the ring eventually causes the death of the system. AS it becomes more and more negatively charged the system attracts the external positive ly charged clouds more and more. This attraction is the Coulomb force between opposite charges. Positive ions rotate in the opposite direction to the ring's electros in the same magnetic field, and they encounter both mechanically and in electrically in a head-on collision in the form of storms breaking out along the ring. In these storms the electron ring is destroyed and the anticyclone ceases to exist.

13 CYCLONES

From Equation (12-1) it can be predicted that the cyclonic rotation is caused by the deflection of positive charges in the vertical component of the Earth's magnetic field. It is only the sign of the electric charge which changes in the anticyclonic equation to yield the cyclonic equation:

$$F_m = +q\left[V_h \times B_v\right] \qquad (13\text{-}1)$$

This change of sign results in the reversal of the rotation: cyclones rotate counterclockwise in the Northern, and clockwise in the Southern

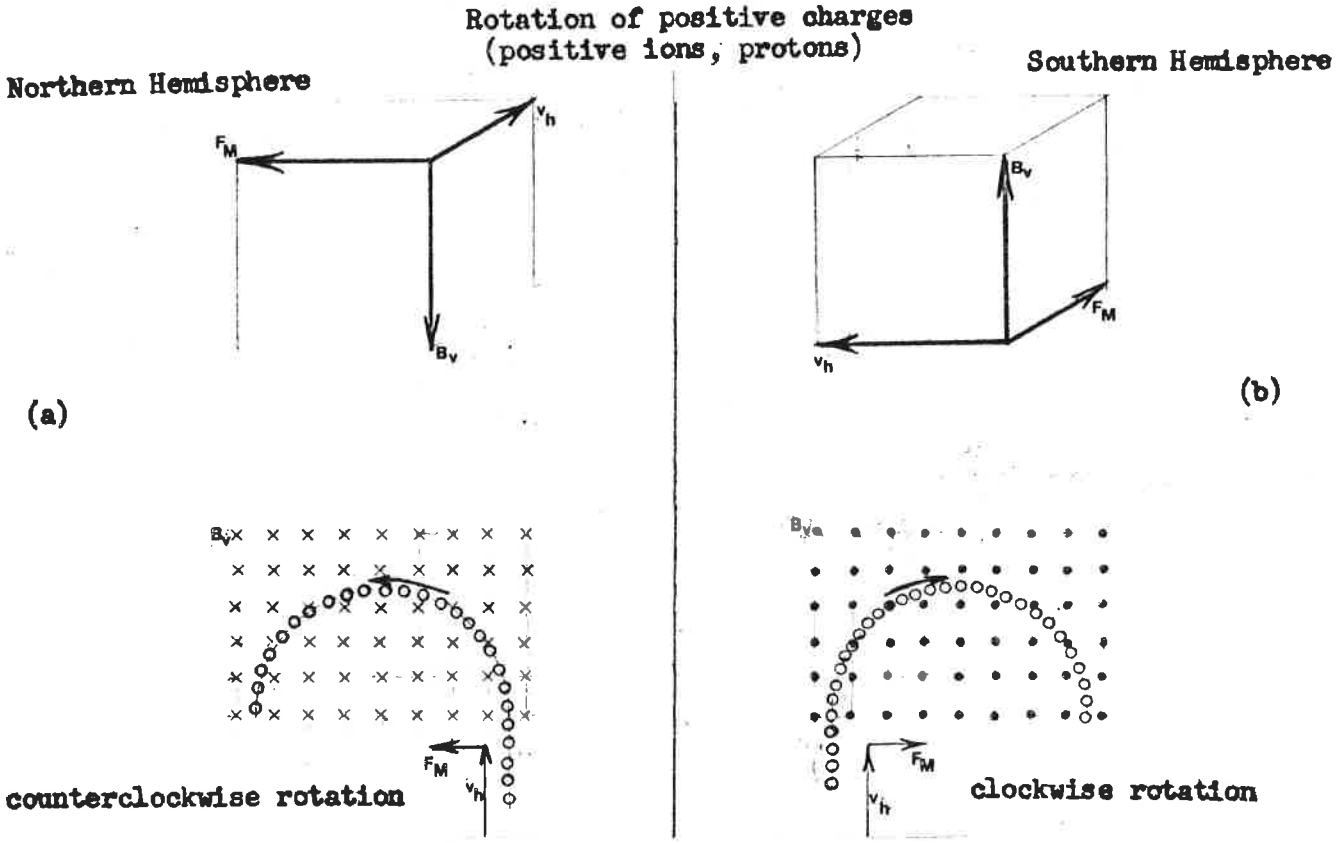

Figure 13-1

Hemisphere (Figure 13-1). Thus, cyclones are caused by the movements of positive charges (positive ions) in the atmosphere.

A significant planetary confirmation exists for this electric nature of the cyclone: Jupiter's Great Red Spot. According to measurements by the space probes Pioneer 10 and 11 (Ref. 13-1), Jupiter's magnetic

field is of reversed polarity: its North Magnetic Pole is in its Southern Hemisphere. Thus, in a reversed magnetic field the rotation of a cyclone should be reversed. Indeed, its cyclonic Great Red Spot is located in its Southern Hemisphere and it does rotate counterclockwise. On the Earth cyclones rotate clockwise in the Southern Hemisphere.

Figure 13-2 summarizes the correspondence between hemispheres, sign of charges, and direction of rotations: (a) and (b) refer to the Earth-type systems, (c) is of general validity regardless of the magnetic polarity.

Type of System	Direction of Rotation	
	Northern Hemisphere	Southern Hemisphere
Cyclone	counterclockwise	clockwise
Anticyclone	clockwise	counterclockwise

(a)

Type of Charge	Direction of Rotation	
	Northern Hemisphere	Southern Hemisphere
Positive	counterclockwise	clockwise
Negative	clockwise	counterclockwise

(b)

Rotation	Charge
Cyclonic	Positive
Anticyclonic	Negative

(c)

Figure 13- 2

14. THE SOURCE OF THE POSITIVE CHARGES

I found the source of the positive charges through the cyclonic rotation of certain cloud formations in the atmosphere. Several papers were published on the observations during the GARP Atlantic Tropical Experiment (GATE), in 1974, which were focused on the tropical cloud systems, especially on the sudden appearance and rapid development of cold clouds of about 100 - 200 km diameter.

A geostationary satellite was positioned over the Equator, near 45 degrees west, which regularly (hourly) produced infrared photographs of that area of the ocean. A large number of the observed cloud structures exhibited the following behaviour (Ref. 14-1):

1. Rapid growth of cold cloud in region where little or no cold cloud had existed. Typical growth period was 2-5 hours

2. Bright mushroom or oval appearance in the growing stage. This is a signature for developing cumulonimbus clouds

3. Mature stage with horizontal dimensions 50-200 km latitude

One observer noted (Ref. 14-2) that "(the infrared pictures) revealed that convection began during the night hours and that the anvil once discovered as a bright dot on the picture would develop exposively like a 'super nova' within the following 2 to 3 hours into a huge storm whose anvil area enlarged by orders of magnitude to thousands of nautical square miles. The decaying state of these storms usually set in during the noon hours." I emphasise here that these sudden storms arise and develop independently on the ambient weather conditions: according to the infrared pictures they frequently emerge under perfectly clear skies, expand upward, and move always westward. Thus their linear longitudinal drift is exactly opposite to that of the electrons.

Even the location of storm outbreaks moves weather-independently and highly regularly. One study (Ref. 14-1) lists locations of 92 systems during the early stages of development (Figure 14-1). I applied the process of linear regression to these figures to see the trend in them and I found two periodicities:

A.) The location of storm outbreaks moves monotonously towards the north during the observation between July 17 and September 6 (Figure 14-2a)

System Number	Date	Time (GMT)	Location
1	July 17–18	2230–0100	30°W– 5°N
2	July 19	0900–1030	33°W– 9°N
3	July 21	0900–1100	26°W– 11°N
4	July 21	1800–2330	28°W– 11°N
5	July 22	0300–0800	26.5°W– 10.5°N
6	July 23	1930–2200	33°W– 3°N
7	July 24	0100–0300	37°W– 8°N
8	July 24	1200–1600	29°W– 7°N
9	July 24	2200–2330	24°W– 9°N
10	July 25	2100–2300	28°W– 12°N
11	July 26	0900–1200	38°W– 11°N
12	July 26	1500–1800	36°W– 11°N
13	July 27	0000–0300	29°W– 8°N
14	July 27	0000–0300	28°W– 9°N
15	July 27	0100–0700	39.5°W– 9.5°N
16	July 28	0000–0500	35°W– 5°N
17	July 29	0500–0730	21°W– 17°N
18	July 29	0500–0730	22°W– 18°N
19	July 29–30	2330–0500	27°W– 8°N
20	July 30	1730–2300	29°W– 7°N
21	July 31	0300–0700	21.5°W– 9.5°N
22	July 31	1530–1830	36°W– 9°N
23	Aug. 1–2	2130–0300	38°W– 7°N
24	Aug. 5	0400–0800	38°W– 8°N
25	Aug. 5	1330–1800	34°W– 8°N
26	Aug. 6	0300–0600	28°W– 10°N
27	Aug. 7	0930–1230	30.5°W– 10°N
28	Aug. 7	1830–2300	27°W– 10°N
29	Aug. 8	0230–0830	28°W– 10°N
30	Aug. 10	0430–0900	26°W– 9.5°N
31	Aug. 10	0430–0900	23.5°W– 9°N
32	Aug. 10	0500–0900	22.5°W– 10°N
33	Aug. 10	0600–1000	23°W– 7°N
34	Aug. 10	0700–1030	30°W– 14°N
35	Aug. 10	0730–1200	25°W– 12°N
36	Aug. 10	0900–1200	26.5°W– 13°N
37	Aug. 10	1800–2200	34°W– 13°N
38	Aug. 12	0000–0500	35°W– 1°N
39	Aug. 12	0000–0500	35°W– 3°N
40	Aug. 12	1400–1800	39°W– 6°N
41	Aug. 14	0330–0900	23°W– 13°N
42	Aug. 14	0500–0900	30°W– 9°N
43	Aug. 14	1730–2330	31°W– 12°N
44	Aug. 15	0100–0400	28°W– 12.5°N
45	Aug. 15	0600–0900	26°W– 12.5°N
46	Aug. 16	0000–0500	39°W– 9°N
47	Aug. 16	0400–0900	20°W– 10°N
48	Aug. 17	0000–0730	30°W– 9°N

Figure 14-1a

System Number	Date	Time (GMT)	Location
49	Aug. 17	0100–0600	36°W– 7°N
50	Aug. 17	0300–0730	27.5°W– 10°N
51	Aug. 18	0100–1000	29.5°W– 8°N
52	Aug. 18	0200–1000	28°W– 9°N
53	Aug. 18	0400–1100	37.5°W– 7.5°N
54	Aug. 18	0600–0900	32.5°W– 8°N
55	Aug. 18	1200–1800	25°W– 10°N
56	Aug. 18	1300–1600	33°W– 8.5°N
57	Aug. 18	1500–2000	27°W– 11°N
58	Aug. 18	2000–2300	30°W– 8°N
59	Aug. 18	2000–2300	36°W– 7°N
60	Aug. 19	0100–0700	30°W– 8°N
61	Aug. 19	0100–0700	34°W– 8°N
62	Aug. 19	0830–1100	22°W– 11°N
63	Aug. 20	0400–0700	25°W– 12°N
64	Aug. 20	0500–0900	31°W– 10°N
65	Aug. 21	2100–2330	27°W– 12°N
66	Aug. 28	0000–0600	27°W– 9.5°N
67	Aug. 28	1300–1800	38°W– 12°N
68	Aug. 28	2130–2330	36°W– 11°N
69	Aug. 29	0200–0800	40°W– 6°N
70	Aug. 29	2030–2230	40°W– 9°N
71	Aug. 30	0100–0600	32°W– 7.5°N
72	Aug. 30	0100–0600	21°W– 14°N
73	Aug. 30	1930–2230	30°W– 11°N
74	Aug. 30	1900–2300	24°W– 12°N
75	Aug. 31	0600–0900	31°W– 12°N
76	Aug. 31	1000–1600	28°W– 4°N
77	Aug. 31	1100–1500	30°W– 12°N
78	Sept. 1	0100–0400	38°W– 8°N
79	Sept. 1	0300–0500	34°W– 10°N
80	Sept. 1	0300–0630	26°W– 5°N
81	Sept. 1	1230–1500	32°W– 13°N
82	Sept. 1	1500–1830	39°W– 9°N
83	Sept. 1	1800–2000	33°W– 7°N
84	Sept. 1	1830–2300	37°W– 11°N
85	Sept. 2	0100–0600	24°W– 7°N
86	Sept. 2	0200–0600	25°W– 11°N
87	Sept. 3	1900–2300	22°W– 7°N
88	Sept. 4	0000–0400	23°W– 8°N
89	Sept. 5	1700–2000	31°W– 11°N
90	Sept. 6	0100–0600	24°W– 12°N
91	Sept. 6	0430–0700	22°W– 8°N
92	Sept. 6	2000–2300	37°W– 9°N

Figure 14-1b

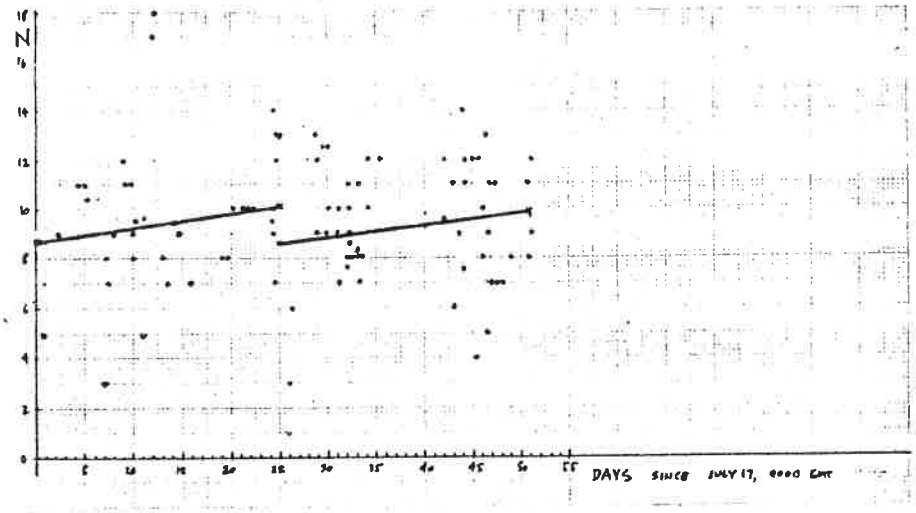

Figure 14-2a

B.) The location of storm outbreaks moves towards the west between midnight and noon, and towards the east between noon and midnight (Figure 14-2b).

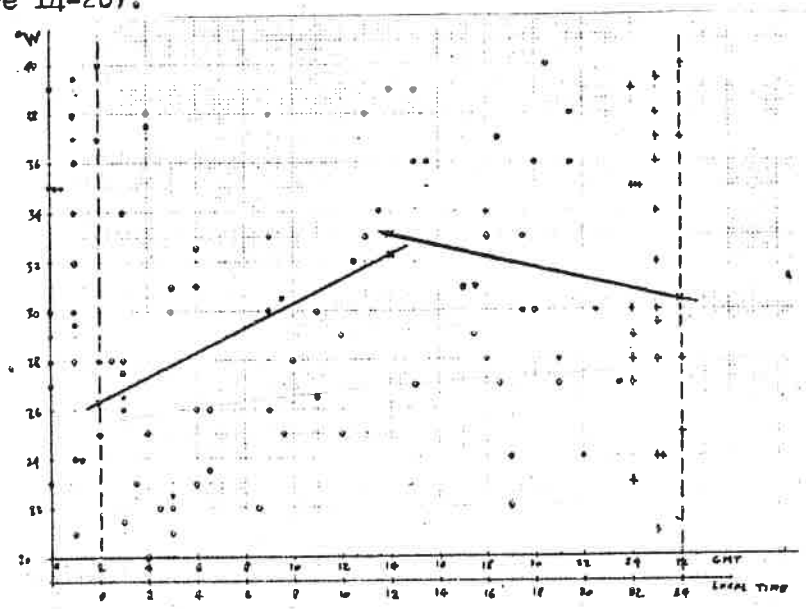

Figure 14-2b

These movements are coincident with the movements of "earth currents" (Chapter &w100) of which I pointed out that their driving force is an electric repulsion force from the direction of the Sun. This repulsion force results in an electron concentration in the night side of the Earth's crust with its maximum at the midnight meridian. This charge concentration is directly involved in the fostering of the storm outbreaks. According to Figures 14-2 the location of storm outbreaks follows the movement of the solar antipode both latitudinally and longitudinally: the shift in the east-west direction is diurnal and in the north-south direction it is seasonal (from June 21 till Decem-

ber 21 it moves northward).

According to the above observations I find the mechanism which gives birth to these storms as follows:

(A) The solid crust acts as a charge separator of charges: it lets the electrons passing through but retains the positive charges as these are located in the protons of the atomic nuclei which can not penetrate the crust because of their size.

(B) Frequent breakup of the ocean floor releases the accumulated positive charges (ions) into the water of the ocean either directly,or by a charge exchange: when the water contacts the molten lava water molecules break up through thermal ionization, and electrons move into the solidifying lava which has been in the state of positive ionization. Thereby the water molecules become positively charged.

(C) The positively charged water moves up in the water of the ocean which acts as an electrolyte, thus positive ions propagate in it. This positively charged water bursts into the atmosphere from the ocean under the driving force of the local electric field. Thus the formation of the cloud at this place is independent of the local weather.

(D) The upward moving positive water-ions drag a large amount of neutral water into the atmosphere. The development of the cloud proceeds from the water surface upward, in the form of a cumulonimbus cloud. "Bright mushroom or oval appearance in the growing stage. This is a signature for cumulonimbus clouds" as I quoted above. As it will be seen later the entire energy of a future hurricane enters into tha atmosphere at this stage.

(E) The lifetime of a fissure on the ocean floor is directly related to the length of the developing phase of these clouds. "Typical growth period was 2-5 hours". In the presence of the water the fissure seals off in a few hours, therefore only a fixed amount of positive charge enters the ocean and eventually into the atmosphere like a great bubble. This develops into a fixed volume of cloud with a sharp cutoff at the bottom. After the cutoff the cloud moves further up into the atmosphere under the electric driving force and a gap develops towards the ocean surface which increases as the bubble moves upward.

(F) The driving force of the cloud in the vertically upward direction is the Coulomb repulsion force

between the locally positively charged surface area of the magma cathode and the similarly positively charged ions in the cumulonimbus cloud. The fast upward driven charged particles transfer a kinetic energy to the neutral molecules through flexible collisions, thus the entire group moves upward. I show later that in a powerful hurricane one charged particle for each million neutral molecules can provide the driving force.

(G) The friction between the driving and the driven molecules develop into a temperature increase inside the cloud. This phenomenon is identical to the Joule heat in a resistive wire when electric current flows in it. The flow of positive ions in the cloud also constitutes an electric current and the neutral water and air molecules represent the resistive medium in this atmospheric conductor. Thus, the temperature gradient inside the cloud is the result, and not the reason, of the drive.

This release of positive ions from the Earth's magma cathode compliments the electron release through the crust, thus the average charge balance of the Earth remains unchanged. I refer here to Figure 1-1 where the "vacuum deposition chamber" is illustrated. Here a thermionic cathode releases both positive ions and negative electrons into the surrounding space. Obviously this cathode would continue releasing particles even if a very thin filmlike layer of broken wet stone was spread over its surface. The only difference would be that the emission would become intermittent, it would be concentrated into packets of bubbles, but the overall emission would continue. These bubbles of packeted charges are the sudden tropical storms on the Earth. The 5 km thick ocean floor on the 12700 km diameter Earth is of the same ratio as 0.0005 centimeter (1/6000-th inch) thick layer on a 1 centimeter (0.4 inch) diameter cathode in the vacuum chamber.